
Helsinki University of Technology

# Aging of iron-based martensites at low temperatures

Kari Ullakko

Thesis for the degree of Doctor of Technology to be presented with due permission for public examination and debate in Auditorium K 216 at Helsinki University of Technology on the 25th of June, 1992, at 12 o'clock noon.

Espoo, March 1992

Report No 3/1992/MTR

ISBN 951-22-1101-7
ISBN 978-951-22-9934-8 (PDF)
ISSN 0785-1294

Author's address:
Helsinki University of Technology
Laboratory of Engineering Materials
Puumiehenkuja 3 A, SF-02150 Espoo, Finland

Otaniemi 1992
TKK Offset/
Valtion painatuskeskus

*ULLAKKO, Kari. Aging of iron-based martensites at low temperatures. Espoo 1992, Helsinki University of Technology*

**Keywords:** martensite, aging, low temperature, deformation, X-ray diffraction, neutron scattering, Mössbauer spectroscopy, internal friction, positron annihilation, electrical resistivity, magnetic susceptibility, dilatometry, shear modulus

## ABSTRACT

In the present work aging of iron-based martensites, defined as all the phenomena preceding the first stage of tempering, is studied using various methods. In some alloys aging was observed to start at very low temperatures, even near 4 K. Abnormally high or abnormally low tetragonality is observed in freshly formed martensite alloyed with Ni or Mn, respectively. The reason for high tetragonality obviously lies in the coherency at the interface between the martensite and the retained austenite. It is shown in the present work that the coherency is broken during aging in the temperature range of 100 - 200 K and it is accompanied by a decrease of tetragonality (first stage of aging). The new internal friction peak centered at 145 K corresponds to the movement of the coherent interface and the break of coherency. Some evidence for correlation between short range atomic ordering in austenite and the high tetragonality of the virgin martensite is given and a contribution of nontransformed ordered austenitic regions inside martensite plates to tetragonality is discussed. It is shown that the second stage of aging at temperatures about 200 - 270 K is controlled by the pinning of the dislocations by carbon atoms and the third stage (mainly above 250 K) by the clustering of carbon atoms in a solid solution. By means of Mössbauer spectroscopy, electrical resistivity and magnetic susceptibility measurements, a striking difference is shown between the redistribution of carbon and nitrogen atoms above 200 K. Evidence for the clustering of carbon and ordering of nitrogen is given and discussed. The dynamics of clustering was studied by means of small angle neutron scattering. Deformation of martensite at subambient temperatures reduced the tetragonality of martensite to cubic and changed the redistribution of carbon atoms. According to different measurements, practically no aging was observed below room temperature in the deformed martensite.

## PREFACE

The present work was mainly performed in the Laboratory of Engineering Materials, Helsinki University of Technology. I wish to express my gratitude to my former and present supervisors Professor J. Pietikäinen and Professor H. Hänninen for their encouraging attitude to my work and for creating the favorable working conditions with an enjoyable atmosphere. It is a pleasure to acknowledge collaboration with Mr. M. Nieminen and the whole personnel of our laboratory. Since 1986, the research has been carried out in close cooperation with the Institute of Metal Physics, Kiev, Ukraine. Especial thanks are due to Professor V.G. Gavriljuk for his significant contribution in this study. To the whole group of Prof. Gavriljuk I would like to express my appreciation for a fruitful cooperation.

Neutron diffraction measurements were of great importance for understanding the early stages of the aging of martensite. I am much indebted to Professor P. Hiismäki, Dr. O. Antson and the whole SFINKS group for the possibility to perform high-resolution neutron diffraction measurements using the "miniSFINKS" facility in Leningrad Nuclear Physics Institute.

Mössbauer experiments were performed in the Laboratory of Biomedical Engineering. I express my appreciation to Professor T. Katila, my former supervisor, and to his Mössbauer group, Mr. I. Tittonen, Mr. J. Lindén and Mr. M. Lippmaa, for discussions and help in fitting the Mössbauer spectra. I am also grateful to Dr. L. Liszkay and Professor P. Hautojärvi for performing positron-lifetime measurements and for advice in the interpretation of the results.

This study was mainly financed by the Academy of Finland and the author was a researcher in the Academy of Finland during this research. The financial support of the following foundations and institutions is also gratefully acknowledged: Japan Society for the Promotion of Science, Academy of Sciences of Ukraine, the Walter Ahlström Foundation, the Jenny and Antti Wihuri Foundation, The Emil Aaltonen Foundation, the Foundation of Technology, the Rautaruukki Foundation and the Oskar Öflund Foundation. Especial thanks are due to the last three for supporting this research during several years. Outokumpu Company is thanked for melting most of the alloys and for financial support for the Finnish - Ukrainian cooperation.

Finally, warm thanks are owed to my wife Mervi and sons Markus, Miika and Petri for their encouragement and patience during the work.

Otaniemi, March 10, 1992
Kari Ullakko

CONTENTS AND LIST OF PUBLICATIONS page

This thesis consists of an introduction and of eight publications:

I K. Ullakko and V.G. Gavriljuk, Effects of coherent interfaces in the freshly formed iron-nickel-carbon martensites, *Overview No. 99 in Acta Metallurgica et Materialia, 1992,* in press

II O. Antson, V.G. Gavriljuk, V.A. Kudryashev, V.M. Nadutov, H. Pöyry, J. Pietikäinen, A. Tiitta, V.A. Trunov, K. Ullakko, V.A. Ul'yanov, P. Hiismäki and Yu.P.Chernenkov, Neutron diffraction study of the martensitic transformation in Fe-Ni-C alloys, *Physics of Metals and Metallography, Vol. 70, No. 4, pp. 108-115, 1990*

III V.G. Gavriljuk, V.M. Nadutov, S.P. Oshkaderov, J. Pietikäinen and K. Ullakko, Phase and magnetic transformations in the Fe-Ni-C alloy at low temperatures, *Physics of Metals and Metallography, Vol. 70, No. 1, pp. 120-125, 1990*

IV V. Gavriljuk, V. Duz' and K. Ullakko, Internal friction of tempered ferrous martensites, *Scripta Metallurgica et Materialia, Vol. 26, pp. 667-672, 1992*

V V.G. Gavriljuk, V.M. Nadutov and K. Ullakko, Low temperature aging of Fe-N martensite, *Scripta Metallurgica et Materialia, Vol. 25, pp. 905-910, 1991*

VI V.V. Runov, A.I. Okorokov, A.D. Tretjakov, L.V. Grigorjev, V.A. Ul'yanov, K. Ullakko and V. G. Gavriljuk, Observation of a relaxation phenomenon during aging of Fe-Ni-C martensite by means of small angle neutron scattering, *Scripta Metallurgica et Materialia, Vol. 236, pp. 661-665, 1992*

VII M.Kajatkari, K. Ullakko and J. Pietikäinen, On the aging of Fe-Ni-C and Fe-Mn-C martensites, *Journal de Physique, Colloque C4, Supplément au n° 18, Tome 43, decembre 1982, pp. 461-466*

VIII K. Ullakko, M. Nieminen and J. Pietikäinen, Effects of low temperature deformation on the lattice structure and carbon distribution in Fe-Ni-C martensites, *Materials Science Forum, Vols. 56-58 (1990), pp. 191-196*

## SUMMARY OF THE PUBLICATIONS

The publications deal with the aging of iron-based martensites at low temperatures. Aging is divided into three stages in the present work. The first stage occurring below 200 K is the main topic of papers I - III. The interface between the freshly formed martensite and retained austenite was observed to be coherent. The coherency was studied in paper I by X-ray and neutron diffraction, internal friction, magnetic susceptibility and electrical resistivity measurements. The new internal friction peak centered at about 145 K was attributed to the movement of coherent interfaces and the subsequent break of coherency. It was shown that the twinned substructure with low martensite start temperature and atomic ordering in austenite are necessary and sufficient conditions for the coherency. The atomic ordering in Fe-Ni-C austenite increases the tetragonality of the virgin martensite due to the coherency at the interface between martensite and retained austenite including the non-transformed small regions of the ordered austenite inside the martensite plates.

Paper II deals with neutron diffraction results of low temperature aging. Unlike X-rays, neutrons penetrate a thick sample and, therefore, neutron diffraction provides real information about stresses arising in austenite and martensite during the martensitic transformation and during the subsequent aging. Some previous models based on X-ray results were shown to be incorrect. The martensitic transformation leads to an increase of strains, owing to coherency of the austenite and martensite lattices and plastic deformation of the austenite. The contribution of the lattice coherency to strains in austenite disappears during heating of the virgin martensite. The aging effects were observed to start at surprisingly low temperature, even between 4 K and 77 K. The neutron diffraction results support the idea that abnormally high tetragonality of iron-nickel martensite is largely caused by the strains due to the lattice coherency between martensite and retained austenite, including nickel-rich austenitic regions inside the martensite plates.

Formation of nickel-rich regions is accompanied by the magnetic ordering which was studied mainly by Mössbauer spectroscopy with the alloy Fe-25Ni-0.7C in paper III. The prevention of the formation of reheat martensite due to a special low temperature stabilization effect of austenite provided an opportunity to study precisely the intensitities of the paramagnetic and magnetically ordered phases. Evidence for magnetic ordering in retained austenite was given by the reversible width and intensity of the austenite Mössbauer peak when the temperature was cycled between room temperature and 77 K. This result is in accordance with the magnetic susceptibility measurements and it indirectly reveals the nonuniform distribution of nickel atoms in the initial austenite, *i.e*, the inhomogeneous short-range ordering, in agreement with the model discussed above.

Ordering of nickel atoms in austenite was evidenced also by internal friction measurements above room temperature, as shown in paper IV. A relaxation peak centered at 160 °C was previously accounted for by the mobility of twin boundaries mainly in Fe-Ni-C martensite. Paper IV shows that the origin of the 160 °C peak cannot lie in the twinned substructure, because this peak does not exist, *e.g.*, in the patterns of the completely twinned Fe-Mn-C martensite. Secondly, the 160 °C-peak appears in an Fe-Ni-C alloy whose structure is not twinned but mainly dislocated. As discussed above, the Fe-Ni-C martensite is characterized by the existence of microvolumes enriched with or depleted of nickel. The carbon atoms prefer to localize in the regions depleted of nickel. The distribution of nickel and carbon is inherited by martensite. We assume that the internal friction peak at 160 °C is caused by the migration of carbon atoms between the different microvolumes. This is supported by the fact that the activation enthalpy of this peak is close to that of carbon diffusion in ferrite.

Low temperature aging of a binary iron-nitrogen martensite is the topic of paper V. Tetragonality (being abnormally high for the virgin martensite) was observed to decrease between 100 and 200 K due to the break of coherency at the austenite-martensite interface. Also, magnetic ordering in the retained austenite below room temperature was observed. Above 200 K nitrogen atoms start to redistribute. An important difference from carbon-based martensites is that nitrogen atoms order without formation of clusters.

Aging of Fe-Ni-C martensites in the room temperature region was studied in papers VI and VII. Both studies revealed formation of carbon clusters. Paper VI deals with dynamical effects of clustering by means of small angle neutron scattering. A relaxation caused by the change in the magnetic structure was observed. It is assumed that redistribution of carbon atoms, clustering, changes the environments of iron and nickel atoms and leads to changes of inhomogeneous magnetic structure of the solid solution.

In paper VII a special Mössbauer fitting model was developed to calculate quantitative carbon contents and "phase" fractions of clusters. It was observed that a short time aging at 35 °C produced a cluster phase whose carbon content is 22 at% which is close to that of the structure $Fe_4C$. Aging for a long time at 38 °C led to the carbon content 25 at% and aging at 100 °C to about

30 at% which corresponds to ε-carbide. Also, the values of the carbon content of the matrix and the phase fractions were very reasonable. Using a simple relationship between carbon content and the unit cell volume of martensite, the macroscopic volume changes of the sample were calculated and tested by dilatometric measurements.

Deformation at low temperature (77 K - 210 K) leads to a drastic decrease of the tetragonality of martensite. In paper VIII it was shown that even cubic lattice structure can be obtained. Mössbauer measurements revealed that carbon atoms are redistributed during the low temperature deformation. It is natural to expect that normal aging of martensite is prevented or, at least drastically changed, which was evidenced by Mössbauer, X-ray diffraction and electrical resistivity measurements in paper VIII.

All these publications are a result of group efforts. Most measurements and equipment used in the present study were made by the present author. In the analysis and interpretation of the results the author had an essential contribution.

## 1 INTRODUCTION

Freshly formed iron-based martensite is characterized by some unusual features at subambient temperatures: low strength and good ductility /1-3/, abnormally high /4,5/ or abnormally low /6,7/ tetragonality and dislocation or twinned substructure depending on the martensitic transformation start temperature $M_s$ /8-10/. When martensite is heated to room temperature, its tetragonality changes (decreases in Fe-Ni-C martensites and increases in Fe-Mn-C and binary Fe-C martensites), it becomes harder and brittle, and even microcracking occurs during low temperature aging /11/.

There is a strong controversy as to the nature of abnormal tetragonality of virgin martensite and the possible mechanisms for its decrease during low temperature aging. Hypotheses have been discussed concerning the distribution of carbon atoms in different sublattices of octahedral interstices in the bcc lattice of α-iron /12,13/ or between the octahedral and tetrahedral sites /14/ and about the effect of coherent interface between martensite and the ordered regions in austenite /15,16/ or merely between martensite and retained austenite /17/. It is important for the explanation of abnormal tetragonality that as-quenched binary Fe-N martensites have a high *c/a* ratio /V/ in contrast to Fe-C martensites.

Mössbauer studies gave the first evidence for the redistribution of carbon atoms ascribed to the formation of carbon clusters during aging below room temperature /18-21/. These Mössbauer data were later supported by transmission electron microscopy observations and atom probe field ion microscopy /22,23/. The concept of modulated structure formation during low temperature aging was proposed by Nagakura /22,24/ and recently summarized by Taylor *et al.* /25/.

According to /25/ a fine-scale modulated structure develops with some "secondary" ordering within the high-carbon regions. The carbon content in these regions was found to be about 11 at %, which was the main reason for supposing that the structure of the carbon enriched regions is isomorphous with the structure of the $\alpha''$ - $Fe_{16}N_2$ phase in Fe-N alloys. The convincing data about two stages of aging of the freshly formed martensite were obtained by Génin with co-workers /26-28/ who used Mössbauer spectroscopy and transmission electron microscopy to study clustering (formation of isolated multiplets according to the terminology proposed in /26-28/) and ordering (extended multiplets). The transmission electron microscopy studies did not reveal any effect of the martensite substructure on the aging of the freshly formed Fe-Ni-C martensite. The authors /25/ did not get any evidence for carbon atom segregation at dislocations and they did not relate the change of mechanical properties to the interactions between the carbon atoms and the dislocations. However, the internal friction data gave strong evidence for pinning of dislocations by the mobile carbon atoms in Fe-Ni-C martensite during aging at temperatures below room temperature /29/. The phenomena occurring during aging of martensite is recently summarized in /30/.

The aim of the present work is to study the aging of freshly formed martensite at low temperatures using several experimental methods focusing attention on the change of the abnormal *c/a* ratio, interaction of carbon atoms with dislocations and redistribution of interstitial carbon and nitrogen atoms. Finally, the effects of low temperature deformation (cryoforming) on aging behavior will be discussed.

## 2 EXPERIMENTAL

### Equipment

Most of the equipment used in the present study, *e.g.*, equipment for internal friction, electrical resistivity, magnetic susceptibility and X-ray diffraction measurements and special sample holders and cryostats for neutron diffraction and Mössbauer facilities, was designed and constructed by the author in the framework of this thesis. In the following sections the main features of these instruments will be presented.

#### *Electrical resistivity and magnetic susceptibility device*

The susceptibility device, shown in Fig. 1, consists of two identical coil sets, a test frame and a compensator /31,32/. In the test frame the sample is magnetized by the magnetic field (0.14 mT at a frequency of 150 Hz) of the primary coil, inducing a voltage in the signal coil which is measured. The voltage of the air flux is compensated for by the antiphase voltage of the compensator.

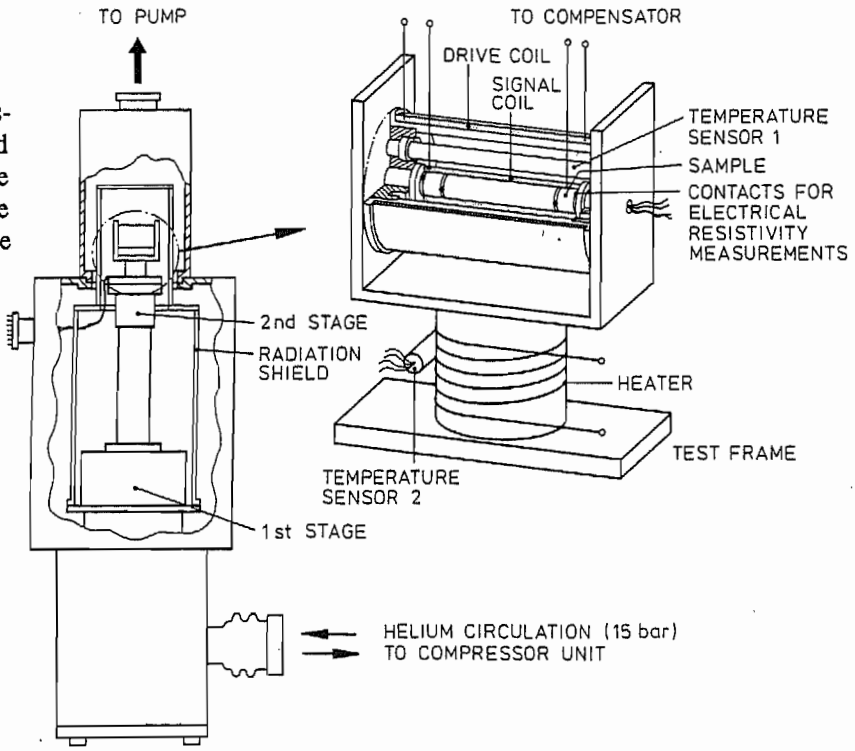


**FIG. 1.** Test frame and cooling system for AC magnetic susceptibility and resistivity measurements. Test frame and compensator are placed side by side on the second stage of the closed cycle cryo-refrigerator.

The voltage induced by the specimen can be expressed as /33/

$$U = U_0 + \Delta U, \qquad (1)$$

where $U_0$ is the voltage caused by the air flux and $\Delta U = A + B$. The vector diagram of the induced voltage is shown in Fig. 2.

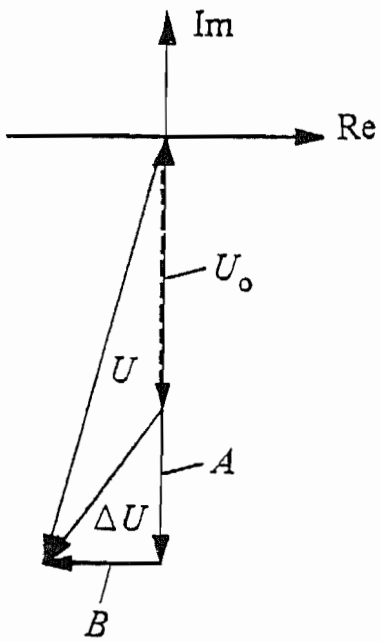


**FIG. 2.** Vector diagram of the induced voltage U. Signals in the test frame and in the compensator are denoted by the solid and dashed lines, respectively.

Component A is proportional to the susceptibility of the specimen and component B is ascribed to the energy dissipated by the eddy currents and, therefore, is primarily caused by the conductivity of the sample. Eddy current measurements serve as a useful method to measure electrical resistivity of, *e.g.*, powder samples. In the multiphase material, eddy currents are mainly induced in the magnetically ordered phases, which provides a unique possibility to measure, for instance, the electrical resistivity of the martensite phase selectively. In conventional resistivity measurements, both martensite and austenite contribute to resistivity.

The magnetizing field is produced using an externally controlled current source. Components B and A of the voltage vector (proportional to the $\chi''$ and $\chi'$ parts of susceptibility) are detected with a two-phase lock-in analyzer. Resolution of the equipment is about 10 nV. The calibration of the magnetic susceptibility scale was performed by $YBa_2Cu_3O_{7-\delta}$ superconductor, the size of which was the same as that of the sample. At the superconducting transition (92 K) the change of susceptibility is close to -1. The calibration was done during the measurement, because the superconductor was placed in the compensator. Four point electrical resistivity can be measured simultaneously using an automatic AC resistance bridge (AVS-100 by RV-Elektroniikka Oy). The frequency of the excitation voltage was 25 Hz. The resolution of the resistance measurements is about 10 μΩ. The block diagram of the measuring system is shown in Fig. 3.

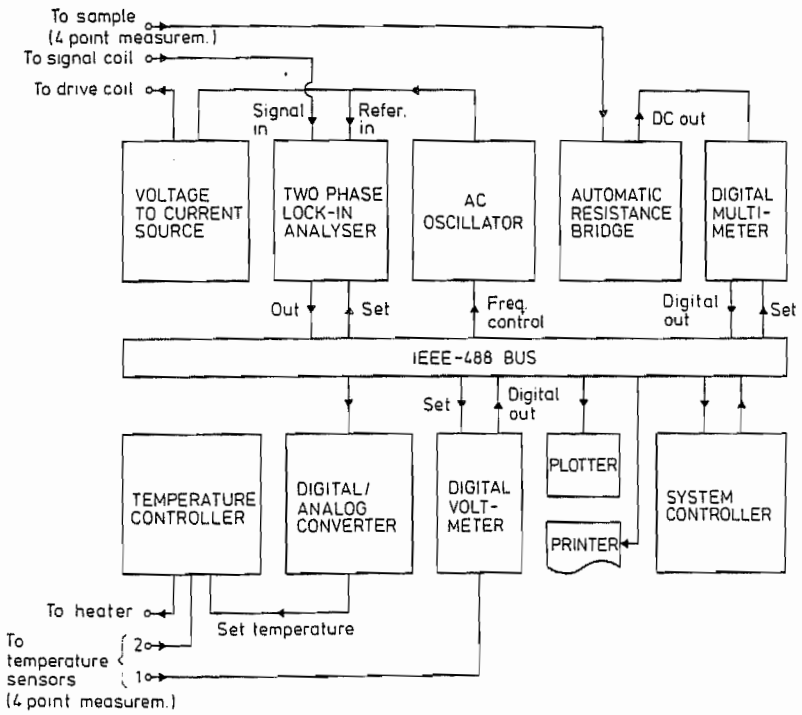


**FIG. 3.** Block diagram of the susceptibility and resistivity measuring system.

The test frame and the compensator are thermally connected to the cold head of a two-stage cryo-cooler (Fig. 1). Iron-rhodium resistors were used as temperature sensors because of their good resolution and quite linear behavior in the whole temperature range. One sensor was used for temperature control and it was placed in contact with the heater and the other, employed for detection, was thermally connected to the sample. Temperature was controlled with an analogical PID controller.

In the cooling system shown in Fig. 1 the set times of temperatures are rather long. For the step-wise heating experiments where temperature must be cycled even hundreds of degrees between the measuring points, a special gas flow cryostat /34,35/ was constructed. Temperature was controlled by warming nitrogen vapour which was led through the sample holder. In this construction, thermal inertia is very small and the temperature changes are rapid (even 50 K/s).

*Internal friction equipment*

Many processes occurring in material cause damping of mechanical vibrations /36/. Internal friction measurements (called also mechanical spectroscopy) are an extremely sensitive method of studying the interaction of dislocations and interstitial atoms. This is because the damping is (inversely) proportional to the fourth power of the average length of the vibrating dislocations. A dislocation can be locked locally (*i.e.*, pinned) by an interstitial atom and the dislocation then vibrates in two parts. Interstitials can also jump between the octahedral sites on different axes in the stress fields of the moving dislocations leading to damping. This damping is frequency dependent and it has a relaxation nature. Vibration of magnetic domain walls also contributes to internal friction. This component is normally eliminated by applying a saturating magnetic field to the sample.

Inverted torsion pendulum equipment (Fig. 4) was constructed for low temperature internal friction measurements /34/. The pendulum is shown in Fig. 5 and the sample holder in Fig. 6. At each temperature the pendulum is excited electromagnetically to the strain amplitude of about $10^{-6}$ and then allowed to oscillate freely. The internal friction ($Q^{-1}$) and frequency (f) values were obtained by computer fitting of the damping sinusoidal curve. Compared to other methods tested this method produces the best resolution and the most reliable absolute values for $Q^{-1}$ and f. Internal friction can also be obtained from the line width of the Fourier transformation of the damping signal. This method is effective if the signal is very noisy. In the present case it turned out to be significantly worse in resolution and accuracy especially for samples with small damping. In the constant amplitude method the damping is compensated for by continuous excitation. An analogically controlled system originally constructed by Kleemola /37/ was further developed and tested, but sensitivity turned out not to be so high as in the freely damping system.

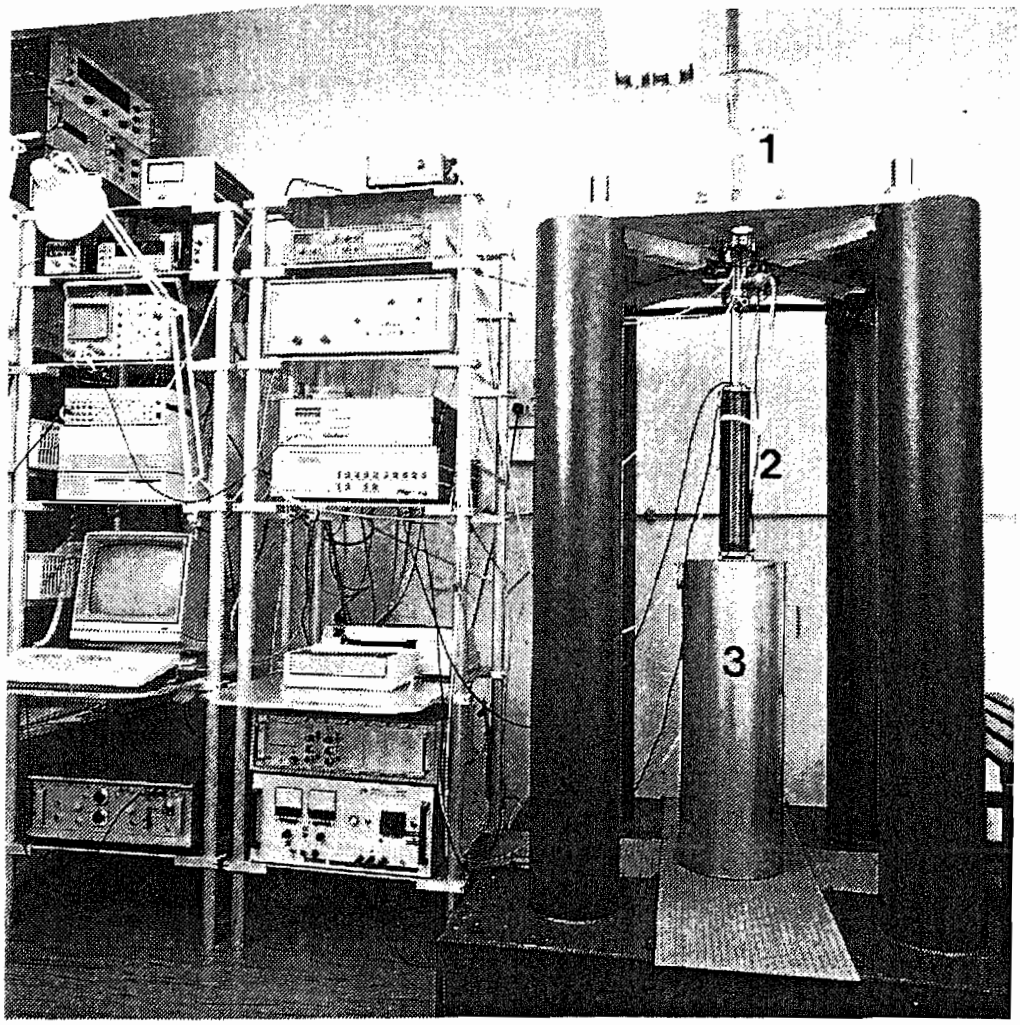


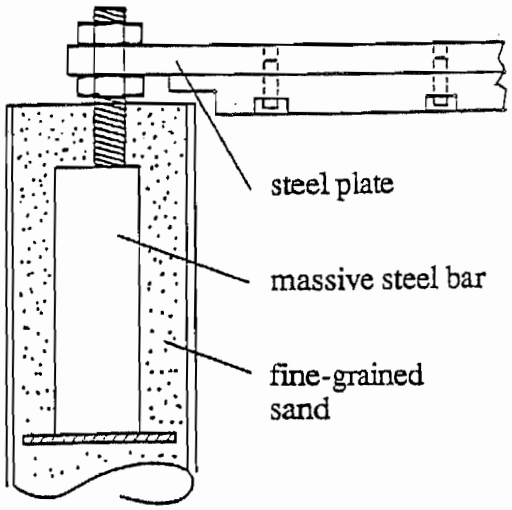


**FIG. 4.** Internal friction equipment (above): 1. pendulum (detail in Fig. 5), 2. sample chamber (see Fig. 6), 3. liquid nitrogen dewar. For insulation of vibrations the pendulum system is connected to steel bars which are floating in fine-grained sand (right).

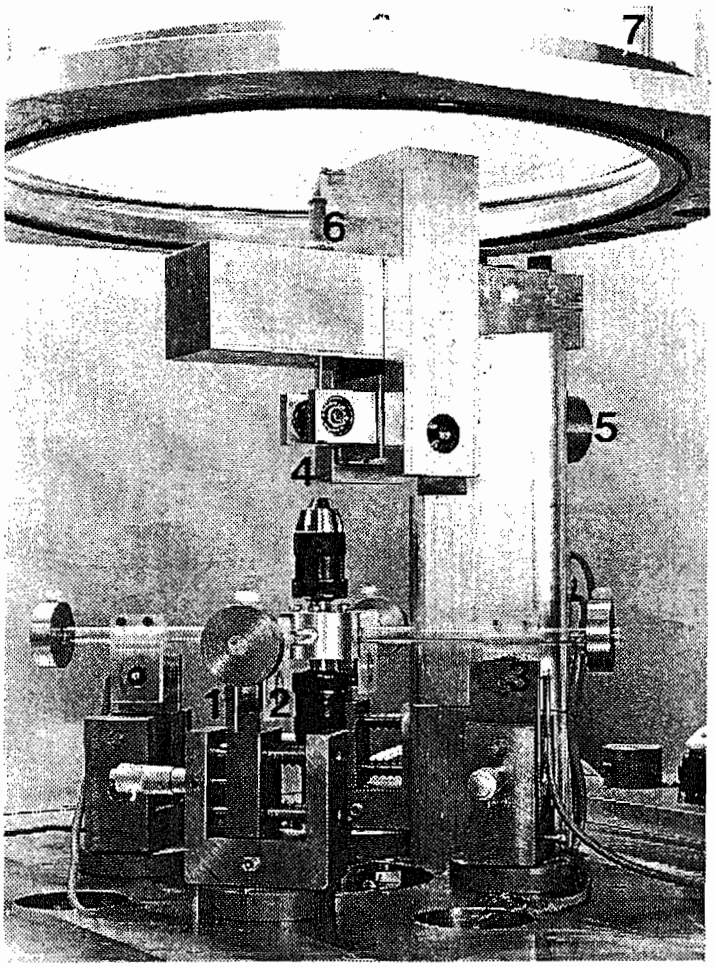


**FIG. 5.** Torsion pendulum: 1. Contactless inductive displacement sensors (Note: sensors are on the same side of the inertia bar thus compensating for the lateral vibrations), 2. ceramic ferrite rings (due to their high electrical resistivity, damping caused by eddy currents is insignificant), 3. excitation coils, 4. Be-Cu suspension wire, 5. counter weight, 6. inductive displacement sensor for measuring the length of the sample (dilatometer), 7. vacuum shield.

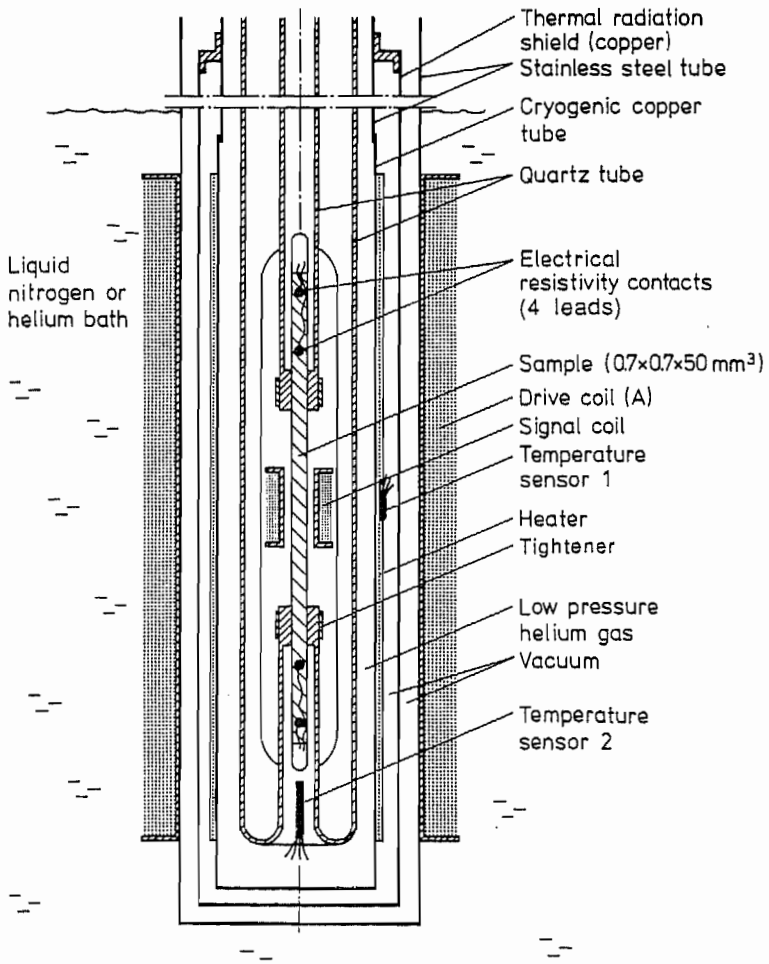


**FIG. 6.** Structure of the sample chamber. The sample holder was made from quartz because of its stiffness, small thermal conduction, small thermal expansion coefficient and high electrical resistivity.

In the present system the torsional movement is detected with a pair of identical inductive sensors which form a half-bridge. The amplified signal is analogically filtered (even 180 dB) and digitized with a computer-controlled DVM. Together with effective insulation of mechanical vibrations this allows a detection of extremely small movements of the bars (less than $10^{-5}$ mm at the end of the bars). Solar eclipse in Helsinki, summer 1990, provided a unique opportunity to test the frequency resolution at low frequencies. Saxl and Allen in Harvard University had observed some anomalies in frequency during the solar eclipse in 1970 /38/ by means of a specially constructed equipment. We repeated their experiment using the oscillation period of about 30 seconds and achieved a resolution of 0.5 ms /39/ which is ten times better than in /38/ (and no anomalies in frequency were observed).

The equipment was combined with a dilatometer (see Fig. 5). This is of great importance, *e.g.*, when accurate values for shear modulus are required. In an isotropic medium the relative change of shear modulus G is expressed as /36/

$$\Delta G/G = 2\ \Delta F/F\ -3\ \Delta L/L, \qquad (2)$$

where F is the frequency and L is the length of the sample. This expression is valid for small changes.

The sample holder is surrounded by coil A (Fig. 6) which can be used to apply a saturation magnetic field in order to avoid the effects of magnetic domain walls on damping. With this internal friction equipment it is also possible to perform simultaneously resistivity and susceptibility measurements. In this case the sample is provided with resistance contacts outside the mechanical connection points of the suspension bar and with a signal coil around the sample (see Fig. 6). Coil A is then used as a drive coil of the susceptibility measuring system. The combination of susceptibility and resistivity arrangements with the internal friction equipment makes possible the studies of the interaction of electromagnetic and mechanical effects (*e.g.*, if magnetic susceptibility is measured synchronously with the frequency of the mechanical twisting, it is possible to observe extremely small reversible variation of the amount of martensite in the periodically alternating stress field, which can be utililized in the studies of the mobility of interfaces).

High sensitivity magnetostriction measurements can be performed by applying an oscillating magnetic field to the sample using coil A and by measuring the output of the amplified dilatometer signal with a lock-in amplifier locked to the frequency of the magnetic field. Using this method it is possible to detect the changes of the lengths much below the resolution of the dilatometer. Damping measurements made with a freely hanging sample in the transverse magnetic field also provide a possibility to study the magnetomechanical effects. This method can be applied, for instance, to the studies of small magnetically ordered clusters (*e.g.*, nickel clusters in austenite). In this case damping is accounted for by the change of the orientation of the magnetization in the clusters.

*X-ray diffractometer*

The X-ray diffraction experiments were performed by means of a Siemens' diffractometer, equipped with a 120° curved position sensitive detector INEL CPS 120. In the present studies, Co $K_{\alpha 1}$ radiation was used. The $K_{\alpha 2}$ and $K_{\beta}$ components were eliminated with a primary Johansson type quartz monochromator. The measurement system is presented in Fig. 7.

The sample holder, equipped with a closed cycle cryo-refrigerator and a special device for deformations, was constructed (Fig. 8). X-ray measurements and deformations could be carried out in the temperature range of 8 - 330 K. Specimens were covered with a thin layer of a high purity silicon powder for internal calibration.

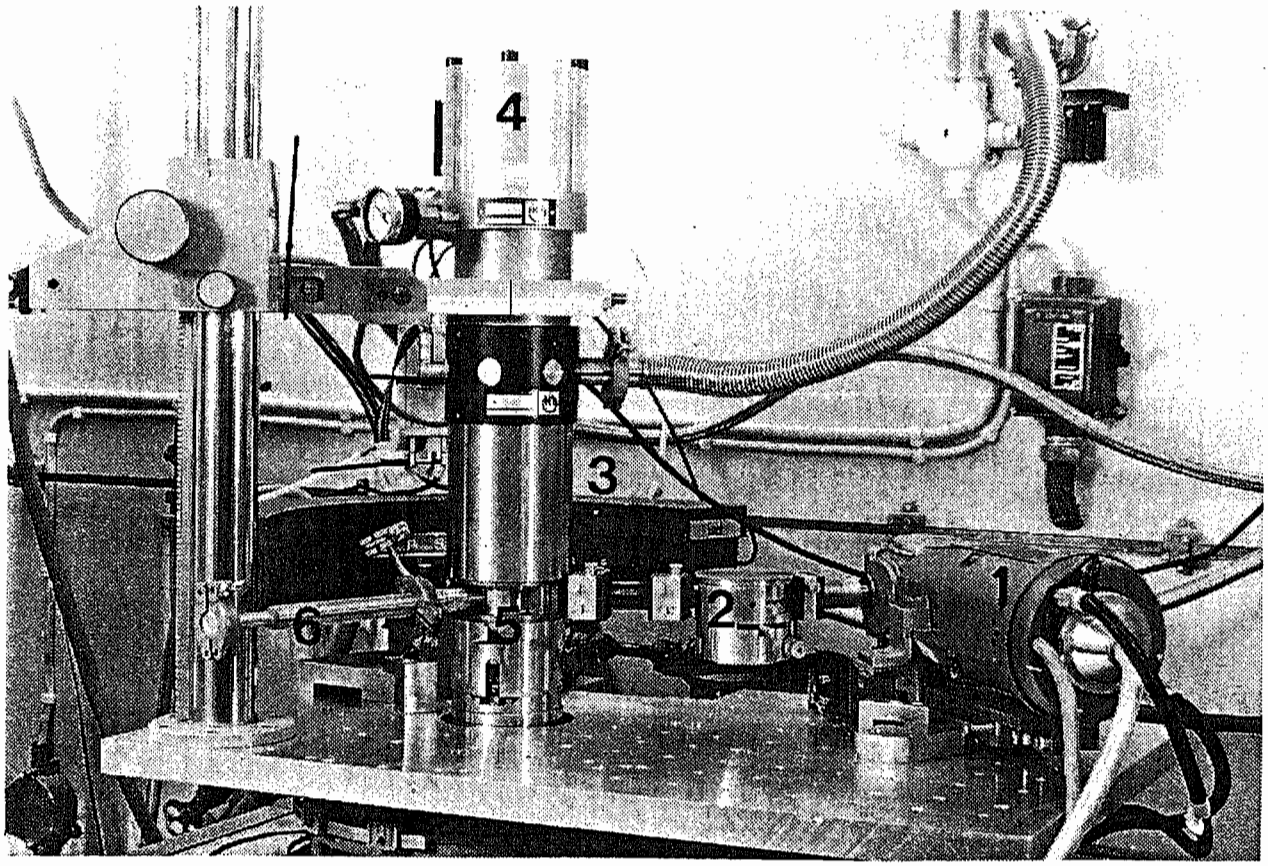


FIG. 7. X-ray diffraction equipment: 1. X-ray tube, 2. monochromator, 3. position sensitive detector (120 degrees), 4. cryo-refrigerator, 5. sample holder (inside), 6. bar of deformation screw.

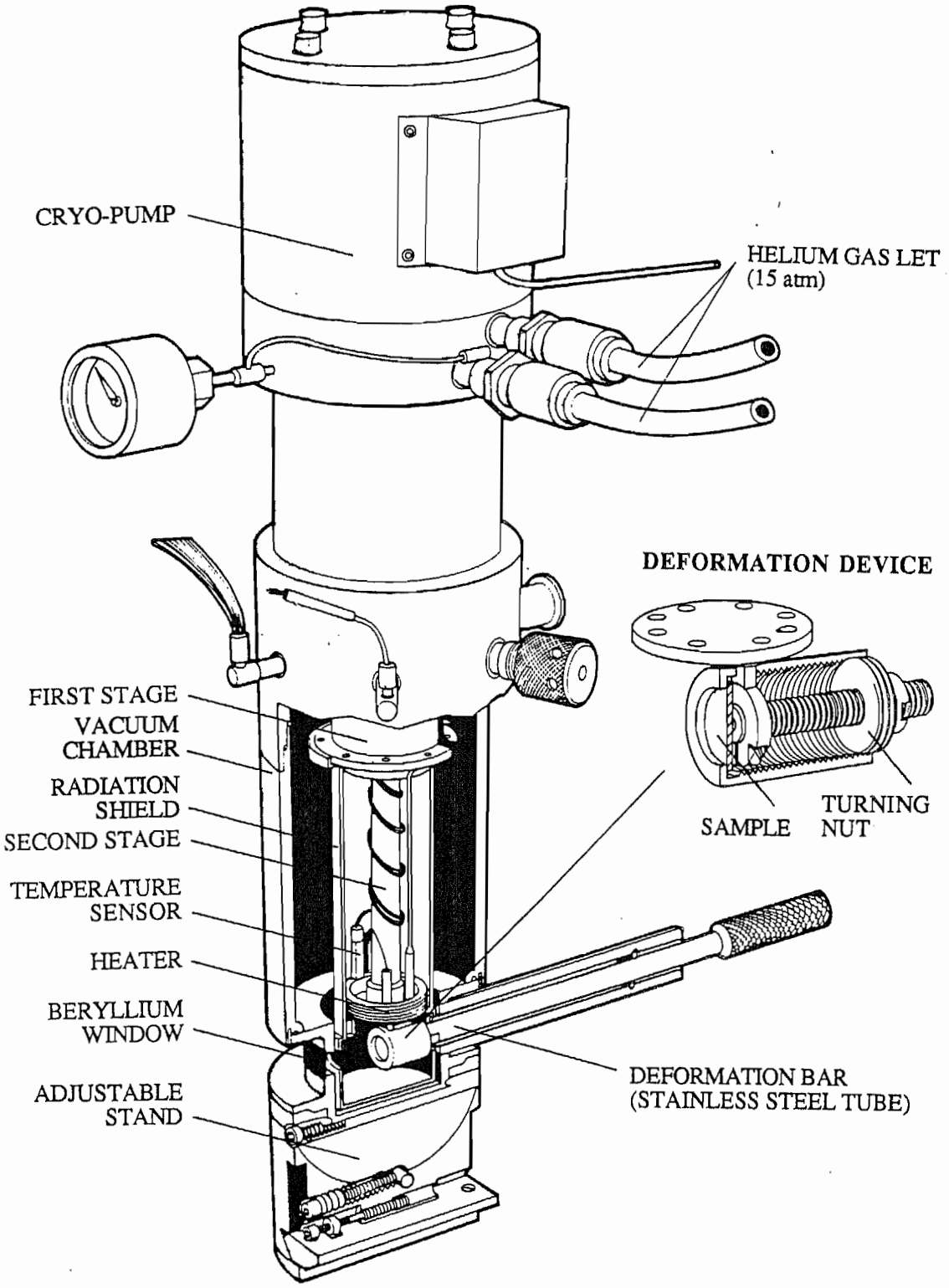


**FIG. 8.** X-ray sample holder: Sample can be deformed *in situ* at temperatures 8 - 330 K with a differential twin screw deformation device. The force is magnified by the small difference of the pitches in the inner and outer screws. One turn of the turning nut causes a bulge in the sample equal to the difference between the pitches (0.1 mm).

*Neutron diffraction facilities*

Neutron diffraction measurements were made with the time-of-flight diffractometer "Mini-SFINKS" which is installed at the VVRM 16 MW reactor in the Leningrad Nuclear Physics Institute, Russia. Due to the unique principle of this diffractometer, intensity and resolution are excellent. The construction is described in detail in /40,41/. The equipment was provided with a cryostat where samples could be quickly quenched in liquid helium /34/. Inside the cryostat there is a furnace into which the samples were lifted for aging. Aging could be performed in the temperature range of 4.2 - 500 K. In order to get more grains in reflection, samples ($\phi$8 x 100 mm$^3$) were rotated during the measurements. Because in some applications it is useful to measure the real volume changes of the specimen during the measurements, the sample holder was provided with a dilatometer (Fig. 9). In the dilatometer the length of the sample is measured by means of an inductive displacement sensor. The dilatometer was placed below the liquid helium level, which ensured the constant temperature during the measuremets. The construction of the cryostat and the sample holder systems are described in /34/.

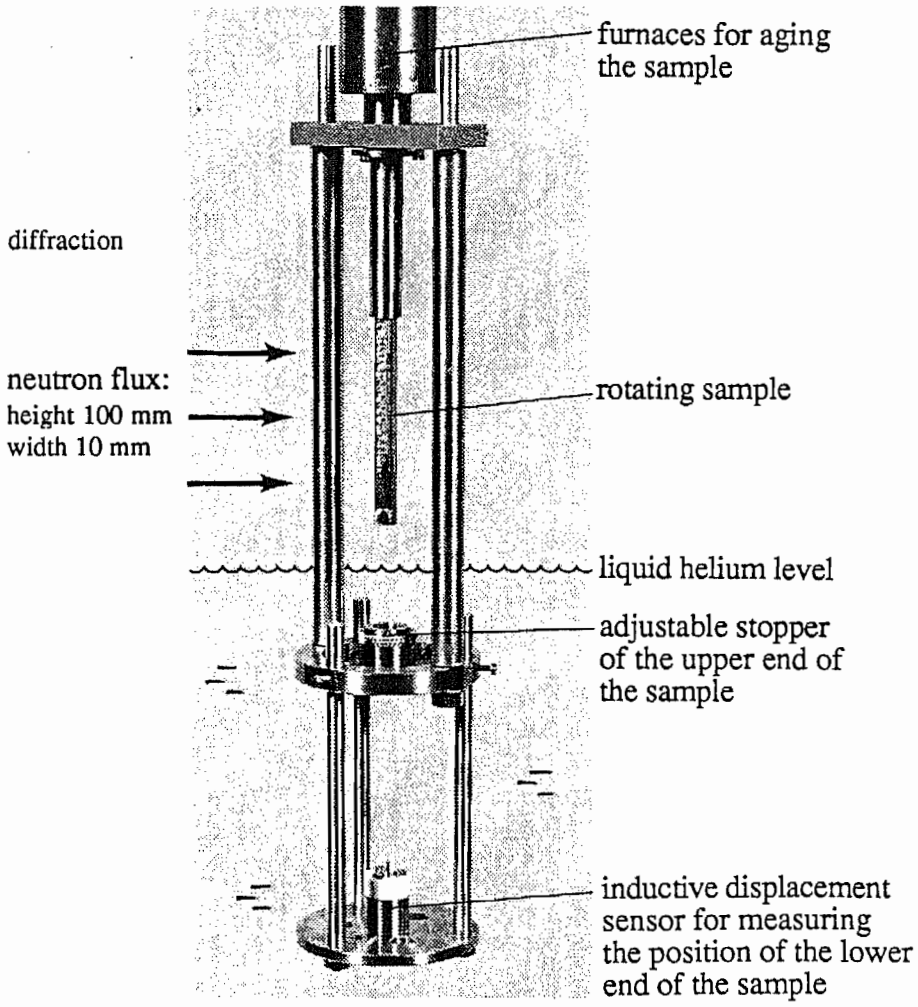


**Fig. 9.** Detail of the neutron diffraction sample holder.

*Mössbauer spectrometer*

Mössbauer spectra were measured using the Halder and NP-255 spectrometers. The $^{57}Co$ in the chromium matrix was used as a source of $\gamma$ quanta. The measuring arrangements made for this purpose are shown in Fig. 10. The cryostats are superisolated and can be used with liquid helium (consumption 0.17 l/h) or with liquid nitrogen. The construction of the sample holder is presented in Fig. 11.

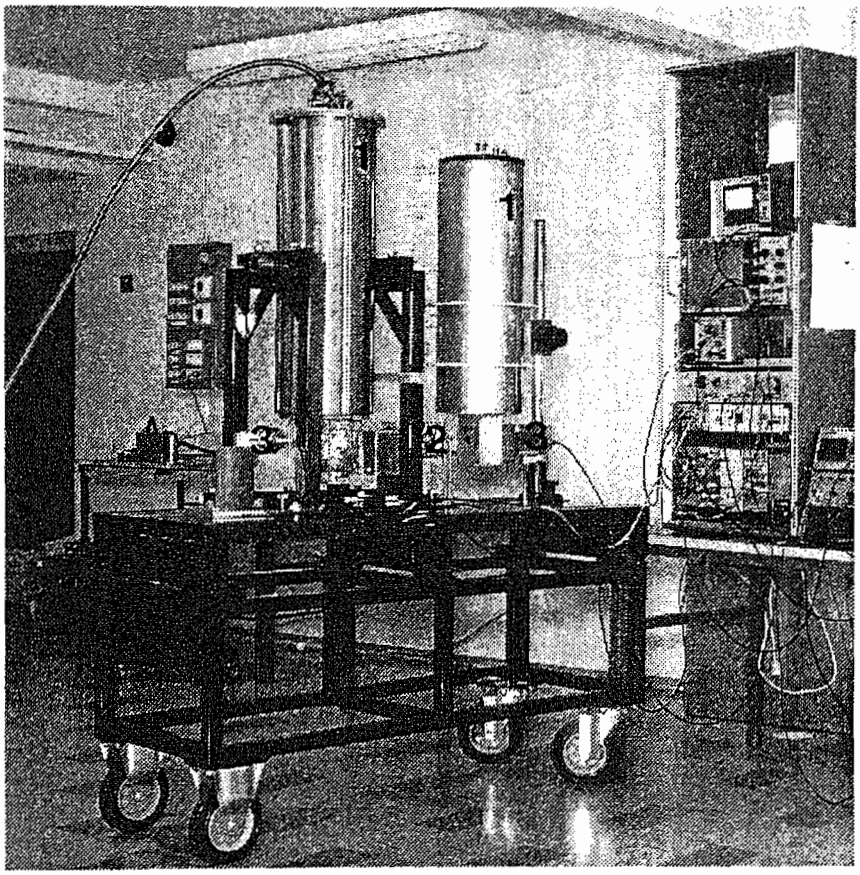


**FIG. 10.** Mössbauer cryostats (1), drive holder with two sources (2) and detectors (3).

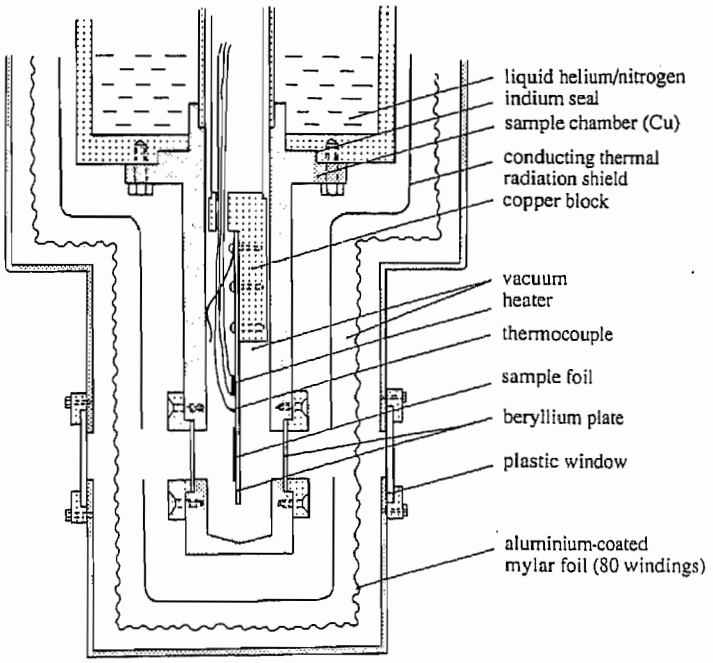


**FIG. 11.** Mössbauer sample holder. The sample can be removed by lifting the holder up. Thin beryllium plate connected to the sample foil enables temperature to be changed very rapidly.

## Experimental material

The Fe-Ni, Fe-Ni-C and Fe-Mn-C alloys were vacuum melted and chill cast. After hot forging, the samples for different experiments were machined. Binary Fe-C and Fe-N samples were produced by carburizing and nitrogenizing the foils of 20 μm thickness in hydrogen-methane and hydrogen-ammonia atmospheres, respectively. Compositions, heat treatments, martensitic transformation start temperatures and morphologies of the alloys are shown in Table 1. By plate martensite we mean here such martensite whose lattice-invariant shear is twinning and the substructure is stacks of twins. Completely twinned "thin plate" martensite of Fe-20Ni-1.2C alloy is shown in Fig. 12a. Typical of this structure are narrow straight plates and smooth planar interfaces. The plates can kink and branch and even cross each other. They can thicken by sidewise growth and by joining with neighboring plates of the same variant /42/. Dislocation density in retained austenite near the austenite-martensite interface is very low /43/. Lenticular martensite is transformed at higher temperatures and its lattice-invariant shear is slip. The substructure is mainly dislocation cells and tangles. In this martensite, also twins exist, especially in the region of midrib. The martensite-austenite interface is irregularly shaped and less mobile than that of the twinned martensite. Dislocation density in austenite near the interface is high. Typical example of lenticular morphology is shown in Fig. 12b.

**TABLE 1.** Treatments, $M_s$ temperatures and morphologies of the alloys studied.

| Fe-based alloy (contents in wt%) | Homogenization temp. (°C) | time (h) | $M_s$ temperature (K) | Morphology of martensite |
|---|---|---|---|---|
| 9Ni-1.4C | 1150 | 3 | 220 | lenticular |
| 18Ni-0.7C | 1150 | 3 | 240 | lenticular |
| 20Ni-0.7C | 1150 | 2 | 208 | lenticular |
| 20Ni-1.2C | 1150 | 3 | 103 | plate |
| 25Ni-0.7C | 1150 | 3 | 140 | plate |
| 28Ni-0.2C | 1150 | 3 | 208 | lenticular |
| 30Ni-0.37C | 1200 | 3 | 160 | plate |
| 30Ni | 1100 | 3 | - | lenticular |
| 33.5Ni | 1150 | 3 | 125 | plate |
| 3Mn-1.6C | 1100 | 1 | 118 | plate |
| 1.76C | 1150* | - | - | plate |
| 2.03C | 1150* | - | - | plate |
| 2.39N | 800** | - | 120 | plate |
| 2.75N | 800** | - | 120 | plate |

* carburized in methane-hydrogen mixture
** nitrogenized in ammonia-hydrogen atmosphere

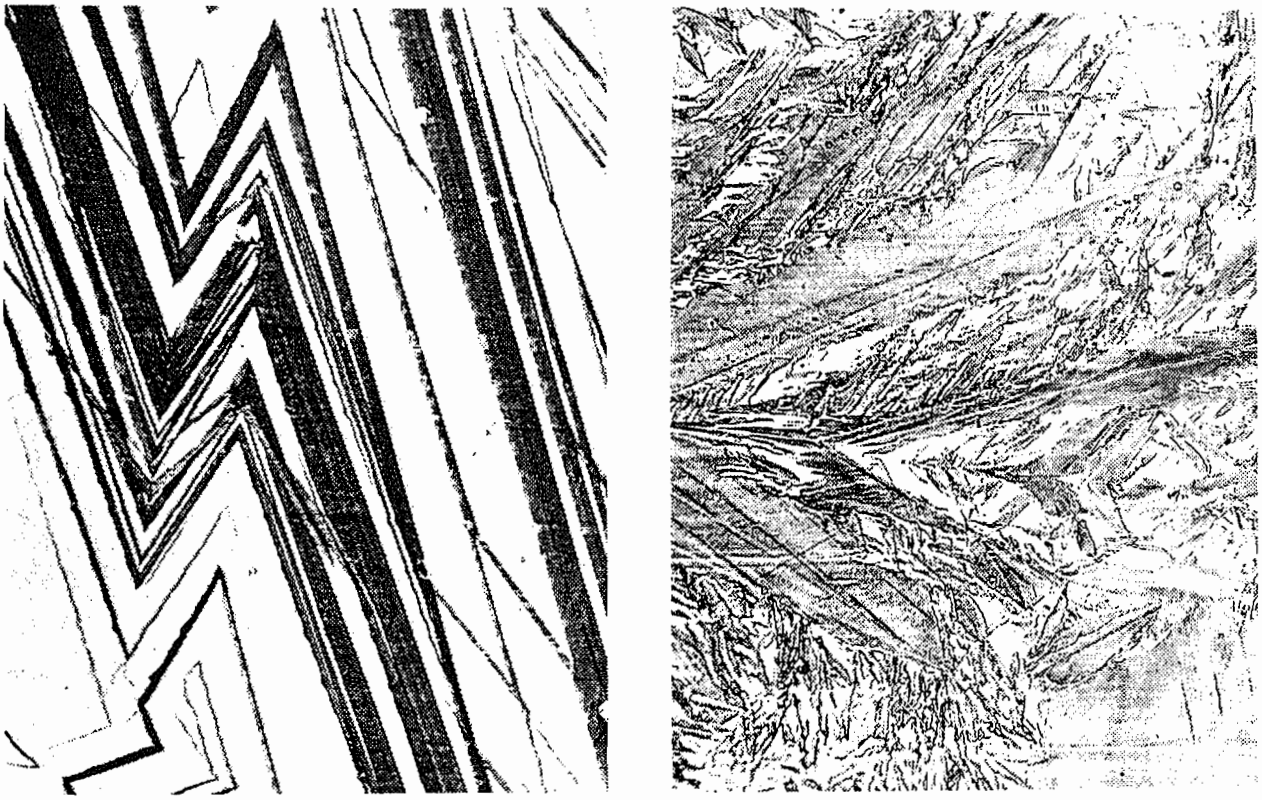

(a) (b)

**FIG. 12.** Optical micrographs of Fe-20Ni-1.2C plate martensite (a) and Fe-18Ni-0.7C lenticular martensite (b). Magnification 700x.

## 3 LOW TEMPERATURE AGING OF MARTENSITE

In the present study, the aging of martensite below room temperature is divided into three stages (denoted by I, II and III in the following): phenomena of coherent interfaces between the virgin martensite and retained austenite (about 100 - 170 K), interaction of carbon atoms with dislocations (about 180 - 240 K) and clustering (in the case of carbon atoms) or ordering (nitrogen atoms) of interstitials (above 200 K). In addition, in the twinned Fe-Ni-C martensites these three stages are preceded by some phenomena which are characterized, *e.g.*, by an abrupt decrease of electrical resistivity between 4 K and 100 K, reduction of the unit cell volume of martensite and the widths of retained austenite peaks, as evidenced by neutron diffraction measurements. These very low temperature phenomena will be discussed in more detail elsewhere. The nature of the *c/a* ratio and the three stages of aging will be the topics of the following sections. Aging was studied by means of different experimental methods. In the following, some results measured with X-ray and neutron diffraction, internal friction, positron annihilation, Mössbauer spectroscopy, electrical resistivity, magnetic susceptibility, shear modulus and dilatometric methods will be reported and discussed. The discussion of each stage of aging is preceded by a short presentation of experimental evidence.

## I EFFECTS OF INTERFACES OF VIRGIN MARTENSITE AND RETAINED AUSTENITE (1st stage of aging)

Abnormally high or abnormally low tetragonality is observed in the freshly formed martensite alloyed with Ni or Mn respectively in accordance with previous studies /4-7/. It is shown that the reason for high tetragonality lies in the coherency at the interface between the martensite and the retained austenite. The coherency is broken during aging in the temperature range of 100 - 200 K and it is accompanied by a decrease of tetragonality. The new internal friction peak observed at 145 K corresponds to the movement of the coherent interface and the break of coherency. Some evidence for correlation between short range atomic ordering in austenite and the high tetragonality of the virgin martensite is given and a contribution of nontransformed ordered austenitic regions inside martensite plates into tetragonality is discussed.

### *X-ray diffraction results*

X-ray diffraction measurements were undertaken to study the behavior of tetragonality during heating of the freshly formed martensites. Figure 13 displays the *c/a* ratios of Fe-Ni-C martensites and Fig. 14 shows the tetragonality behavior of Fe-2.39N, Fe-1.76C and Fe-3Mn-1.6C alloys.

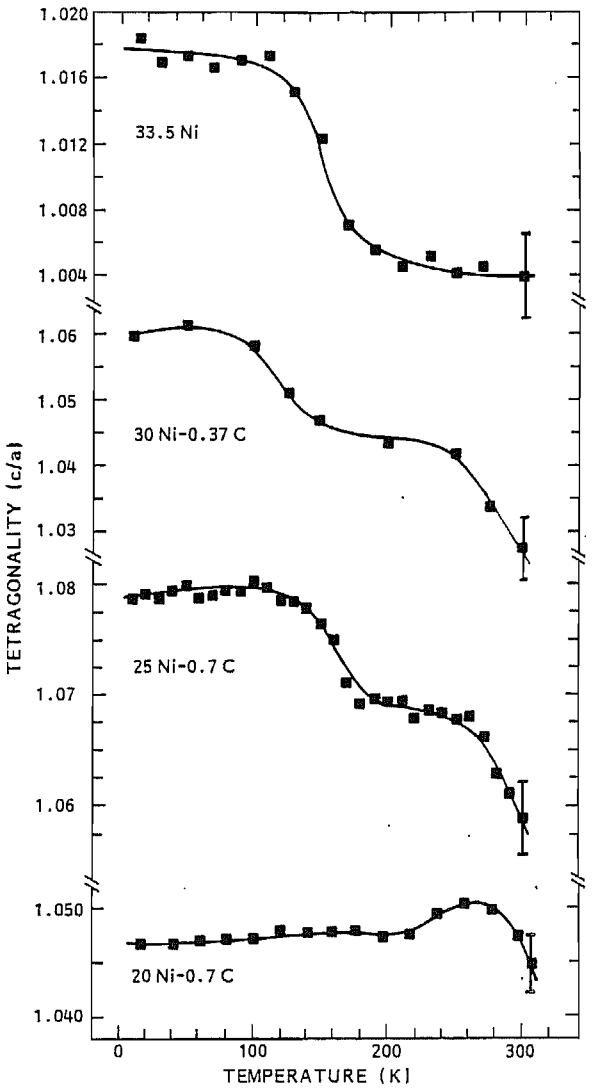


**FIG. 13.** Tetragonality of the freshly formed Fe-Ni-C martensites during heating.

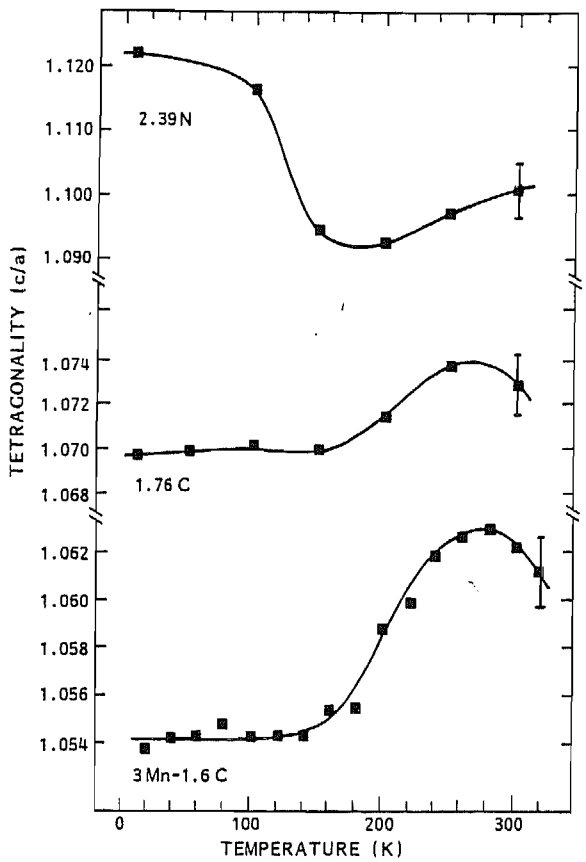


**FIG. 14.** The change of the *c/a* ratio during heating of the freshly formed iron-based martensites containing 2.39N, 1.76C and 3Mn-1.6C.

For the twinned Fe-Ni-C martensites and for the nitrogen alloyed martensites, tetragonality is abnormally high and it is reduced during aging at 100 - 200 K. Usually abnormally high tetragonality occurs in the martensites with a low $M_s$ temperature and a plate morphology with a completely twinned substructure containing few dislocations. Tetragonality of Fe-20Ni-0.7C, Fe-1.76C and Fe-3Mn-1.6C martensites does not decrease in this temperature range. During heating above 200 K the *c/a* ratio remains unchanged in Fe-33.5Ni martensite, decreases in the iron-nickel-carbon alloys, except Fe-20Ni-0.7C, and increases in Fe-2.39N, Fe-1.76C and Fe-3Mn-1.6C alloys. The increase of tetragonality of Fe-1.76C and Fe-3Mn-1.6C martensites begins even below 200 K.

In order to obtain additional information about the nature of abnormally high tetragonality, the effect of the low temperature deformation on the *c/a* ratio of Fe-33.5Ni martensite was studied (Fig. 15). The sample was deformed by bending *in situ* in the cryostat of the X-ray diffractometer (shown in Fig. 8). Deformation at 40 K led to a significant decrease in the distance between the doublet peaks (Fig. 15b), but during further deformation at 110 K the martensite lattice became completely cubic (Fig. 15c). Decrease of tetragonality is similar to that caused by heating in the temperature range of 110 - 170 K (Fig. 13).

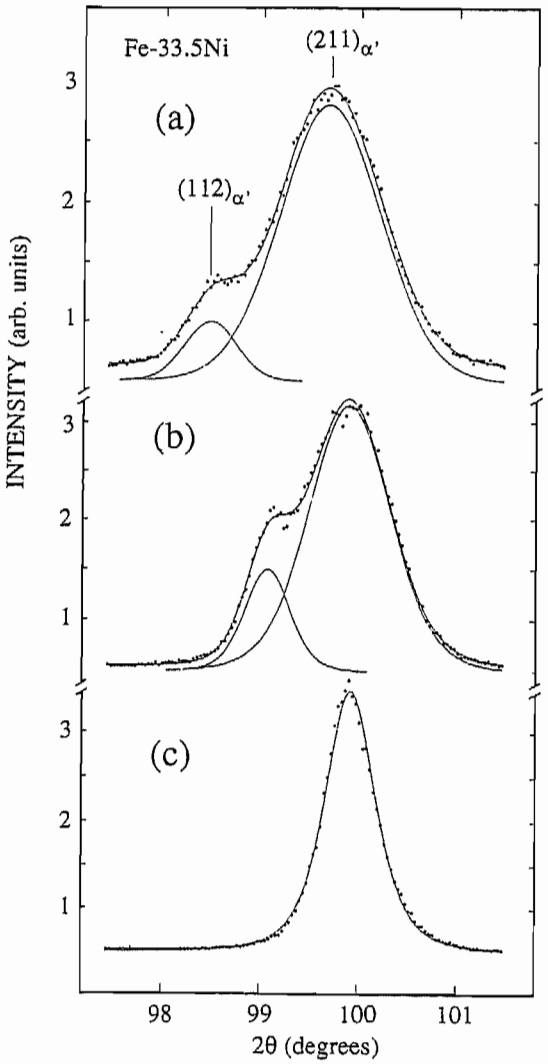


**FIG. 15.** The effect of deformation *in situ* on the doublet $(112)_{\alpha'}$ / $(211)_{\alpha'}$ in the freshly formed Fe-33.5Ni martensite: (a) undeformed, (b) deformed at 40 K, (c) further deformed at 110 K. The measurements were made at 40 K.

*Neutron diffraction results*

The inverted time-of-flight Fourier chopper diffractometer /41/ employed in the neutron diffraction measurements has an excellent resolution and intensity. Because of the large bulk samples used, the intensity ratios of different reflections are very reliable. A diffraction pattern of Fe-18Ni-0.7C alloy measured for 4 hours at 77 K is presented in Fig. 16. Several martensite and austenite peaks are resolved. We observed that some neutron diffraction results differ from the X-ray

diffraction results. Chen *et al.* showed that there is an extra peak between the tetragonal doublet reflections (002) and (200) of polycrystalline Fe-18Ni-0.9C martensite (which is very close to the present alloy) even in the freshly formed state and it remains during aging /44/. Fitting of the neutron diffraction pattern of the martensite aged at 190 K revealed no extra peak (see inset of Fig. 16). The explanation for the discrepancy can lie in the difference of the experimental methods: neutrons are diffracted from the lattice of nuclei, but X-rays are scattered from charge density (which normally forms the same lattice). The additional peak in the X-ray spectra could reveal some interatomic charge density which does not lead to an essential change of the positions of nuclei observed by neutron diffraction. Another difference from X-ray results is that the ratio of the integrated intensities $I_{112}$ / $I_{211,121}$ of the neutron diffraction peaks nearly equals the ideal value 1:2 as shown in the inset of Fig. 16. In the case of X-ray diffraction, this ratio is always significantly smaller, *e.g.*, about 0.34 for $I_{002}$ /$I_{200,020}$ /44/. The attenuation of the intensities is accounted for by the static displacements of the iron atoms caused by the neighboring carbon atoms in the *c*- axis octahedral sites according to the point defect model by Krivoglaz /45/. The displacements are larger in the *c*- direction than in the *a*- and *b*- directions, which leads to the smaller than the ideal value of the intensity ratio. The nearly ideal value of the intensity ratio in the case of neutron diffraction may reveal that the nuclear lattice is less disturbed by carbon atoms than the lattice formed by charge density or, at least, it is disturbed more uniformly in different lattice directions. The magnetic scattering contributing to neutron diffraction peak intensities is small and cannot serve as an explanation for the difference between the neutron and X-ray diffraction results.

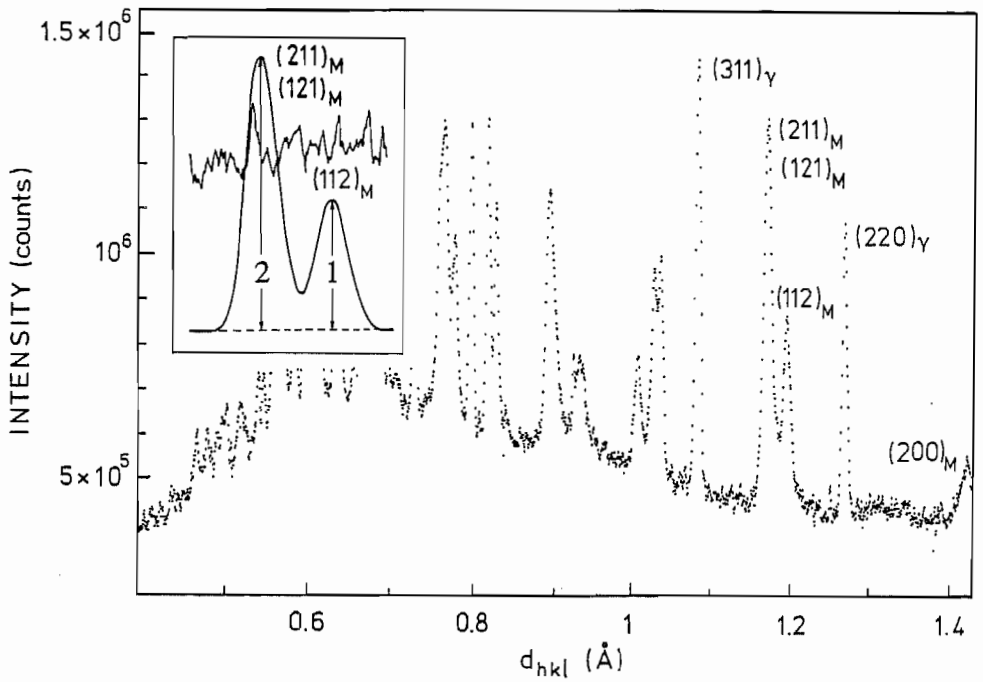


**FIG. 16.** Neutron diffraction pattern of the virgin Fe-18Ni-0.7C martensite run at 77 K. Inset: the fitted doublet $(112)_{\alpha'}$ / $(211)_{\alpha'}$ of the martensite aged for 3 hours at 190 K.

The positions of the martensite doublet peaks $(112)_{\alpha'}$, $(211)_{\alpha'}$ and the retained austenite peak $(311)_{\gamma}$ of the virgin Fe-20Ni-1.2C martensite after heating from liquid helium temperature to room temperature are shown in Figure 17.

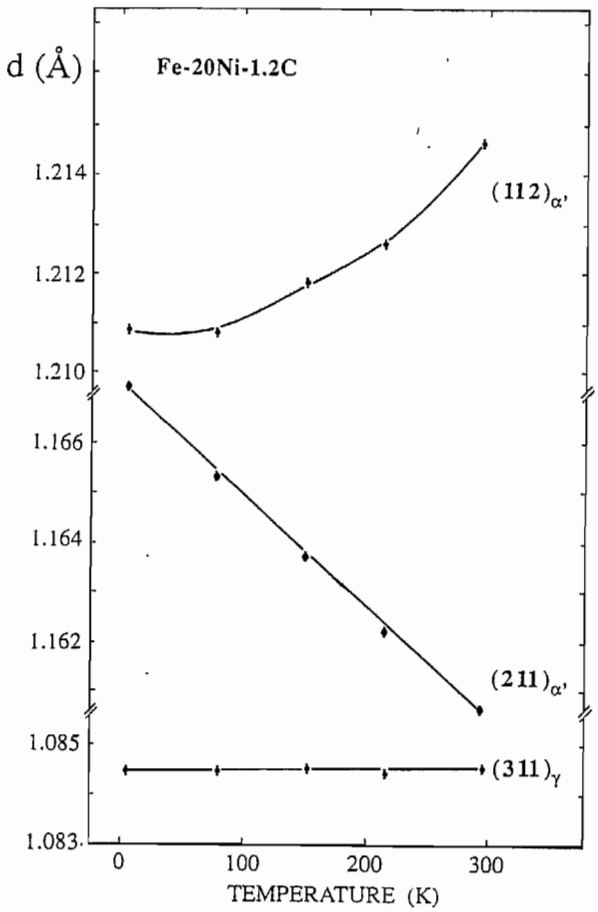


**FIG. 17.** The change of d-values of the martensite peaks $(112)_{\alpha'}$ and $(211)_{\alpha'}$ and of the austenite peak $(311)_{\gamma}$ after heating of the Fe-20Ni-1.2C martensite freshly formed during quenching in liquid helium. The data are obtained from the neutron diffraction spectra.

The *c/a* ratio determined for the freshly formed martensite significantly exceeds the tetragonality expected from the equation $c/a = 1 + \gamma p$, where p is the carbon content in wt % and $\gamma = 0.046 \pm 0.001$. During heating to room temperature, the tetragonality of the Fe-20Ni-1.2C martensite is reduced due to the decrease of the *c* parameter and the increase of the *a* parameter while the position of the retained austenite peak remains unchanged. Other martensite doublets and retained austenite peaks display similar behavior during heating. The behavior of the *c/a* ratio in the Fe-20Ni-1.2C martensite agrees with the results of the X-ray studies of the freshly formed high-nickel martensites obtained by Hayakawa *et al.* /46/ and Kajiwara *et al.* /47/.

The positions of the austenite peaks (d-values) in the neutron diffraction pattern do not change during cooling and during the subsequent heating but the peaks are broadened in the course of the martensitic transformation. Figure 18 displays the broadening of the $(311)_{\gamma}$ peak during cooling and the change of the peak widths during the following heating of the two alloys with different $M_s$ temperatures (see Table 1). The reduction of the widths of the austenite reflections $(220)_{\gamma}$, $(222)_{\gamma}$ and $(420)_{\gamma}$ of Fe-20Ni-1.2C alloy during heating is shown in Fig. 19. The behavior is

dependent on the indices of the reflections, which reveals that the relaxation process is not isotropic. It is natural to expect that the orientation relationship of the martensite and austenite lattices affects the relaxation process.

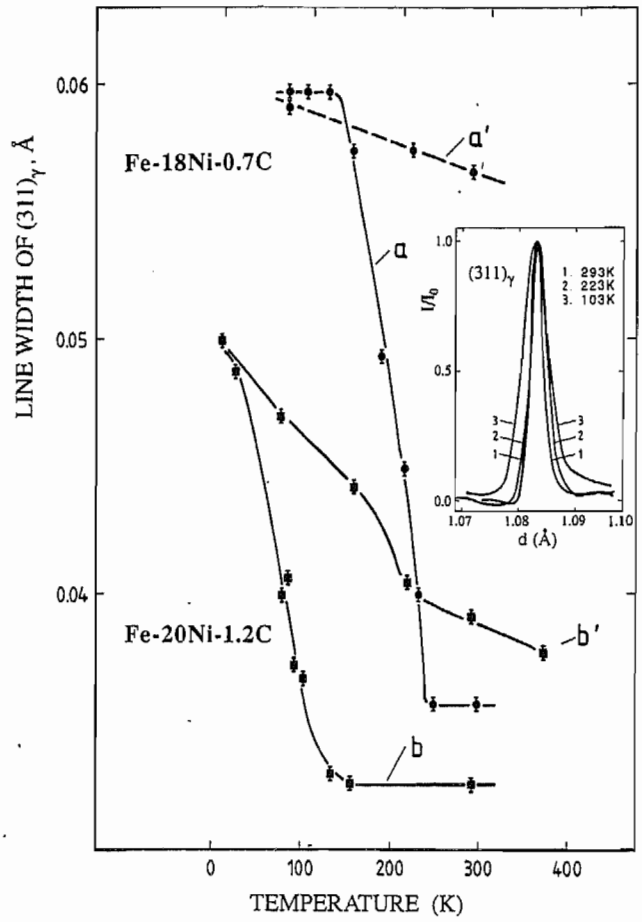


**FIG. 18.** The changes of the widths of the neutron diffraction peaks $(311)_\gamma$ during the martensitic transformation when cooling the alloys Fe-18Ni-0.7C (a) and Fe-20Ni-1.2C (b) and after subsequent heating from temperatures 77 K (a') and 4.2 K (b'), respectively. During cooling the measurements were performed at the temperatures shown in the plot but during the heating stages they were made at 4.2 K after aging for three hours at each temperature. The $(311)_\gamma$ peaks of the alloy Fe-18Ni-0.7C at three temperatures during cooling are shown as inset.

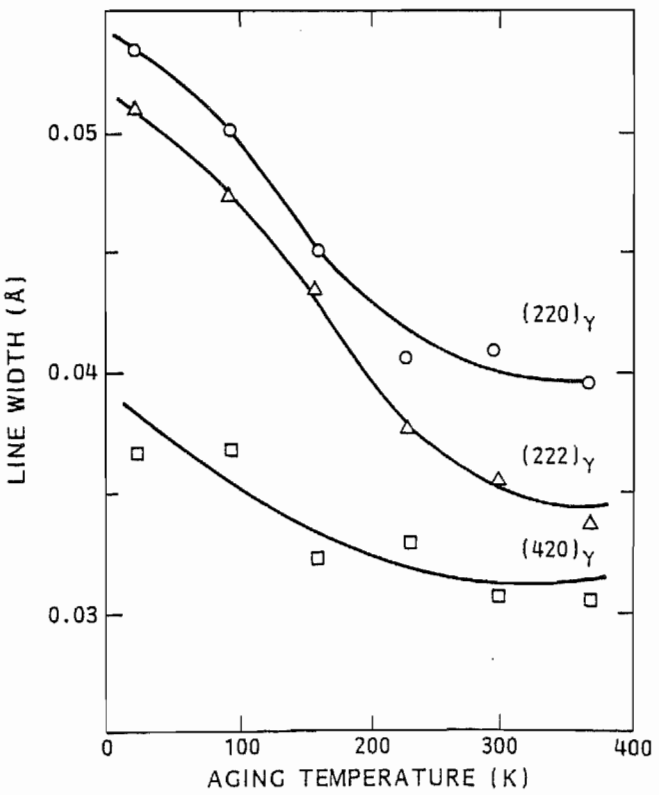


**Fig. 19.** Evolution of the line widths of the retained austenite in Fe-20Ni-1.2C alloy during heating after a rapid quench in liquid helium. Measurements were made at 4 K.

The broadening of $(311)_\gamma$ austenite peak in Fe-20Ni-1.2C during cooling gives evidence for strains created in the retained austenite by the martensitic transformation. The data obtained contradict the X-ray data obtained by Hayakawa and Oka /48/ who claimed that stresses in austenite appear only as a result of rapid cooling before martensitic transformation and then relax during the transformation. The reason for such a difference in interpretations lies in the different techniques applied. X-ray diffraction provides information from the surface layers only. However, interplane distances may be distorted in a complex way in these layers (contracted or elongated) depending on the cooling conditions or other factors and these distortions are compensated for by opposite changes in deeper layers. In contrast, with neutron diffraction, real average stresses in the bulk of the sample can be measured. Neutron diffraction gives precise information regarding stresses in the initial and the retained austenites and the changes of the unit volume of austenite.

The noteworthy difference between the two alloys is the "irreversibility" (during cooling and heating) of the broadening of the austenite peaks of the alloy Fe-18Ni-0.7C and the remarkable decrease of the line width of the Fe-20Ni-1.2C alloy during heating. The "reversible" part of this broadening is attributed to the strains arising from coherency between the virgin martensite and the retained austenite lattices. The connection between abnormally high tetragonality and the coherency effects will be shown below.

***Internal friction results***

Low temperature internal friction patterns were found to be quite different for Fe-Ni-C martensites with different $M_s$ temperatures (Fig. 20, see also Table 1). The computer fitting of the internal friction curves was performed by four Debye peaks with positions at 110, 145, 200 and 250 K. For the dislocation martensite Fe-28Ni-0.2C ($M_s$ = 208 K), peaks $A_1$, $A_3$, $A_4$ are clearly resolved and can be interpreted in accordance with Prioul *et al.* /29,49,50/. Peak $A_1$ is caused by the isothermal martensitic transformation during heating /49/.

As shown in /29/ peak $A_3$ can be interpreted in terms of the increased mobility of dislocations (the left side) and their pinning by carbon atoms during aging above 200 K (the right side). Thus, this peak is not attributed to a relaxation phenomenon, which is confirmed by the low, close to zero value, of the activation enthalpy. Peak $A_4$ reflects the real relaxation process - the formation of Snoek athmospheres, *i.e.*, the ordering of carbon atoms due to their jumps into more favorable octahedral interstices when a dislocation passes through the array of single carbon atoms /50/. The activation enthalpy of this peak was evaluated, as a rough approximation, to be 0.4 eV, which is near the value of enthalpy for the formation of the Snoek atmospheres determined in /51/. The height of the peak depends on the heating rate, because the pinning of dislocations by the carbon atoms during aging diminishes it. Peaks $A_3$ and $A_4$ will be discussed in Chapter II (pinning of dislocations by carbon atoms).

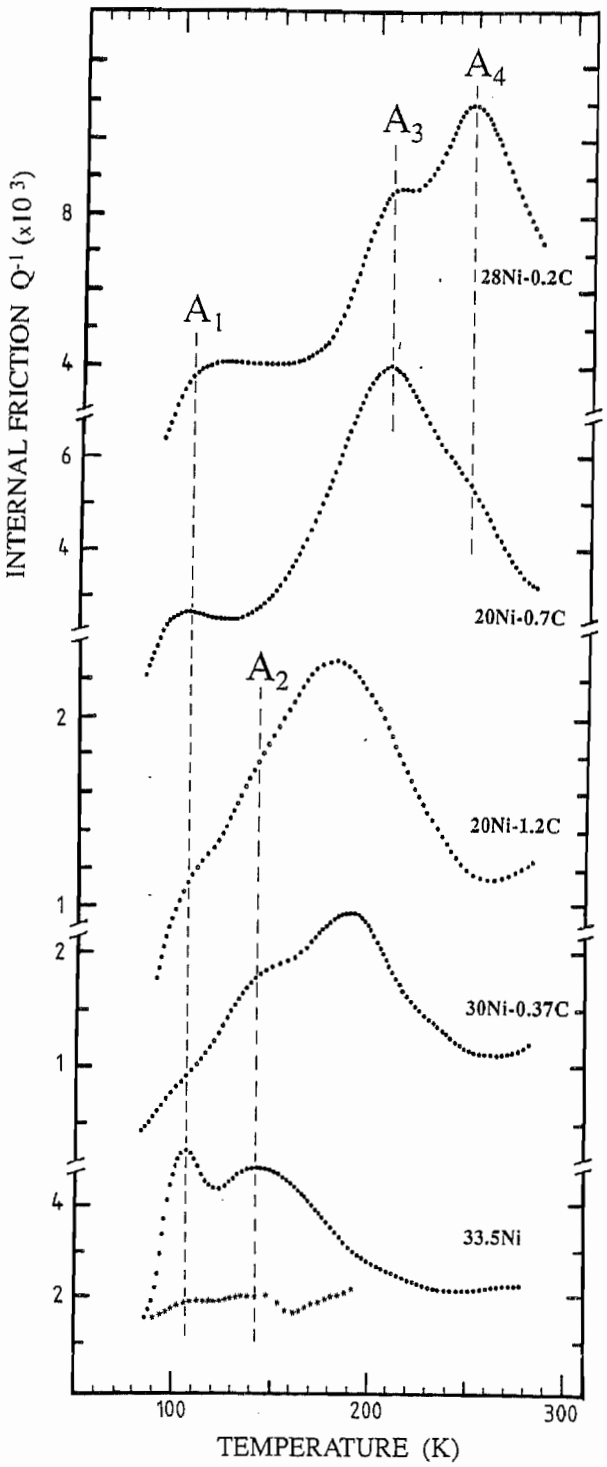


**FIG. 20.** Internal friction of the freshly formed Fe-Ni-C martensites with lenticular morphology (28Ni-0.2C and 20Ni-0.7C) and plate morphology (20Ni-1.2C, 30Ni-0.37C and 33.5Ni) during low temperature aging. Internal friction curve of the 33.5Ni martensite initially deformed at 77 K is denoted by stars (the lowest curve).

Peak $A_2$ was studied in detail in /I/. It is absent in Fe-28Ni-0.2C and Fe-20Ni-0.73C alloys, but it is clearly resolved in the low carbon alloy with 33.5 % of Ni and it overlaps with peak $A_3$ in Fe-20Ni-1.2C and Fe-30Ni-0.37C alloys. Peak $A_2$ appears in the twinned martensites with low $M_s$ temperatures and its height clearly increases with increasing nickel content. It practically disappears during deformation at 77 K as shown in Fig. 20 (the lowest curve denoted by stars). The nature of peak $A_2$ will be discussed below.

**Nature of abnormally high tetragonality**

Three main hypotheses have been proposed to explain the decrease of the high tetragonality of Fe-Ni-C martensite during the low temperature aging: perfect occupation of octahedral interstices on the *c*- axis in the freshly formed martensite with subsequent disordering and a partial redistribution of carbon atoms on the *a*- and *b*- axes during heating /12,13,52/; a redistribution of carbon atoms between octahedral and tetrahedral interstitial sites /14,15/ and a coherent bond between the crystal lattices of virgin martensite and high tetragonal clusters in austenite /15,16/. The last idea has its origin in the theoretical study by Koval and Kokorin /53/ who showed that even in the absence of carbon atoms, tetragonality of martensite can be accounted for by the coherency between solid solution and the ordered precipitates which remain austenitic during the martensitic transformation. In the X-ray study of the carbon free Fe-Ni alloy /17/ coherency between austenite and martensite was considered a sufficient condition to provide tetragonality. However, in this study ordering in the austenite was not taking into account. We observed that short range ordering of nickel atoms in austenite (which leads to a formation of nickel-rich regions) increases the tetragonality of martensite: austenitizing at lower temperature leads to a higher degree of ordering, as evidenced by the Mössbauer and the susceptibility results in /I/, and also to higher tetragonality.

It is clearly seen in Figures 17 and 13 that hypotheses suggesting redistribution of the carbon atoms are not valid because a reduction of the *c/a* ratio is observed starting from such a low temperature that the movement of carbon atoms is excluded. It has to be noted that the $(110)_\alpha$ twinning proposed by Roitburd and Khachaturjan /54/ as the mechanism for redistribution of carbon atoms over *a* - and *b*- octahedral sites does not agree with the increase of the intensity ratios $I_{200,020} / I_{002}$ and $I_{211,121} / I_{112}$, observed by Hayakawa *et al.* /55/, because the opposite effect of the intensity ratios should be expected according to the calculations presented in /55/. The $(110)_\alpha$ twinning was indeed observed by Lysak *et al.* /56/ and Danil'chenko /57/ after the low temperature aging. However, the twins observed in /56,57/ were not the thin polysynthetic twins supposed by Roitburd and Khachaturjan and could not affect the *c/a* ratio.

Mössbauer spectra /21,58/ (see Fig. 31a, shown below) give clear evidence for the absence of the redistribution of carbon atoms from tetrahedral to octahedral interstitial sites, because such a redistribution has to be accompanied by the appearance of components in the spectra with other values of quadrupol splitting in the case of the movement of carbon atoms into the octahedral interstitial sites on the *a*- and *b*- axes and other values of the hyperfine field in the case of the occupation of tetrahedral interstitial sites. However, practically no changes in the spectra were observed after aging at temperatures below 200 K (compare with spectra in Fig. 31a).

### Strains at the interface between virgin martensite and retained austenite

We consider the changes of the retained austenite peaks of the neutron diffraction patterns during martensitic transformation and during aging (Fig. 18) as important for the explanation of abnormally high tetragonality and its reduction in Fe-Ni-C martensite. The broadening of the austenite peaks during martensitic transformation contradicts the X-ray data by Hayakawa and Oka /48/ who concluded that stresses in austenite relax during martensitic transformation. According to the present results, the martensitic transformation is accompanied by an increase of stresses in the retained austenite. The broadening is larger for the Fe-18Ni-0.7C alloy because of the greater amount of martensite formed and as a result of a larger volume effect of martensitic transformation (see also /II/). Behavior of the austenite peak widths during heating is clearly different for the two alloys: the width decreases only slightly in the Fe-18Ni-0.7C alloy while nearly 50 % reduction occurs in the Fe-20Ni-1.2C alloy (Fig. 18).

The reason for such a difference lies in the difference of the $M_s$ temperatures of the two alloys. The high $M_s$ temperature 240 K in Fe-18Ni-0.7C alloy allows martensitic transformation to develop when dislocations are mobile. It means that the broadening of the retained austenite peaks is caused by strains from dislocations which were generated in the retained austenite to decrease the elastic distortions arising from the volume effect of the transformation. These dislocations in the retained austenite remain unchanged during low temperature aging and that is why broadening of the austenite peaks in the alloy Fe-18Ni-0.7C is almost irreversible. The density of the dislocations is insignificant in Fe-20Ni-1.2C martensite, because the martensitic transformation occurs mostly between liquid nitrogen and liquid helium temperatures. Dislocations are essentially immobile at these temperatures and elastic distortions at the coherent interface between the freshly formed martensite and the retained austenite cannot relax during transformation by means of plastic deformation, which is the main reason for the broadening of the retained austenite peaks. When heated, the dislocations become mobile and the coherency is broken due to the generation and slip of dislocations in austenite causing the decrease in the width of the austenite peaks. It is natural to expect that the process breaking the coherency is not isotropic but orientation dependent as revealed by Fig. 19, where the evolution of the linewidths of austenite peaks with different indices was different. Thus stresses in the retained austenite exist though they are not the ones assumed on the basis of the X-ray diffraction studies /59-61/ where the decrease of the austenite lattice parameter was observed and the conclusion was made that the retained austenite is in state of overall hydrostatic compression. Figures 17 and 18 reveal that martensite lattice parameters and the austenite line widths start to change even at temperatures between 4.2 and 77 K during heating, the reason for which is not so far very clear. A relaxation of macrostresses induced in the sample during cooling is not a probable explanation, because the same effects were observed independent of whether the sample was cooled slowly (during several days) or quenched rapidly in liquid helium.

The lattice parameter of the retained austenite remains unchanged during the martensitic transformation (see Fig. 17), which means that neither hydrostatic compression nor dilatation occurs in the retained austenite and stresses are compensated for in the bulk of the sample. The broadening of the peaks for the most part reflects coherent distortions at the martensite-austenite interface in the case of twinned martensite with low $M_s$ temperature or is caused by elastic distortions from the crystal lattice imperfections in the retained austenite in the case of dislocation martensite with the higher $M_s$ temperature.

We can use the model proposed above for the broadening of the retained austenite peaks to explain the high *c/a* ratio in Fe-Ni-C martensites. The decrease of the austenite peak width during heating of the Fe-20Ni-1.2C alloy is accompanied by a reduction of the *c/a* ratio, which can be considered as evidence for the main contribution of distortions at the coherent interface between the virgin martensite and the retained austenite to the abnormally high tetragonality. A break of coherency during heating causes a reduction of tetragonality. In the case of the Fe-18Ni-0.7C alloy, coherency at the austenite-martensite interface has been broken during transformation because of the high mobility of the dislocations. That is why the *c/a* ratio is not high and it is not reduced by heating. Some small excess of tetragonality above the value calculated from the relation $c/a = 1 + \gamma p$ remains in both of the alloys after heating to room temperature, which can be explained by the short range atomic order in the Fe-Ni solid solution as suggested in /62,63/.

The break of coherency at the interface between the freshly formed martensite and retained austenite is also evidenced by the decrease of tetragonality of the twinned high-nickel Fe-Ni-C and nitrogen alloyed martensites (Figs. 13 and 14) in the temperature range of 100 - 200 K. This was not observed in the plain carbon and the Fe-Mn-C steels (Fig. 14) nor in the Fe-20Ni-0.7C alloy the morphology of which is lenticular (Fig. 13).

The idea that coherency between the retained austenite and the virgin martensite is a reason for abnormally high tetragonality can be tested using deformation at low temperatures. If a break of coherency, assisted by some dislocation process, causes a decrease of the *c/a* ratio at temperatures below 200 K, as we assume, tetragonality should be reduced by an external stress, too. The data shown in Fig. 15 confirm that abnormally high tetragonality disappears after deformation at temperatures below the temperature interval where the *c/a* ratio decreases during heating (Fig. 13). The peak becomes very narrow after deformation (see Fig. 15c), which indicates that stresses have really relaxed. The fact that the low temperature external loading makes martensite cubic supports the idea that coherency between lattices of the retained austenite and the freshly formed martensite could be a reason for the abnormally high tetragonality.

**Mobility of the martensite - austenite interface**

It was first recognized by Kurdjumov and Khandros /64/ that a necessary condition for a reversible growth of martensite plates is that the accommodation strains are elastic. Later, modelling of the elastic stress fields associated with a growing plate has been developed by Owen and co-workers (see, *e.g.*, /65/). Most of that work was concerned with ordered $Fe_3Pt$ alloys and it provides a basis for understanding the behaviour of the reversible growth of martensite plates.

The data about the coherent austenite-martensite interface in the alloys with low $M_s$ temperatures shown above can be used to interpret the internal friction pattern of twinned martensites. The second peak $A_2$ in the internal friction patterns of the Fe-25Ni-0.7C, Fe-20Ni-1.2C and Fe-33.5Ni martensites (see Fig. 20) is attributed by the present author to the movement of the coherent interface and to the subsequent break of coherency. Such an interpretation is supported by the following experimental results: (a) peak $A_2$ exists only in the martensites with the plate morphology; (b) its temperature range coincides with the range of the decrease of tetragonality during heating of the Fe-Ni-C twinned martensites (compare with Figs. 13 and 20); (c) low temperature deformation causes a decrease of tetragonality and leads to the disappearance of peak $A_2$ (Fig. 20). We observed /I/ reversibility of the left side of this peak and irreversible behaviour after heating to temperatures above the internal friction maximum (145 K), which means that the peak has a complicated nature: vibration of the coherent interface (the left side) and the subsequent break of coherency when the temperature increases (the right side). Peak $A_2$ is not observed in the internal friction patterns of the dislocation martensites Fe-28Ni-0.2C and Fe-20Ni-0.7C (Fig. 20) with higher $M_s$ temperatures and lenticular morphology. This is in accordance with the absence of the tetragonality reduction at 100 - 200 K as evidenced in Fig. 13 for the latter alloy.

It should be noted that the morphology of the freshly formed martensite, not the low $M_s$ temperature itself, controls the presence or the absence of a coherent bond at the austenite - martensite interface. The following experiment proves the connection between the morphology of the martensite, the break of coherency and the internal friction peak $A_2$. A two-stage cooling method /34/ provides a possibility to decrease the $M_s$ temperature of an alloy, as illustrated in Fig. 21a for the alloy Fe-20Ni-0.7C by means of electrical resistivity measurements. The martensitic transformation started at 208 K during cooling. Then cooling was interrupted at 150 K and the sample was heated to room temperature. At the second cooling, the start of the martensitic transformation in the retained austenite was decreased to 110 K due to the effect of thermal stabilization caused by the aging of the previously formed martensite /66/. However, in spite of the low $M_s$ temperature this second stage martensite possesses a dislocation substructure /67/. In accordance with the interpretation presented here it means that no coherency at the interface and no peak $A_2$ can be observed. The results obtained here confirm this assumption.

During the second heating, the isothermal martensite is transformed as revealed by the decrease in electrical resistivity (Fig. 21a). The third heating was performed to exclude the reversible thermal effects. The difference in the electrical resistivity between the second and third heatings (see Fig. 21b) clearly shows that the isothermal martensitic transformation occurred in the temperature range below 120 K producing about 2.5 % of the total amount of martensite. It is also confirmed by the internal friction measurements presented in Fig. 22b where peak $A_1$, attributed to the isothermal martensitic transformation, is seen. At the same time peak $A_2$ does not exist. Because of the lenticular morphology, *i.e.*, the dislocation substructure of the second stage martensite, peak $A_3$ appears during the second heating (Fig. 22b), though its intensity is rather small due to a small amount of the newly formed martensite. For comparison, the internal friction curve for the first heating is given in Fig. 22a where peak $A_3$ reflecting movement of dislocations and their pinning by carbon atoms and peak $A_4$ caused by the Snoek ordering of carbon atoms in a stress field of moving dislocations are clearly seen.

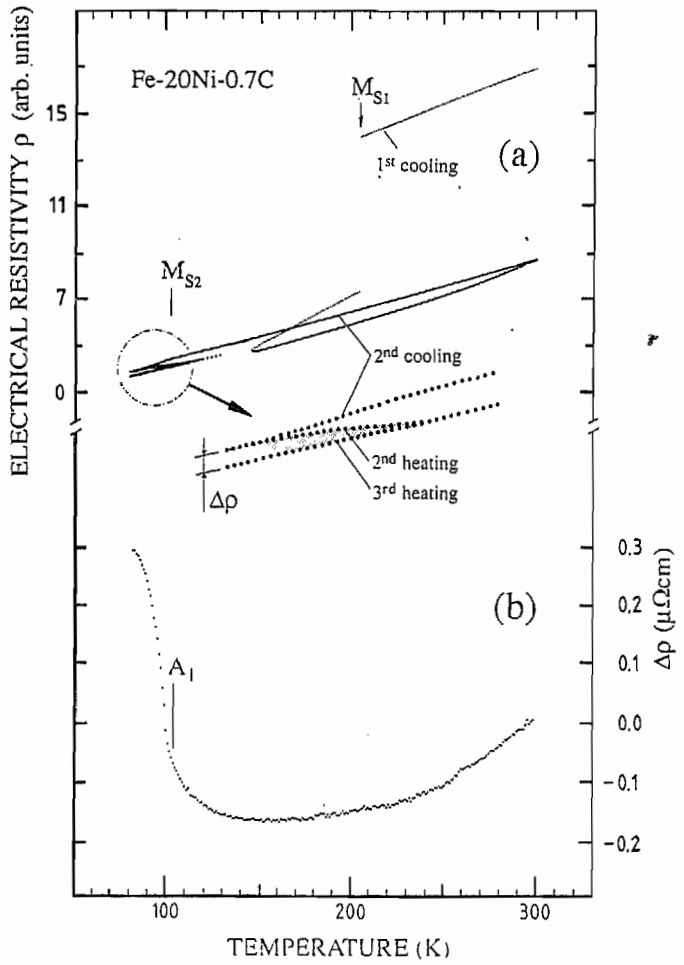


**FIG. 21.** (a) Electrical resistivity of the alloy Fe-20Ni-0.7C during successive coolings and heatings ($2^{nd}$ and $3^{rd}$ heating curves are not shown above 120 K), (b) the difference of electrical resistivity between the $2^{nd}$ and $3^{rd}$ heatings (the shaded area in Figure a).

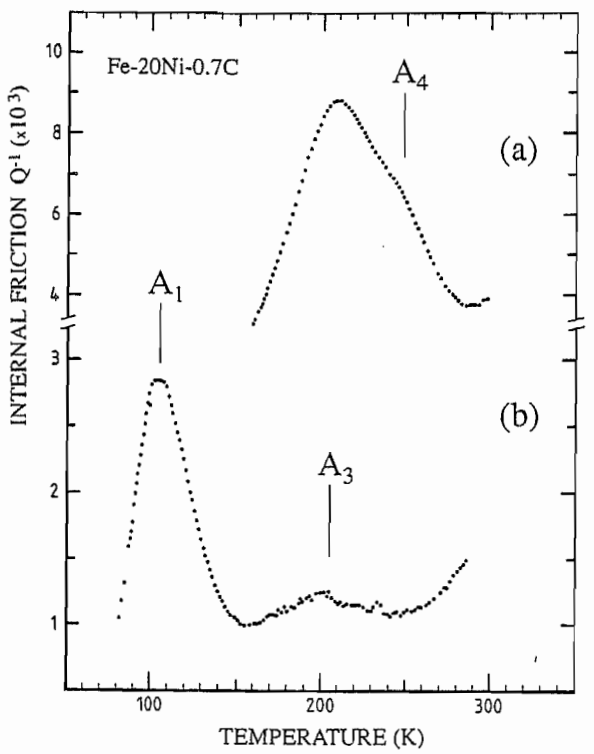


**FIG. 22.** Internal friction of the Fe-20Ni-0.7C martensite in the two-stage cooling experiment during the first (a) and the second (b) heatings (compare with Fig. 21).

In the case of low temperature aging of the twinned Fe-33.5Ni martensite, the behavior of the electrical resistivity is quite different (Fig. 23). The martensitic transformation starts at 125 K and during the burst, nearly 90 % of martensite is transformed (see Fig. 23a). The difference between the first and second heating curves makes it possible to observe the irreversible effects separately from the reversible thermal effects in the same way as was done in Fig. 21. It is noteworthy that the electrical resistivity continues its decrease above temperatures where the isothermal martensitic transformation has been completed (Fig. 23b). As seen in Fig. 20 the break of coherency occurs after the isothermal martensitic transformation, resulting in a decrease of the *c/a* ratio (Fig. 13). Therefore, electrical resistivity decreases at these temperatures due to the stress relaxation caused by the break of coherency. Magnetic susceptibility measurement /I/ made simultaneously with the same sample revealed a decrease below 110 K and an increase between 110 - 200 K. This confirms that the decrease of resistivity must also be caused by two different effects although they cannot be resolved. For comparison, in the alloy Fe-20Ni-0.7C (see Fig. 21b) the electrical resistivity decreases mainly at temperatures below 120 K, *i.e.*, in the temperature range of the formation of isothermal martensite. This is in accordance with the absence of coherency at the interface between the retained austenite and the virgin martensite in this alloy.

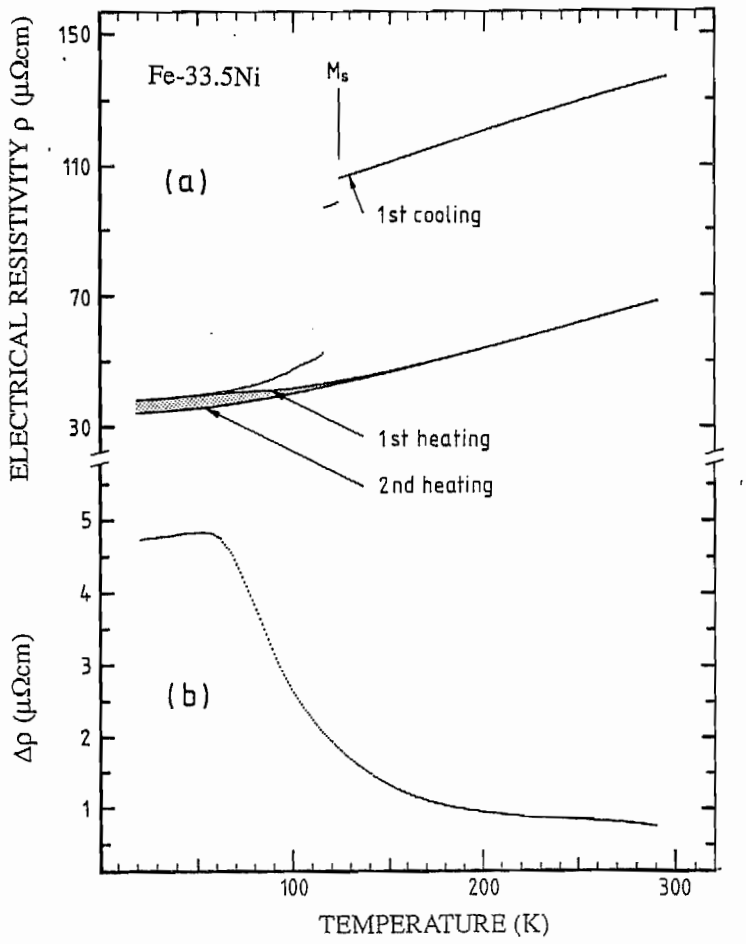


**FIG. 23.** The change of electrical resistivity in the alloy Fe-33.5Ni during coolings and heatings: (a) the change of electrical resistivity during two subsequent coolings and heatings between 10 K and room temperature, (b) difference between the first and second heatings, *i.e.*, the shaded area in Figure (a), (the curve plotted without smoothing).

Thus, we can explain the change of internal friction and electrical resistivity during the aging of the freshly formed martensite at temperatures below 200 K in a consistent way on the basis of the idea of coherency at the austenite - martensite interface and the break of this coherency.

### Short range atomic ordering in Fe-Ni-C austenite and its contribution to abnormally high tetragonality and to coherency effects

An important question is whether the coherent interface between the freshly formed martensite and the retained austenite is sufficient, by itself, to cause the abnormally high *c/a* ratio or if the atomic order in the retained austenite, coherently bound to the martensite, plays any role in tetragonality.

The contribution of the short range atomic order in Fe-Ni alloys to tetragonality of martensite was discussed by Winchell *et al.* /62,63/. According to Winchell, one kind of atoms surrounded by the other kind of atoms in austenite (tetragonal clusters) tend to sustain the former atomic configuration in martensite, which resists the Bain strain and can cause the tetragonal distortion of the martensite crystal lattice. The effect of coherent regions in austenite on the crystal structure of martensite (for example, $Ni_3Ti$ in Fe-Ni-Ti or $Fe_3AlC$ in Fe-Al-C alloys) is concerned with the fact that these particles do not transform to martensite and retain a coherent bond with the crystal lattice of the martensite (see, for example, /53,68-70/). Having a higher elastic modulus they cause a shear deformation in martensite resulting in its tetragonality. In the twinned Fe-Ni martensite, where the thickness of twins is about 100 - 200 Å, particles of the order of 30 - 50 Å in size have to sustain their coherency according to calculations performed by Kokorin /70/.

The idea of coherency between the freshly formed martensite and the ordered regions in the retained austenite was used in /15,16/ to explain the abnormally high tetragonality of Fe-Ni-C martensites. Magnetic ordering is illustrated in Fig. 24 for the alloy Fe-30.6Ni by Mössbauer spectroscopy and in Fig. 25 for Fe-25Ni-0.7C by magnetic susceptibility. Figure 24 shows that annealing of the deformed alloy results in the magnetic broadening of the Mössbauer pattern. It is important that annealing at 900 °C causes larger broadening than at 1100 °C, which is accounted for by the ordering of nickel atoms. The correlation between the magnetic and atomic ordering exists in Fe-Ni alloys /71,72/. It was also shown for the alloy Fe-33.5Ni in /I/ by means of Mössbauer spectroscopy that the degree of magnetic ordering is higher in the retained austenite as compared to the initial austenite. This is because $M_s$ temperatures of the nickel-rich regions are lower and the most ordered regions transform to martensite last or remain untransformed during cooling. The difference between the amounts of the retained austenite evaluated by means of different methods is consistent with the existence of the small nontransformed austenitic regions enriched with nickel. In Mössbauer spectroscopy all austenite is detected independent of the size of the regions, and significantly higher amounts of martensite were observed than, *e.g.*, by optical methods by which only austenite regions larger than about 0.5 μm can be detected.

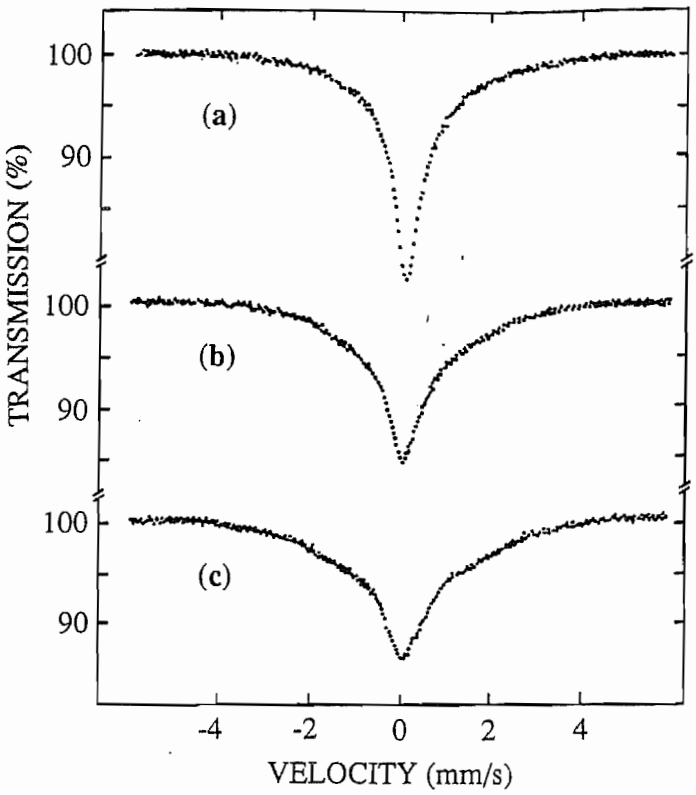


**FIG. 24.** The Mössbauer spectra of the Fe-30.6Ni austenite after deformation (a) and after subsequent annealings at 1100 °C (b) and 900 °C (c).

Figure 25 shows that the annealing temperature affects the Curie temperature and the saturation level of magnetic susceptibility. The saturation level for the sample corresponding to the higher degree of ordering (annealed at 1050 °C) is lower, which can be ascribed to the decreased mobility of magnetic domain walls due to their interaction with the magnetically ordered nickel-rich regions. It is noteworthy that the martensite start temperature is also lower for the sample annealed at 1050 °C in spite of the possible graphitization (which raises the $M_s$ temperature). This is also clear evidence for the ordering of nickel atoms.

Partial magnetic ordering in the retained austenite of the alloy Fe-25Ni-0.7C was also observed by Mössbauer spectroscopy in /III/. For the validity of the model proposed here, it is important that ordering of nickel atoms accompanied by magnetic ordering is observed for all the alloys which possess coherency effects. A crucial question arises if magnetic ordering can be observed also in the Fe-20Ni-1.2C martensite whose nickel content is lowest and whose coherency peak $A_2$ in the internal friction pattern is very small. Figure 26 shows Mössbauer spectra of the aged Fe-20Ni-1.2C martensite measured at 30 and 10 K. The height of the central retained austenite peak is significantly smaller (integrated intensities about the same) and the width is larger for the pattern measured at 10 K. Because these changes are reversible during successive coolings and heatings and because the central peak is broader at lower temperature, we conclude that magnetic ordering has really occurred between 10 and 30 K. This effect cannot be caused by the reversible growth of martensite plates.

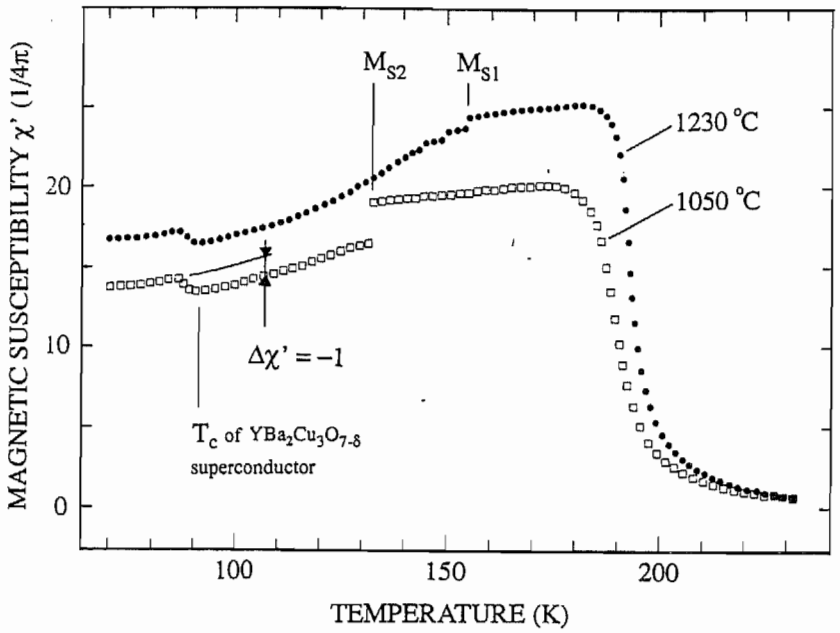


**FIG. 25.** Magnetic susceptibility of the alloy Fe-25Ni-0.7C after austenitizing for 3 h at 1230 °C (upper curve) and in addition for 17 h at 1050 °C (lower curve). The susceptibility scale was calibrated by a high-$T_c$ superconductor placed in the compensator coil.

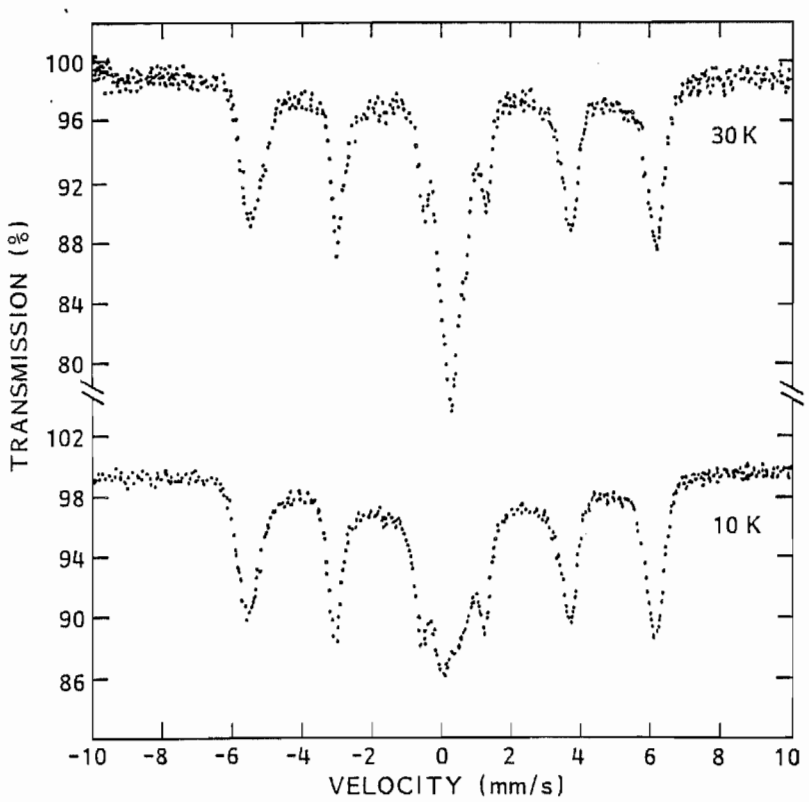


**FIG. 26.** Mössbauer spectra of aged Fe-20Ni-1.2C martensite, measured at 10 K and at 30 K.

The existence of nickel-rich clusters can be indirectly evidenced also by internal friction measurements. The high-nickel regions should inhibit the movement of the austenite-martensite interface, which should appear as a decreased intensity of peak $A_2$. This behavior is illustrated in Fig. 27 for the alloy Fe-33.5Ni. Austenitizing at lower temperature 900 °C (corresponding to higher degree of short range ordering) leads to smaller coherency peak $A_2$, as expected.

Coherency at the interface of the ordered nontransformed austenitic regions inside the virgin martensite can make a significant contribution to tetragonality. Tetragonality of the Fe-33.5Ni martensite was measured after austenitizing at 1230 °C and 1000 °C and it was really higher for the treatment at lower temperature. In addition, the changes of the austenite lattice parameter caused by the ferromagnetic transformation can affect the strains at the coherent interface and also the *c/a* ratio of martensite. The magnetic transformation in Fe-Ni-C austenites can occur before or during the martensitic transformation (see, *e.g.*, /I/).

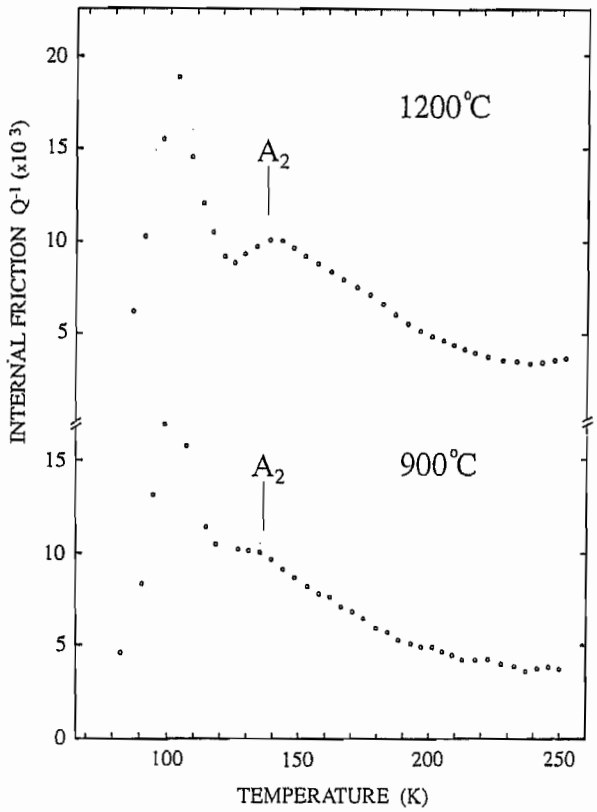


**FIG. 27.** Internal friction (f=0.28 Hz) of the alloy Fe-33.5Ni during heating. Sample was austenitized at 1230 °C for 1 h (upper curve) and further at 900 °C for 17 h (lower curve).

According to /I/ and the present results, we can conclude that the twinned microstructure and the ordering of nickel atoms are necessary and sufficient conditions for the effects of coherent interfaces between martensite and retained austenite. By means of a two stage cooling experiment it was shown that the low $M_s$ itself is not a sufficient condition. Measurements (X-ray diffraction, internal friction, magnetic susceptibility and electrical resistivity /I/) made with the Fe-Mn-C martensite, whose $M_s$ temperature is low and microstructure is twinned, revealed no sign of coherency effects, which indicates that the twinned structure alone is not a sufficient condition either.

## II INTERACTION OF CARBON ATOMS WITH DISLOCATIONS (2nd STAGE)

The second stage of aging at temperatures 200 - 270 K is controlled by pinning of the dislocations by carbon atoms and the formation of Snoek atmospheres, which can be evidenced by internal friction (results shown above) and positron-lifetime measurements. Morphology of martensite affects the density of dislocations and, therefore, the extent of their interaction with carbon atoms.

### *Positron annihilation results*

Positron-lifetime measurements were performed in order to study the interaction of carbon atoms with dislocations and vacancies during aging of the freshly formed martensite. Two alloys, Fe-20Ni-0.7C and Fe-20Ni-1.2C, were chosen on account of their different morphology and substructure. After solution treatment at 1150 °C and cooling in water, the samples were inserted in the cryo-refrigerator. Aging was performed for one hour at temperatures 50, 100, 150, 200, 250 and 300 K and the positron-lifetime was measured at 25 K between each aging (Fig. 28).

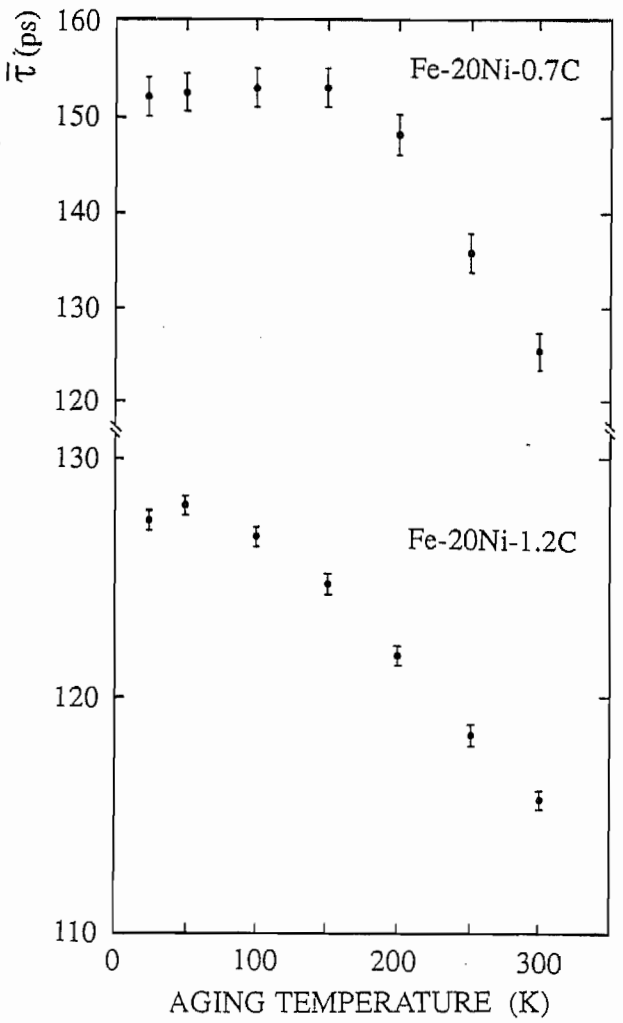


**FIG. 28.** The change of the positron mean lifetime after low temperature aging of the virgin Fe-20Ni-0.7C and Fe-20Ni-1.2C martensites. Measurements were made at 25 K between each aging.

The different mean lifetimes in the freshly formed martensites and different temperature ranges of the change of lifetime during aging are clearly seen. After subtracting the contribution of the source and the background the multiexponential spectra were decomposed into two intensities $I_1$, $I_2$ and lifetimes $\tau_1$, $\tau_2$. The changes of $\tau_2$ and $I_2$ with the aging temperatures can be seen in Figures 29 and 30.

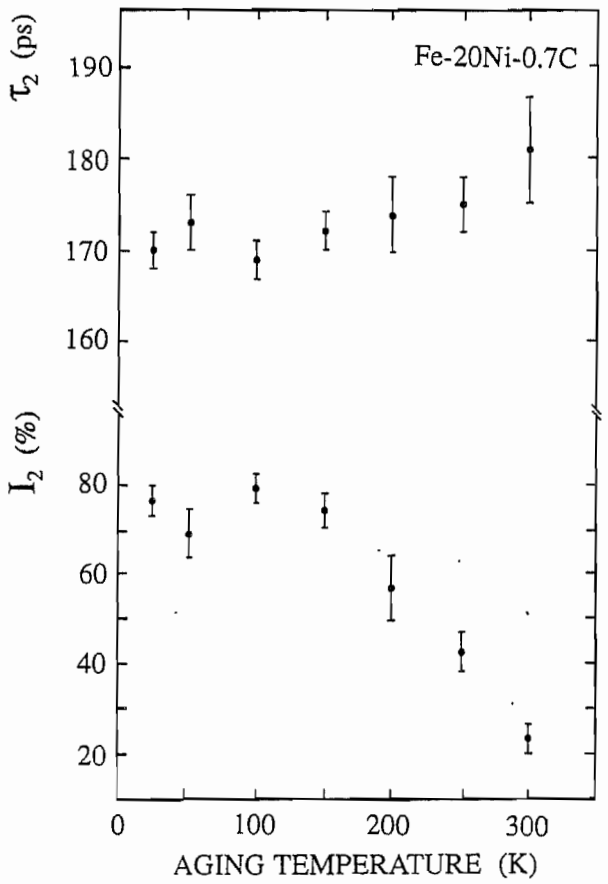


**FIG. 29.** The change of lifetime $\tau_2$ and intensity $I_2$ of positrons trapped in dislocations after low temperature aging of the virgin Fe-20Ni-0.7 martensite.

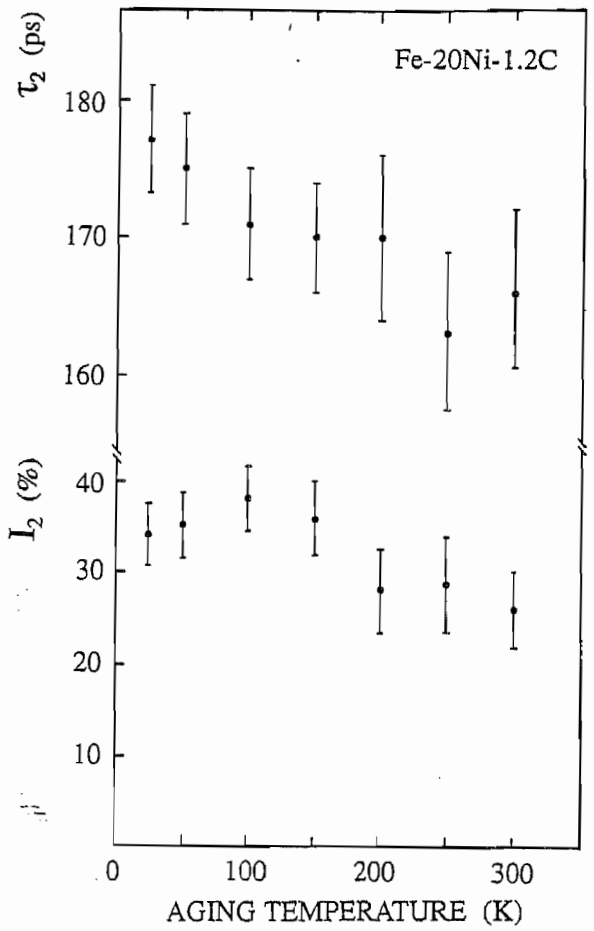


**FIG. 30.** The change of lifetime $\tau_2$ and intensity $I_2$ after low temperature aging of the virgin Fe-20Ni-1.2C martensite.

Lifetime $\tau_1$ is close to 100 ps which corresponds to annihilation in a solid solution /73,74/. The value of $\tau_2 = 170 \pm 5$ ps can be attributed to trapping of positrons by vacancies or dislocations in accordance with /75/. It should be noted that unlike plastic deformation, the martensitic transformation produces a more ordered dislocation substructure and leaves a less possibility for nonconservative movement of the dislocations, *i.e.*, for generation of vacancies or selfinterstitials. For this reason we can assume dislocations to be the most probable traps for positrons in the freshly formed martensite. For the Fe-20Ni-0.7C martensite, the mean lifetime is much greater (Fig. 28) and correspondingly the intensity of the long-lifetime component $I_2$ prevails as compared to the Fe-20Ni-1.2C martensite (compare with Figs. 29 and 30), which is consistent with the dislocation

substructure of the former and the twinned substructure of the latter. It confirms indirectly that lifetime $\tau_2$ corresponds to positron lifetime in dislocations. The different temperature behavior of the mean lifetime $\tau$ and of the intensity $I_2$ during the aging of both martensites will be discussed below.

**Pinning of dislocations by carbon atoms**

During low temperature aging of the freshly formed lenticular martensites, the internal friction peaks $A_3$ and $A_4$ can be clearly distinguished (see Fig. 20). Peak $A_3$ is attributed to the movement of the dislocations (left side of the peak) and the pinning of them by carbon atoms (right side), while peak $A_4$ is related to the Snoek ordering of carbon atoms in a stress field of moving dislocations in accordance with the results shown in references /29,50/. The occurrence of these peaks in the internal friction patterns of dislocation martensites (alloys Fe-20Ni-0.7C and Fe-28Ni-0.2C), their small intensity in the patterns of twinned martensites (Fe-20Ni-1.2C, Fe-30Ni-0.37C and Fe-33.5Ni) and their disappearance after the first heating clearly prove that pinning of dislocations by carbon atoms takes place during aging below room temperature.

The positron annihilation measurements are a very sensitive tool for studying the interaction of interstitials with dislocations or vacancies. The data shown in Figs. 28-29 provide the opportunity to compare martensites with twinned and dislocation substructures. Mean lifetime $\tau$ and intensity $I_2$ display the different behavior during aging of these martensites. A decrease of $\tau$ and $I_2$ begins at 200 K in the Fe-20Ni-0.7C martensite (Figs. 28 and 29), which can be attributed to the capture of carbon atoms by dislocations resulting in a decrease of the probability of positron trapping by these defects. After aging at room temperature only a few of the dislocations can serve as traps for positrons according to the present results. The value of $\tau_2$ seems to increase about 10 ps during aging above 200 K (Fig. 29). This means an increase in the average size of positron traps. One possible source for the larger traps is microcracking which occurs during the low temperature aging of the lenticular martensites. Perhaps some low-intensity unresolved component appears in the spectra with a lifetime much larger than $\tau_2$.

Surprisingly, the value of $\tau$ decreases in the Fe-20Ni-1.2C martensite starting from aging at 100 K (Fig. 28). The reason for such behavior lies in the decrease of both intensity $I_2$ and lifetime $\tau_2$ (Fig. 30). Such a low temperature for the change of $I_2$ and $\tau_2$ was not observed in the irradiated $\alpha$-iron (see, for example, /74,75/). As discussed above, the Fe-20Ni-1.2C martensite with plate morphology is characterized by a coherent bond with retained austenite and a low density of dislocations. The value of lifetime $\tau_2$ of the virgin Fe-20Ni-1.2C martensite exceeds that of the Fe-20Ni-0.7C alloy (Figures 29 and 30) and it decreases during aging, which gives evidence that some traps, more effective than dislocations, exist in the freshly formed state and disappear with heating. According to the results mentioned above, it can be assumed that the coherent interfaces producing the long range stresses, can effectively trap positrons as long as martensite remains virgin. If this assumption is correct, the number of traps should decrease when the coherency at the interface

between martensite and austenite is broken. It is noteworthy that intensity $I_2$, proportional to the number of traps, really decreases between 100 and 200 K, which is the temperature range where the coherency is broken according to the present X-ray diffraction and internal friction results. The small value of $I_2$ for the Fe-20Ni-1.2C alloy and its slight decrease after aging as compared to the alloy Fe-20Ni-0.7C also confirms that the density of dislocations is really small in this twinned martensite.

Thus, a part of the carbon atoms leave the solid solution and pin dislocations during aging above 200 K. The fraction of carbon atoms captured by dislocations is small and cannot be revealed by means of transmission electron microscopy. Therefore, it it impossible to observe the pinning of dislocations by carbon atoms during the aging of the Fe-C alloys using this method. However, as in the case of strain aged iron and pearlitic steels, the contribution of this carbon-dislocation interaction to the striking change of mechanical properties is important, in addition to clustering in the solid solution. As shown (see, for example, /76/), dislocations do not break off carbon atoms at yield stress in aged plain carbon steels, but new dislocations are emitted and they interact with the pinned ones, which may be responsible for the increase in the yield strength of the freshly formed martensite after the low temperature aging /1-3/. Pinning of dislocations also increases the brittleness of martensite, because the stresses cannot be relaxed by the plastic deformation. Hence, microcracking during aging /11/ can also be understood, taking into account the pinning of the dislocations by carbon atoms (together with the dimensional changes of martensite lenses during aging), while it is not so clear if only the effect of clustering is considered.

## III CLUSTERING AND ORDERING OF INTERSTITIALS (3rd STAGE)

By means of Mössbauer spectroscopy, electrical resistivity and magnetic susceptibility measurements, it will be shown that carbon atoms form clusters but nitrogen atoms order without formation of clusters during aging above 200 K.

### *Mössbauer spectroscopy*

Mössbauer measurements gave strong evidence for the clustering of carbon atoms during aging of the virgin martensite below room temperature long before the transmission electron microscopy studies /18-21/ were made. It is simpler to illustrate the effects of low temperature aging on Mössbauer spectra using the plain carbon martensite, because nickel causes the magnetic broadening of lines hiding some details of the spectra. The change of the Mössbauer pattern of the alloy Fe-2.03C after aging in the temperature range of 65 - 293 K is shown in Fig. 31a where the outer line corresponding to the transition -1/2 -> -3/2 is present.

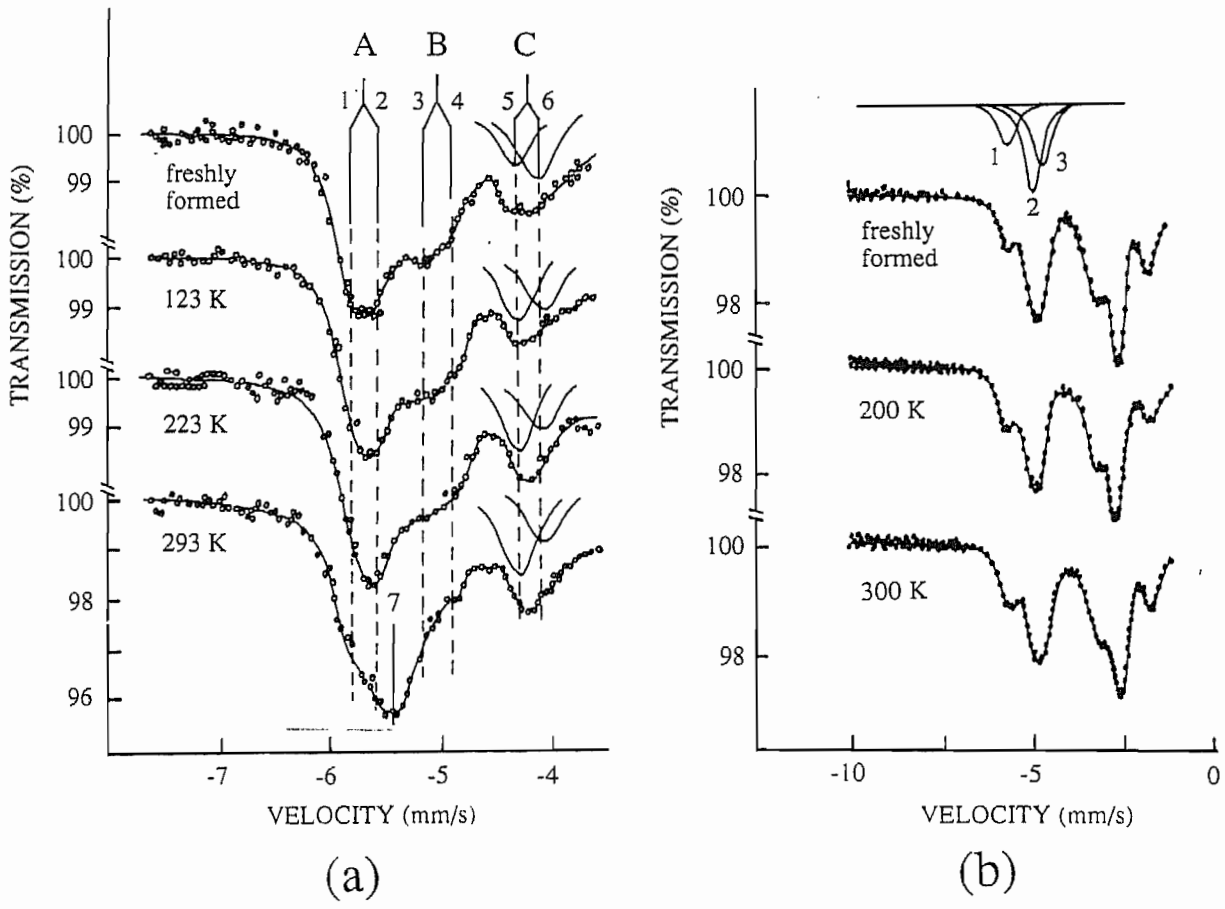


**FIG. 31.** The Mössbauer spectra of virgin and aged martensites:
(a) the outer line (transition -1/2 -> -3/2) of the Fe-2.03C martensite spectrum after quenching to liquid helium and after the following heating to 123, 223 and 293 K. These spectra were measured at 65 K /21,58/;
(b) the left part (transitions -1/2 -> -3/2 and -1/2 -> -1/2) of the Fe-2.75N martensite spectrum after quenching to liquid nitrogen and subsequent aging at 200 and 300 K. These spectra were measured at 5 K.

The line is split into components A, B and C, each of them having a fine internal structure, according to the fitting performed in /21,58/ (see Table 2). During aging, component B disappears for the most part, component A shifts to the right and component C increases and shifts to the left as a result of the change in its internal structure. The same hyperfine structure in the Mössbauer spectra of virgin and aged plain carbon martensites was observed in /18-20/ and in other available studies and the controversy exists only in the interpretations.

The same behavior is observed in the Mössbauer spectra of the virgin Fe-Ni-C martensite during low temperature aging (see for instance /77/). The application of an external magnetic field /26,78/ resulted in the detection of a new very weak component with a field of about 18 T /26/ or 16.5 T /78/ masked by a strong high-field component. The weak component was found by Ino *et al.* /78/ only after aging at 363 K, but Génin /26/ observed it even in the freshly formed martensite with an intensity of about 2 % and its intensity did not change after aging at room temperature for one month.

The outer lines of the Mössbauer spectrum of the Fe-2.75N alloy after quenching in liquid helium and aging at 200 and 300 K are shown in Fig. 31b. The lines consist of three components. The martensite spectra are overlapped by the patterns of ordered $Fe_4C$ clusters in retained austenite. When cooling to 5 K, the clusters undergo magnetic ordering which is reversible /V/. During aging, the structure of the Fe-N Mössbauer spectrum remains unchanged (Fig. 31b).

*Electrical resistivity and magnetic susceptibility*

The behavior of electrical resistivity of the Fe-Ni-C alloys during low temperature aging is presented in Fig. 32. All of the curves reveal an abrupt increase of the resistivity starting at about 250 K. This effect is attributed to the static displacements due to clustering of carbon atoms (see, *e.g.*, /79/) and it is shown to be independent of the morphology of martensite. A smaller increase in resistivity occurs already in the temperature range of 160 - 250 K.

Because resistance value also depends on the geometry of the sample, *i.e.*, the length and the cross-section of the specimen, and because aging changes them as shown in Fig. 36, it was necessary to evaluate the contribution of the change of the sample dimensions to resistance. The shape of the dilatometric curve of the Fe-18Ni-0.7C alloy (Fig. 36) is indeed very similar (up side down) to that of the resistivity curve of the same alloy shown in Fig. 32 and it would be tempting to try to explain resistance results simply by geometrical effects. However, using the data of the dilatometric measurement (Fig. 36) it was calculated that only 20 % of the resistance change of the Fe-18Ni-0.7C alloy in the temperature range of 160 - 250 K could be accounted for by the diminishing of the dimensions of the specimen. In other temperature ranges the contribution of the geometrical effects on resistance was still smaller. Hence, we can conclude that the main part of the resistance changes shown in Fig. 32 is caused directly by the aging process. The initial increase in resistivity of the Fe-25Ni-0.7C alloy is more pronounced than in the other alloys, probably due to

the higher nickel content that increases the mobility of carbon atoms.

The decrease of resistivity in the very beginning of the aging of Fe-18Ni-0.7C martensite is attributed to the formation of isothermal martensite. This reduction was significantly smaller when the measurement was preceded by holding at 77 K for two weeks during which the isothermal transition was almost completed /34/. The behavior of resistivity of Fe-20Ni-0.7C alloy during aging is very similar. In the case of Fe-20Ni-1.2C and Fe-25Ni-0.7C alloys, the contribution of the isothermal martensite is not resolved. Alloy Fe-2.39N reveal another kind of behavior of resistivity (Fig. 34). Unlike in the Fe-Ni-C alloys, resistivity decreases consistently above 200 K. The reduction of resistivity for the Fe-2.39N alloy is surprisingly high (35 %).

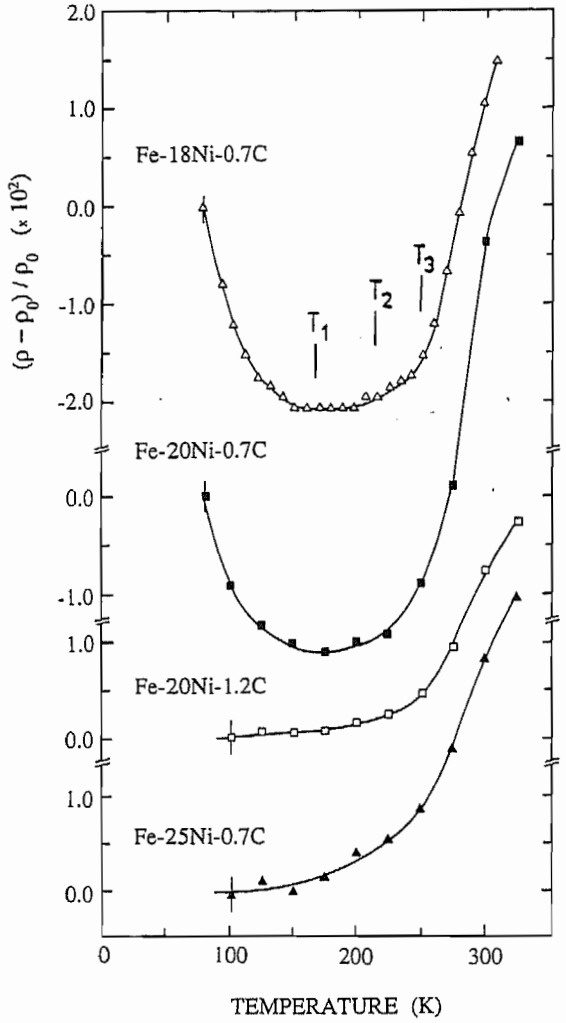


FIG. 32. Relative resistivity of the Fe-Ni-C martensites as a function of aging temperature. Measurements were made at 77 K. The resistivity of the virgin martensite is denoted by $\rho_0$.

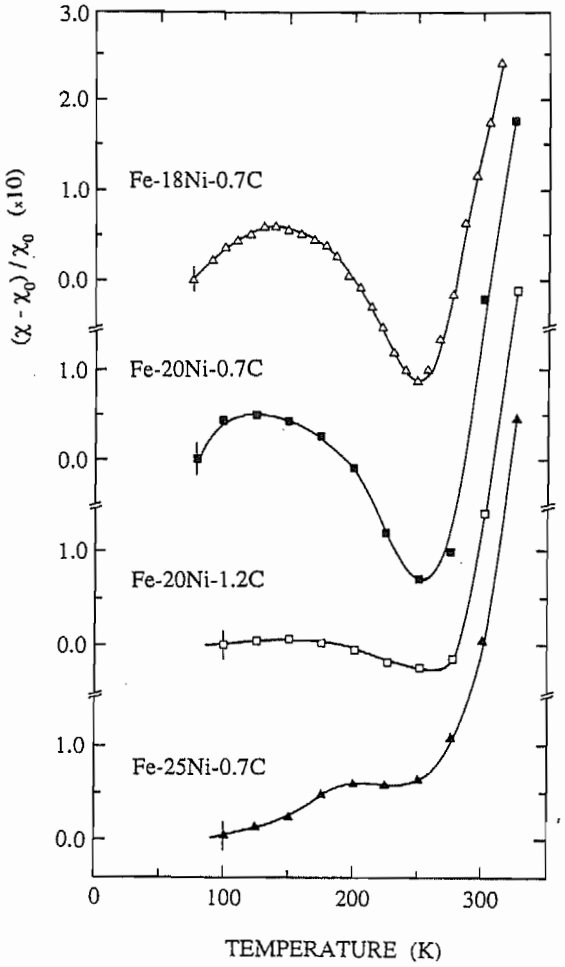


FIG. 33. Magnetic susceptibility of the Fe-Ni-C martensites versus aging temperature. Measurements were made at 77 K. The susceptibility of the virgin martensite is denoted by $\chi_0$.

Magnetic susceptibility is a new method for studying the low temperature aging of martensite /34,35,V/. Susceptibility was measured simultaneously with electrical resistivity. As shown in Fig. 33, susceptibility also increases abruptly above 250 K as does resistivity in the case of the Fe-Ni-C alloys. This increase is preceded by a reduction of susceptibility during the early stage of aging. For the lenticular Fe-18Ni-0.7C and Fe-20Ni-0.7C martensites, this reduction is largest. The increase in the range of 80 - 130 K observed in these alloys is attributed to the isothermal martensitic transformation. Susceptibility of the alloys Fe-25Ni-0.7C and Fe-20Ni-1.2C increases until 200 K, but for the second alloy the increase is very small.

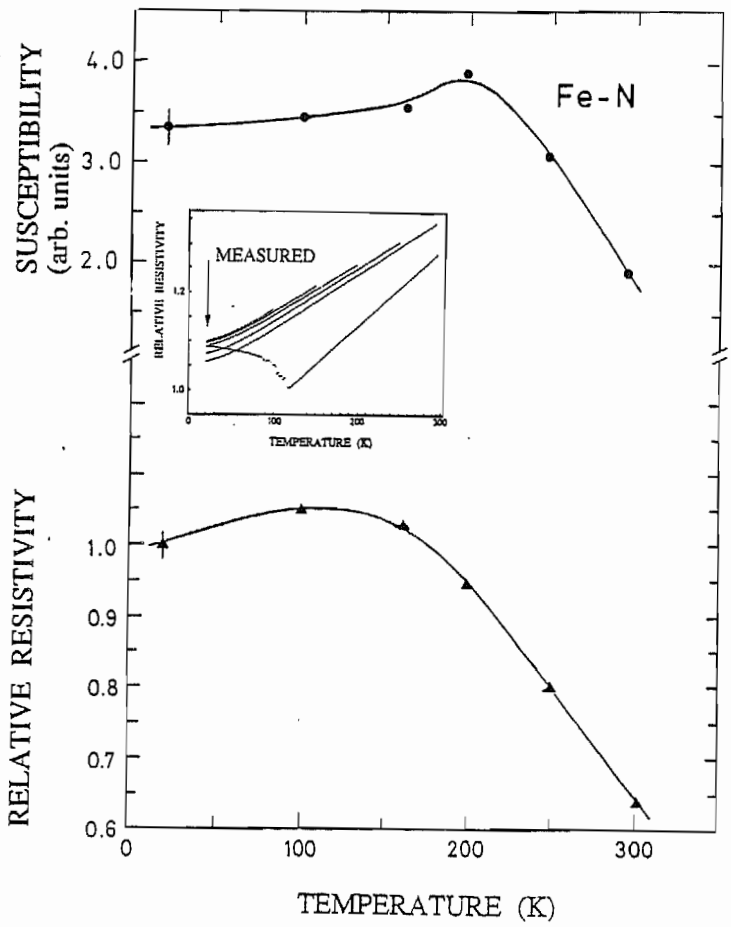


**FIG. 34.** Electrical resistivity and magnetic susceptibility of the Fe-2.39N alloy as a function of aging temperature, measured at 20 K after subsequent coolings, as illustrated in the inset.

Magnetic susceptibility of the Fe-2.39N martensite after aging at different temperatures is shown in Fig. 34. It reveals another kind of behavior as compared to the Fe-Ni-C alloys. Susceptibility increases until 200 K and decreases consistently above 200 K.

*Neutron diffraction data*

Figure 35 shows the relative structure factors $F^2$ of the Fe-18Ni-0.7C martensite for the reflections $(211)_{\alpha'}$ and $(112)_{\alpha'}$. The structure factors are proportional to the integrated intensities of the neutron diffraction peaks and they are reduced by an increase of the mean-square displacements

of the interatomic distance, the origin of which may be thermal vibration of atoms or static distortions caused by, for instance, interstitials. The structure factors of the reflections (211) and (112) are nearly equal at 77 K, which proves that the intensity ratio $I_{(112)} / I_{(211),\,(121)}$ is about 1:2 as shown in Fig. 16. The structure factor is slightly smaller for the reflection (112), which may be accounted for by the larger amplitude of the thermal vibrations in the *c* - direction than in *a* - and *b* - directions. It is noteworthy that the difference between the factors $F^2_{(112)}$ and $F^2_{(211)}$ remain unchanged after aging at 200 K. This indicates that the static mean-square displacements do not increase at these temperatures.

The values of $F^2$ of the martensite aged at 200 K are about 5 % higher than those of the virgin martensite. This increase can be attributed to the formation of isothermal martensite during heating ($F^2$ is also proportional to the amount of phase).

After aging at 300 K both of the structure factors have clearly decreased revealing the increase of the static displacements. $F^2_{(112)}$ is reduced more than $F^2_{(211)}$, which is in accordance with the decrease of the intensity ratio $I_{(112)} / I_{(211),\,(121)}$ observed by the neutron and X-ray diffraction.

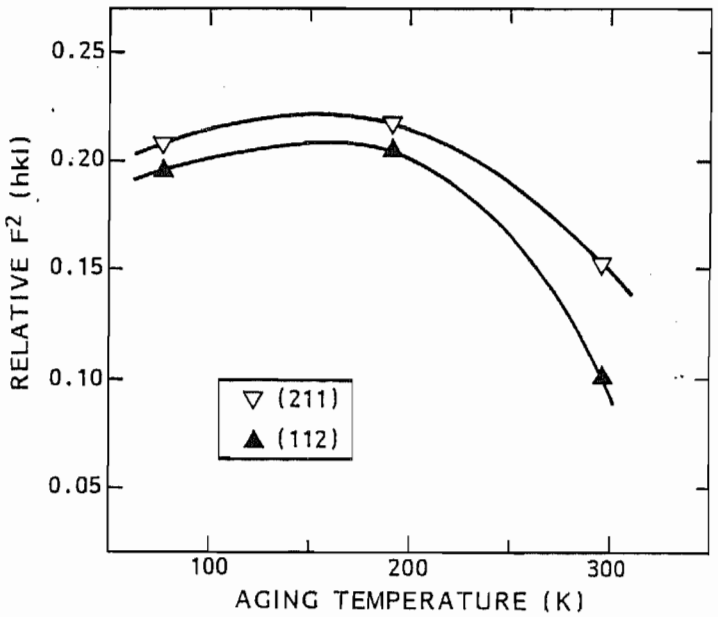


**FIG. 35.** Relative structure factors for the neutron diffraction reflections (211) and (112) of the Fe-18Ni-0.7C martensite. The austenitic sample was quenched in liquid nitrogen and aged at 200 and 300 K. The measurements were made at 77 K.

*Dilatometric results*

Dilatometric, internal friction and frequency measurements were performed simultaneously with the same sample using the internal friction facility described in Chapter 2. The sample was aged for one hour at temperatures 77, 83, 90, 100, 110, ... , 290 and 300 K. Measurements were made both at these temperatures and at 77 K between each aging. The thermal cycle is presented in Fig. 37 as inset. Figure 36 shows the changes of the length of the Fe-18Ni-0.7C martensite on aging,

measured at 77 K. Because the average size of the martensite lenses is substantially smaller than the diameter (1 mm) of the sample and because the lenses are oriented randomly, we assume that the dilatation is isotropic.

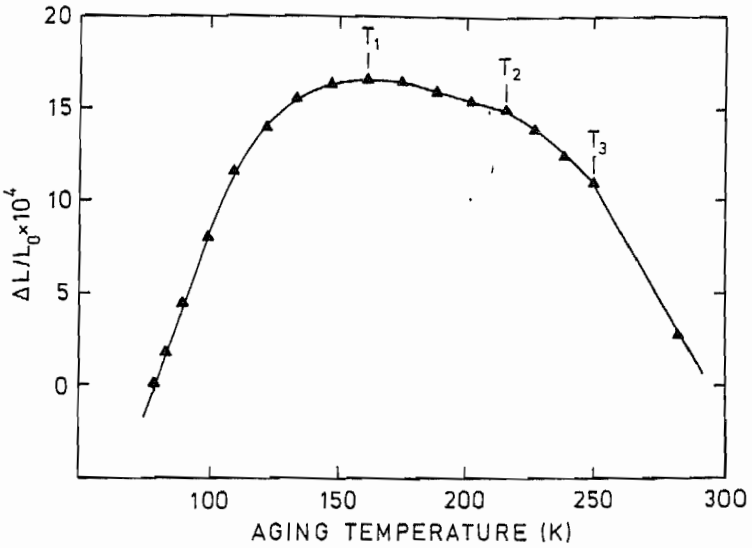


**FIG. 36.** Dilatation of the Fe-18Ni-0.7C martensite on aging. The measurements were made at 77 K.

An abrupt elongation of the sample below $T_1$ is attributed to the formation of isothermal martensite. The changes of the unit cell volume of martensite on aging do not serve as an explanation for the elongation of the sample because these changes are opposite and small according to the neutron diffraction measurements. The present temperature range 77 - 160 K of the isothermal martensitic transformation coincides with the results of internal friction (for the Fe-20Ni-0.7C alloy, Fig. 20), electrical resistivity and magnetic susceptibility (Figs. 32 and 33, respectively). Using the unit cell volumes of martensite and austenite and the phase fraction of martensite at the virgin stage obtained from the neutron diffraction measurements, it was calculated from the present dilatometric data that a few percent of martensite was formed on heating below $T_1$. This is in accordance with the results of the structure factor measurements of the neutron diffraction reflections presented above.

Shrinking of the sample is observed above $T_1$. According to the interpretation of the internal friction data and the results of the positron-lifetime measurements (Figs. 28 and 29) carbon atoms are trapped by lattice defects, mainly dislocations. This results in the volume decrease observed by dilatometry. The two knees $T_2$ and $T_3$ coincide with those in electrical resistivity curves and they will be discussed below.

*Shear modulus*

Figure 37 shows frequency, which was measured simultaneously with the dilatometric measurement presented in Fig. 36. The lower curve is measured at aging temperatures and the upper curve at 77 K. The fact that the lower curve is identical to those obtained on continuous heating (see, *e.g.*, /29,35,80/), indicates that cycling procedure itself does not affect the results. The monotonous, quite linearly increasing behavior of the upper curve is very interesting. This curve possesses no

remarkable changes in slope at about 200 K, which indicates that the typical minimum at this temperature observed in the previous frequency measurements (*e.g.*, /29,80/) is of some dynamical origin (there may be also a contribution of thermal expansion) and does not represent any permanent effects caused by aging. Another notable feature of curve 37a is the rather large overall increase of the frequency. Our previous measuremets made with the same alloy /81/ showed that the frequency curve levels off above room temperature and starts to increase again at about 370 K probably due to the formation of ε-carbide.

The relative change of shear modulus is obtained from the relative change of frequency by performing a dilatation correction with the expression (2) shown on page 16. For the correction to be exact, it is of great importance that dilatometric and frequency measurements are made simultaneously with the same sample as was done here. The relative shear modulus was calculated from the relative frequency (Fig. 37a) using the dilatometric data (Fig. 36). The result is shown in Fig. 38.

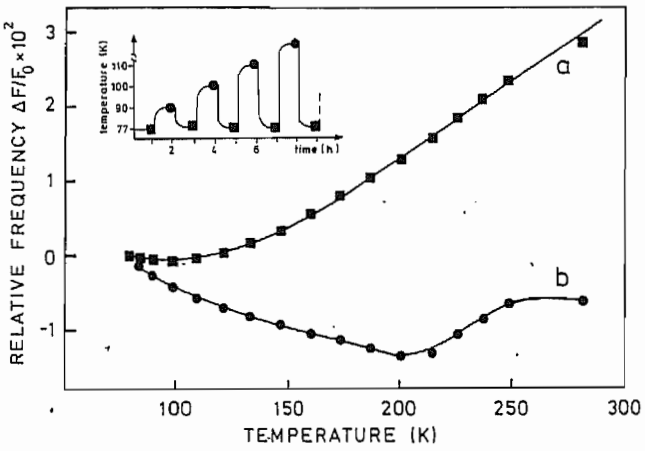


**FIG. 37.** Relative frequency measured at 77 K (a) and at aging temperatures (b). The thermal cycle is shown as inset. Alloy: Fe-18Ni-0.7C /34,35/.

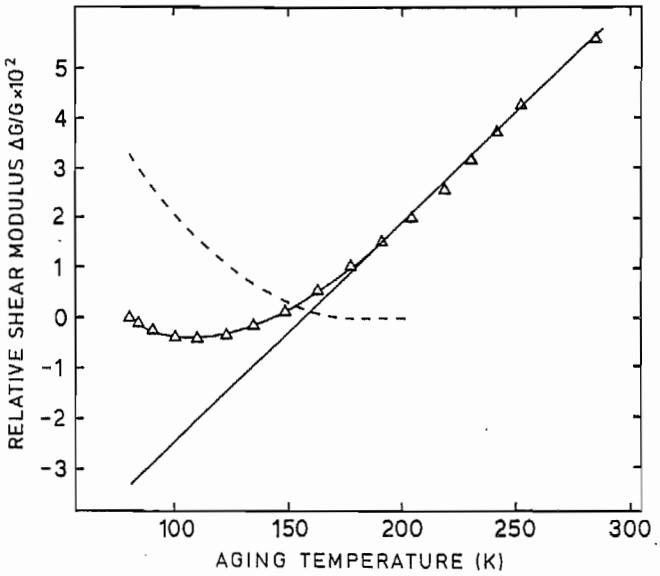


**FIG. 38.** Relative shear modulus of the Fe-18Ni-0.7C martensite (at 77 K). The dashed line represents the deviation of the shear modulus from linear behavior.

It is seen in Fig. 38 that above 170 K the increase is rather linear. The deviation from linear behavior is denoted by a dashed curve. This curve decreases monotonously and levels off at about 160 K and it is attributed to the formation of isothermal martensite. The shear modulus of martensite is smaller than that of austenite. The shape of this curve is very similar to the resistivity curve below 200 K shown in Fig. 32.

It is surprising that the behaviour of shear modulus is so linear and insensitive to the details of the low temperature aging: all other physical quantities presented above revealed a great variety of effects during the 2nd and 3rd stages of aging (the 1st stage does not exist in the Fe-18Ni-0.7C alloy). To clarify the role of carbon in the behavior of shear modulus, the results of a nearly carbonless

Fe-33.5Ni alloy (carbon content 0.01 %) are compared. In this alloy, only the 1st stage of aging occurs. Because this is nearly an invar alloy, the thermal expansion is small and continuous heating can be used instead of the cycling procedure, and no dilatation correction is needed for calculating the values of the relative shear modulus. Figure 39 shows the frequency during cooling of the austenitic Fe-33.5Ni sample from 370 K to 80 K and during the subsequent heating back to 370 K. The decrease of frequency on cooling was observed to be reversible and it is due to the softening of the austenite lattice. As mentioned above, thermal expansion is very small and cannot serve as an explanation here (besides, its effect on frequency would be opposite). The neutron diffraction measurement (Fig. 18) showed that the austenite line width remains unchanged during cooling. This means that no strains appear in austenite which could explain the frequency behaviour in Fig. 39. Martensitic transformation starts at 125 K (compare with Fig. 23) with a large burst. This leads to a decrease of the frequency as expected due to the less rigid lattice of martensite. Further martensitic bursts cause the large scattering of the points below $M_s$ temperature.

During heating of the freshly formed martensite, the frequency increases about 8 %. In Figure 3 in Ref. /I/, it was shown that this increase is irreversible and is caused by the aging: heating of the aged martensite (at different temperatures) revealed constant frequency. It is surprising that the shape of the heating curve in Fig. 39 so closely resembles the curve of the Fe-18Ni-0.7C martensite shown in Fig. 38, although the aging behaviour of these two alloys is completely different. The fact that the shapes of the line width curves of the different austenite peaks measured by neutron diffraction (shown in Figs. 18 and 19) are very similar to the shear modulus curves (upside-down) give a sign that the inrease of the shear modulus could be caused by stress relaxation (in austenite and martensite). Another notable feature in the heating curve in Fig. 39 is that it reaches the value which initial austenite had at $M_s$ temperature.

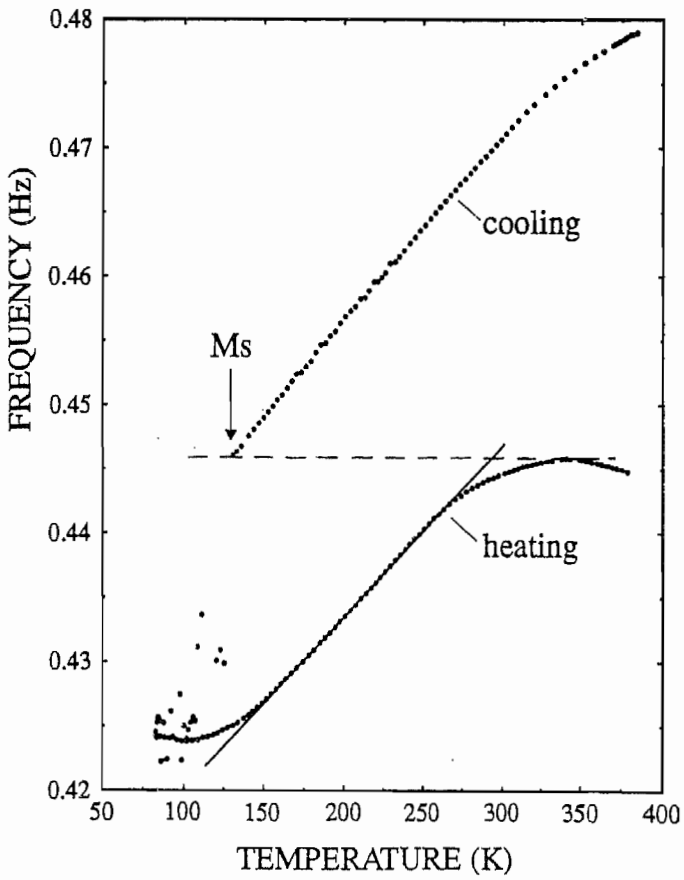


**FIG. 39.** Frequency of the Fe-33.5Ni alloy during cooling of the initial austenite and during heating of the freshly formed martensite.

Finally, after presenting in this work the results obtained with different experimental methods which revealed several phenomena occurring during the three stages of aging, the shear modulus turned out to be rather insensitive to the details of the aging. The validity of the present observations made using only two alloys and conclusions proposed here will be tested by further experiments.

**Redistribution of carbon and nitrogen atoms**

Let us define clustering as a redistribution of interstitial atoms which leads to an increase in the number of interstitials in the immediate surroundings of the metal atoms. Therefore, ordering of interstitials in a solid solution, which usually has a repulsive character, is not necessarily accompanied by clustering. The Mössbauer spectra of the Fe-2.03C martensite reveal clustering of carbon atoms during low temperature aging at 223 - 293 K (Fig. 31a) according to the interpretation given in /18-21/. The aging mechanisms of the virgin iron-carbon martensite with some features of spinodal decomposition has been modelled on the basis of the transmission electron microscopy studies /22-25/. The early Mössbauer data were interpreted in terms of the formation of the $Fe_4C$ structure during aging /19-21/. However, the content of carbon in the carbon-rich regions of the modulated structure was evaluated as about 11 at% by means of atom probe field-ion microscopy (APFIM) /23/, which is closer to the $Fe_8C$ (or $Fe_{16}C_2$) stoichiometry. On the basis of the APFIM data, Taylor *et al.* /25/ drew the conclusion, that 'the high carbon phase which forms spinodally during the aging of Fe-C martensites will be isomorphous with the $\alpha''$ - $Fe_{16}N_2$ phase that precipitates during the tempering of Fe-N martesites' and tried to reassess the available Mössbauer data on Fe-N and Fe-C martensites.

The data for hyperfine fields and abundances for different sites according to studies /21,26,58,78/ are presented in Table 2. We have used the notations in the original papers in each column of Table 2. The interpretations are given in the last two columns using the notations proposed by Rochegude and Foct /82/. The notations $I_{\alpha'}$, $I'_{\alpha'}$ and $I''_{\alpha'}$ correspond to the first, second and third nearest iron neighbors of a carbon atom in octahedral interstitial sites and $0_{\alpha'}$ designates iron without interstitials in the three nearest neighbor shells. Iron atoms in ferrite are marked by $0_{\alpha}$. Two carbon atoms in a shell are denoted by II. The configurations are presented in Fig. 41. The interpretation given by Taylor *et al.* /25/ is based on the reassessment of the Mössbauer data on Fe-C martensite. The present interpretation is more traditional and is founded mostly on the results /18,21,58/. Before the discussion of the Mössbauer data on the aging of Fe-C martensite some comments on this reassessment will be given.

The interpretation /25/ of Fe-C martensite is based on the measurements of Fe-N martensite by DeCristofaro and Kaplow /83/ and more recently by Gochegude and Foct /82/ and was already discussed in /84,85/. The interpretation /25/ of spectral components A, B and C (Fig. 31a) as $0_{\alpha'}$, $I'_{\alpha'}$ and $I_{\alpha'}$ does not take into account the multicomponent structure of each line, which was evidenced, *e.g.*, in /21,26/.

**TABLE 2.** Hyperfine fields (in Tesla) and abundances (in Pct) for different sites in the Mössbauer spectra of Fe-C martensites.

| | Ino *et al.* [78] | | Génin *et al.* [26] | | | Gridnev *et al.* [21,58] | Sites according to | |
|---|---|---|---|---|---|---|---|---|
| | H(T) | Pct | H(T) | | Pct | H(T) | Taylor *et al.* [25] | present interpretation |
| | Quenched and measured at 77 K | | Quenched and measured at 77 K | | | Quenched at 4.5K and measured at 65 K | | |
| Freshly | - | | (E) | 37.6 | 6 | (A) (1) 37.4 | - | $I''_{\alpha'}$ |
| formed | (a) 35.5 | | (A) | 36.5 | 44 | (A) (2) 35.7 | $0_{\alpha'}$ | $0_{\alpha'}$ |
| martens- | (a) 34.1 | | | - | | - | - | - |
| ite | (a) 33.0 | | | - | | - | - | - |
| | - | | ($B_c$) | 33.4 | 10 | (B) (3) 33.5 | $I'_{\alpha'}$ | $I'_{\alpha'}$ |
| | (b) 31.5 | | ($B_a$) | 33.1 | 19 | (B) (4) 31.6 | - | $I_{\alpha'}$ |
| | (c) 27.0 | | (C) | 28.3 | 15 | (C) (5) 28.0 | $I_{\alpha'}$ | $II_{\alpha'}$ |
| | - | | (D) | 26.2 | 4 | (C) (6) 27.8 | - | $II_{\alpha'}$ |
| | - | | (F) | 16.5 | 2 | - | - | - |
| | Aged and measured at 300 K | | Aged at 293 K and measured at 77 K | | | Aged at 293K and measured at 65 K | | |
| Aged | (e) 37.1 | 8 | (E) | 37.6 | 8 | (A) (1) 38.2 | $0_{\alpha''}$ | $II'_{\alpha'}$ ($Fe_4C_x$) |
| martens- | (a) 35.5 | 11 | (A) | 35.5 | 54 | (A) (2) 35.9 | $I'_{\alpha''}$ | $0_{\alpha'}$ |
| ite | (a) 34.1 | 29 | | - | | (7) 34.6 | - | $0_{\alpha}$ |
| | (a) 33.0 | 23 | | - | | - | - | - |
| | - | | ($B_c$) | 32.4 | 4 | (B) (3) 33.5 | - | $I'_{\alpha'}$ |
| | (b) 31.5 | 12 | ($B_a$) | 32.4 | 8 | (B) (4) 31.6 | $0_{\alpha}$ | $I_{\alpha'}$ |
| | (c) 27.0 | 12 | (C) | 28.3 | 14 | (C) (5) 27.7 | - | $II_{\alpha'}$ ($Fe_4C_x$) |
| | (d) 26.4 | 5 | (D) | 26.2 | 10 | (C) (6) 27.9 | $I_{\alpha''}$ | $II_{\alpha'}$ ($Fe_4C_x$) |
| | (f) 18* | - | (F) | 16.5 | 2 | 19.4* | $II_{\alpha''}$ | ε-carbide* |

* aged at 363 - 373 K

The authors /25/ assume a larger reduction of the hyperfine field for Fe atoms with C neighbor as compared to the Fe-N case on the basis of the unpublished data obtained by Krasko in 1986. However, this statement does not agree with the larger electrical exchange between Fe and N atoms clearly seen when comparing the Mössbauer spectra of Fe-C and Fe-N austenites (see Fig. 40 and also /82,83-87/). The positive isomer shift of a doublet that belongs to the iron atoms with interstitials as nearest neighbors, is several times greater in the Fe-N austenite than in the Fe-C austenite (compare the relative shift between the doublets and the central line of the Fe-C and Fe-N austenites in Fig. 40). According to the interpretation of the isomer shift on the $^{57}Fe$ nuclei given by Walker *et al.* /88/, it means that nitrogen atoms contribute more electrons to the 3d-band of iron than

the carbon atoms, which can result in a greater reduction of the magnetic moment at the neighboring iron atoms in the Fe-N martensite.

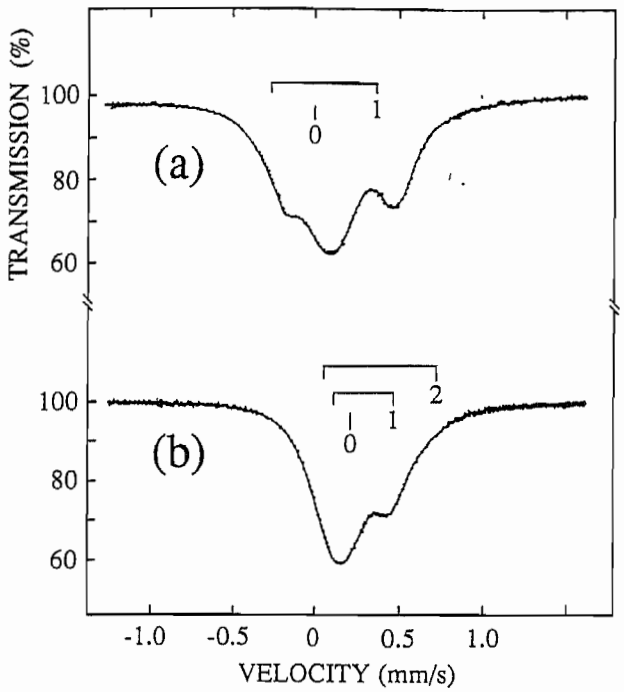


**FIG. 40.** Mössbauer spectra of the Fe-1.76C (a) and Fe-2.67N (b) austenites /89/.

In the Mössbauer spectrum of the aged martensite, Taylor *et al.* /25/ denoted the component A or (a) with H = 34.1 - 35.5 T as $I'_{\alpha''}$ and attributed it to the iron atoms which are now the second neighbors of carbon, while the component $B_a$ or $B_c$ with H = 31.5 - 32.4 T was denoted as $0_\alpha$ (iron atoms without carbon in the immediate surroundings; see Table 2, Fig. 41 and also /25,27,78/). It does not seem probable that iron atoms, occupying the planar positions of the octahedral interstitial sites in α-iron (Fig. 41a) and therefore having an immediate electronic exchange with the carbon atom are characterized by a larger magnetic moment than atoms of "pure iron". They denoted component B (Fig. 31a) of the virgin martensite as $I'_{\alpha'}$, *i.e.*, (b) in notation /78/ or $(B_c,B_a)$ in notation /26/ with H = 31.5 - 33.4 T (Table 2). This component almost disappears after aging. In the spectrum of the aged martensite, the authors /25/ denoted component A (Fig. 31a) as $I'_{\alpha''}$ that means component (a) in notation /78/ or A in notation /26/ with H = 34.1 and 35.5 T respectively (Table 2). On the basis of such an interpretation, it is not clear why the hyperfine field at the nuclei of iron atoms $I'_{\alpha'}$ should increase during clustering. It is not clear either how the fraction of these atoms, the second neighbors to the carbon atoms (Fig. 41a), can increase during aging, which occurs according to the interpretation /25/ (see, for example, intensities of the components in the spectra of virgin and aged martensites in /26,78/).

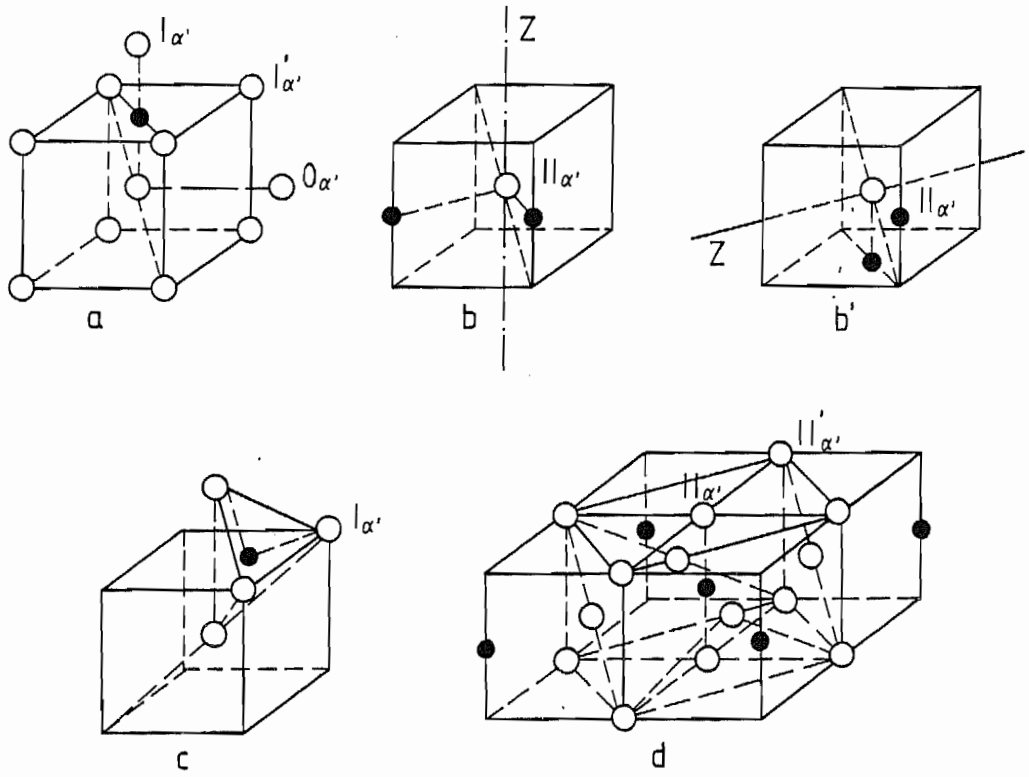


**FIG. 41.** Possible atomic configurations in the virgin and aged martensites (see also Table 2): iron atoms in the vicinity of a single carbon atom in the octahedral interstitial site (a), iron atoms with two carbon atoms as second neighbors (b), and one carbon atom in the first and one in the second neighbor shell (b'). Iron atoms in the vicinity of a single carbon atom in the tetrahedral interstitial site is shown in (c) and the structure of $Fe_4C$ in (d). Orientations of the electrical field gradient are denoted by *z*. The axis of easy magnetization is assumed to be (001).

Another question arises concerning the Mössbauer data on the kinetics of clustering. The structure of the type $\alpha''$ - $Fe_{16}N_2$ has no iron atoms with two carbon atoms as nearest neighbors $II_{\alpha'}$ and at the same time, according to the interpretation /25/, these iron atoms do not exist in the virgin martensite either. It means that the fraction of iron atoms $I_{\alpha'}$, the first neighbors of carbon (see Fig. 41a), cannot be changed during spinodal decomposition, if the interpretation /25/ is valid, and therefore this component has to remain unchanged after clustering. However, the studies /18-21, 26,58,78/ clearly revealed that component C, denoted as $I_{\alpha'}$ by Taylor *et al.* /25/, substantially increases during aging (according to Fig. 31a, see also abundances of the same iron environments C and D in /26/).

In the following, we shall compare the redistribution of interstitials during aging of the virgin Fe-C and Fe-N martensites and discuss the possible isomorphism /25/ between the carbon-rich phase in the aged Fe-C martensite and the $\alpha''$ - $Fe_{16}N_2$ phase in the Fe-N martensite. Shown in Fig. 31b is a part of the Mössbauer spectrum of Fe-2.75N (wt%) alloy after cooling to 9 K, aging at 200 K and at room temperature for 30 min. The spectra were measured at 9 K. These data have been published in detail elsewhere /V/ together with X-ray diffraction, electrical resistivity and magnetic

susceptibility results. Let us compare the changes of the Mössbauer patterns during the low temperature aging of the Fe-C (Fig. 31a) and Fe-N (Fig. 31b) martensites. Independent of the interpretation, it is clearly seen that aging essentially changes the nearest neighborhood of iron atoms in the Fe-C martensite: it increases the fraction of Fe atoms with the two C atoms in the first neighbor shell $II_{\alpha'}$ and diminishes the fraction of Fe atoms with one C atom as the nearest neighbor $I_{\alpha'}$, if one follows the interpetation of the Mössbauer spectra given in /18-21/. In contrast, no significant changes take place in the immediate neighborhood of Fe atoms during the low temperature aging of the virgin Fe-N martensite (Fig. 31b). Also, when taking into account the higher mobility of nitrogen atoms in α-iron as compared to carbon atoms, one can conclude that there is a significant difference in the low temperature aging mechanisms of the virgin Fe-C and Fe-N martensites. No clustering occurs during aging of the Fe-N martensite because the immediate neighborhood of the iron atoms does not change. The present results support the concept of Mittemeijer /90,91/ who proposed that at early stages of aging of the Fe-N martensite ordering of nitrogen occurs without the cluster formation. Ordering in the Fe-N martensite below room temperature was earlier observed by Suyazov *et al.* /92/ using transmission electron microscopy.

The structure of the carbon-rich phase formed during low temperature clustering of the Fe-C martensite remains unclear. The structure $Fe_4C$ (Fig. 41d) was suggested for carbon-rich regions in the early Mössbauer studies /19-21/ and later the model was corrected by Génin *et al.* /26-28/ who proposed that the structure of extended multiplets could be expressed by the formula $Fe_6C$. The $Fe_4C_x$ structure was also proposed by Ino *et al.* /78/ on the basis of their observations of a weak component with H = 18 T in the spectrum of Fe-C martensite aged at 363 K. However, taking into account the fact that during aging at 363 K, the Fe-C martensite is significantly decomposed and ε-carbide begins to precipitate according to the well known results of the electron microscopy studies (see, for example, /93,94/), we can attribute this component to iron atoms in ε-carbide. The hyperfine structure of ε-carbide consists of two components /95/ and one of them has a hyperfine field near 18 T.

Thus, the Mössbauer spectra give clear evidence for clustering during aging below room temperature and the change of component C (see Fig. 31a and Table 2) is consistent with the expected behavior of the iron atoms with two carbon atoms as the first and second neighbors. Also, convincing data about ordering of carbon atoms in clusters (extended multiplets according to the terminology in /28/) were obtained in TEM studies by Génin *et al.* /28/.

In accordance with the interpretation of the Mössbauer spectra of the aged Fe-C martensite based on the existence of two carbon atoms as nearest neighbors of an Fe atom (Table 2), which in our opinion is the most acceptable of the interpretations available, it can be assumed that $x < 1$ in the structure $Fe_4C_x$ of these regions. This agrees with the APFIM data /23,25/ of the carbon content in the carbon-rich regions of aged martensite. Formation of the structure $Fe_4C_x$ can be understood on the basis of the insufficient mobility of carbon atoms below room temperature. It can be also added, that the component with the highest hyperfine field, about 37 T, which is denoted as $II'_{\alpha'}$ in our

interpretation, as (e) in /78/ and as E in /26/ (see Table 2), is naturally attributed to iron atoms in the corners of the elementary unit of the $Fe_4C$ structure as shown in Fig. 41d.

The behavior of the *c/a* ratio of virgin martensites during the third stage of the low temperature aging (250 - 300 K, see Fig. 13) needs some comments in relation to clustering. In this temperature range tetragonality does not significantly change in the alloy Fe-33.5Ni, but it decreases in the twinned Fe-Ni-C martensites (shown in Fig. 13) and increases in the Fe-2.39N martensite (Fig. 14). In the plain carbon and Fe-3Mn-1.6C martensites the increase of tetragonality occurs even below 200 K. It is natural to expect a decrease of the *c/a* ratio in Fe-Ni-C martensites during aging as a result of the decomposition of the solid solution. Nickel increases the thermodynamic activity of carbon in α-iron and assists decomposition of martensite. At the same time, the increase of the nickel content shifts the beginning of the reduction of the *c/a* ratio at the third stage of aging to lower temperatures as shown in Fig. 13.

Changes of electrical resistivity of the Fe-Ni-C alloys during the low temperature aging are shown in Fig. 32. The behavior observed is typical of aging of virgin Fe-C martensites (see, *e.g.*, /79/). The increase of resistivity is attributed to static displacements of atoms caused by clustering at an early stage. By means of an analogy between the thermal vibrations and the static displacements it is possible to evaluate the increase of resistivity using the data of the attenuation of the X-ray diffraction peaks of martensite /96/. Such an evaluation was performed by the present author for the alloy Fe-18Ni-0.7C using the martensite (002) reflection. The shape of the resistivity curve could be explained successfully by this simple model. The results of the neutron diffraction structure factor measurements (shown in Fig. 35) revealed no increase of static displacements during aging below 200 K. This is in accordance with the electrical resistivity results (Fig. 32) which do not show any significant increase in this temperature range either. Between 200 and 300 K, the structure factors $F^2_{(112)}$ and $F^2_{(211)}$ clearly decreased indicating an increase of the static displacements due to clustering of carbon atoms. This result is also in agreement with an abrupt increase of resistivity starting at about 250 K (denoted by $T_3$ in Fig. 32).

An increase of magnetic susceptibility during aging (Fig. 33) means that magnetic domain walls can move more easily in the regions depleted of carbon as a result of clustering. In the case of the Fe-25Ni-0.7C alloy, the increase of susceptibility between 100 and 200 K is ascribed to the relaxation of stresses due to the break of coherency at the interfaces between martensite and retained austenite. For the alloy Fe-20Ni-1.2C this increase is not observed, because the coherency effects are smaller due to the lower nickel content and because of the overlapping with the decrease of susceptibility caused by the early stages of the redistribution of carbon atoms. This decrease is largest for the alloys Fe-18Ni-0.7C and Fe-20Ni-0.7C. The onsets of the abrupt increase of resistivity and susceptibility are slightly shifted to lower temperatures with increasing nickel contents, which also gives evidence that the third stage of aging starts earlier in the high nickel martensites. This effect is in agreement with the *c/a* measurements (Fig. 13) which revealed that the inrease of nickel content shifted the reduction of tetragonality to start at lower temperatures.

The dilatometric measurement made with the Fe-18Ni-0.7C alloy confirmed that isothermal martensite is formed in the temperature range of 77 - 160 K. This is in agreement with internal friction, resistivity, susceptibility and neutron diffraction results. Contraction of the sample, observed above 160 K (possibly even below 160 K, but it may be masked by the antagonistic effect of the formation of martensite), is an evidence for pinning of dislocations by carbon atoms, which occurs in this temperature region according to the present positron-lifetime and internal friction measurements. Further contraction of the dilatometer sample at higher temperatures is attributed to the redistribution of carbon atoms. Knee $T_2$ in the dilatometric curve may be a sign of the start of carbon diffusion leading to the formation of small clusters. The temperature of the abrupt increase in resistivity and susceptibility coincides with the second knee $T_3$ in the dilatometric curve. The proper clustering of carbon atoms is started in this temperature range as also evidenced by Mössbauer measurements.

The change of electrical resistivity and magnetic susceptibility during aging of Fe-2.39N martensite reflects a different kind of redistribution of nitrogen as compared to carbon. Unlike in Fe-C alloys, electrical resistivity of the Fe-2.39N alloy increases during martensitic transformation. Therefore, formation of isothermal martensite during low temperature aging is accompanied by an increase of resistivity below 100 K (Fig. 34). Resistivity starts to decrease above 100 K possibly due to the break of coherency at the austenite-martensite interface and continues to decrease at higher temperatures as a result of long range atomic ordering. Magnetic susceptibility increases first during the martensitic transformation and during the break of coherency at about 100 - 200 K. Similar effect was observed also in the Fe-33.5Ni martensite /I/. The decrease of the susceptibility of the Fe-2.39N alloy occurs in the same temperature range as the increase of tetragonality in Fig. 14 and is attributed to the third stage of aging of the Fe-N martensites caused by the long range atomic ordering corresponding to the structure $Fe_{16}N_2$.

Mössbauer measurements revealed that no clustering of nitrogen atoms occurred in the Fe-2.39N martensite during aging. The resistivity and susceptibility results support this conclusion. No increase in resistivity and susceptibility, typical of Fe-Ni-C martensites above 250 K and which is attributed to clustering of carbon atoms, was observed during aging of the nitrogen martensites. In contrast, both susceptibility and resistivity decreased consistently.

It is noteworthy that the overall decrease of resistivity (even 35 %) for the Fe-2.39N alloy is significantly larger than the resistivity changes in the Fe-Ni-C alloys. The explanation may lie in the high nitrogen content (8.9 at%) of the alloy which is quite near the stoichiometric composition (11.1 at%) of the structure $Fe_{16}N_2$. Hence, the ordering of nitrogen atoms during aging can occur throughout the whole volume of martensite without any local increase of nitrogen concentration.

Special attention should be paid to the increase of tetragonality in the Fe-C and Fe-Mn-C martensites. This increase begins at temperatures below 200 K, where the carbon atoms are essentially immobile during the measurements. Thus, it cannot be caused by a decomposition of the solid solution. The nature of the abnormally low tetragonality observed in the plain carbon /6/ and

manganese alloyed /7/ martensites has been the object of many discussions, resulting so far in no success (see, for example, /54, 97/). One of the most promising theoretical studies regarding this topic was performed by Mirzajev *et al.* /98/ who showed that thin planar defects, like twins (110) <110>, affect the distribution of the intensity of the scattered X-rays and can shift the positions of the X-ray diffraction peaks. The reason for such a shift does not lie in superposition of the normal and twin reflections as proposed in /53/. It means that deviations of tetragonality from the normal values obtained in such alloys are apparent and probably do not indicate any real change in the crystal lattice parameters. Thus, the reason for the increase of tetragonality during aging observed in the temperature region where diffusion of carbon atoms does not occur, can lie in some relaxation of stresses changing the distribution or thickness of such planar defects.

Shear modulus was measured for the alloys Fe-18Ni-0.7C and Fe-33.5Ni. In both cases shear modulus increased quite linearly with increasing aging temperature. The behavior of shear modulus turned out to be very similar both in the dislocated carbon-alloyed Fe-18Ni-0.7C martensite possessing the 2$^{nd}$ and 3$^{rd}$ stages of aging and in the twinned, practically carbonless Fe-33.5Ni martensite in which only the 1$^{st}$ stage is present. The fact that shear modulus is rather insensitive to the details of the aging process (at least of the 2$^{nd}$ and 3$^{rd}$ stages) unlike most of the other physical quantities measured in this work, may be a sign of some universal factor which is common to the aging of different alloys. In addition to the explanation proposed in /I/, the contribution of some changes in the electronic structure or in the interatomic bonds due to some stress relaxation cannot be excluded. Neutron diffraction measurements provide information about stresses and strains in austenite and martensite. Figures 18 and 19 revealed rather linear decrease of austenite line width during heating, which supports the assumption that some stress relaxation could explain the behaviour of the shear modulus. However, before performing systematic measurements on different alloys with different kinds of moduli measurements this question cannot be answered exhaustively.

## EFFECTS OF LOW TEMPERATURE DEFORMATION ON THE LATTICE STRUCTURE AND AGING OF MARTENSITE

The effects of aging on the deformation mechanisms of martensites at low temperatures has been studied little /99,100,101/. The most detailed studies were performed by Kajatkari with Fe-18Ni-0.7C martensite /99/ . Kajatkari deformed virgin and aged martensites mainly at 213 K and observed that the deformation mechanism was twinning in both cases. The twins were very irregularly shaped in the virgin martensite when deformed at a slow compression rate and straight in the aged martensite. Aging of the low temperature deformed martensite is not studied in detail so far. Only some preliminary results have been reported in /102,VIII/.

Alshevskii and Kurdjumov observed that tetragonality decreased during deformation of Fe-14Ni-1C martensite at 77 K /103/. These measurements were made at room temperature. They assumed that carbon atoms were redistributed partially also to *a*- and *b*-octahedral sites. Aging of the

deformed martensite was not discussed in /103/. Independently of those results, we observed that the tetragonal lattice of the Fe-25Ni-0.7C martensite (*c/a* about 1.08) is collapsed to a completely cubic structure when the virgin martensite is deformed at 210 K /102/. Some years earlier, a significant reduction of tetragonality in the Fe-20Ni-1.2C martensite was found during an *in situ* deformation at 77 K in the X-ray sample holder. We obtained also evidence for the redistribution of carbon atoms by Mössbauer measurements made with this alloy at 77 K after forging a foil sample in liquid nitrogen and subsequently in alcohol at 210 K /102,VIII/. This experiment revealed that carbon distribution was drastically changed during deformation at 210 K. Both X-ray and Mössbauer results could be explained by the assumption that carbon atoms are able to move during deformation possibly by some slip mechanism from the octahedral sites on the *c*-axis to the sites on the *a*- and *b*-axes. This process must lead to a decrease of the energy stored in the stress fields of distortion dipoles around carbon atoms. Assuming that clusters are formed during aging (in undeformed martensite) to minimize the total strain energy, it was expected that deformation prevents clustering, which was evidenced by X-ray diffraction, Mössbauer, resistivity /102,VIII/ and later by magnetic susceptibility and dilatometric measurements. Gavriljuk *et al.* /104/ have studied the redistribution of carbon atoms in a binary iron-carbon martensite after deformation at room temperature by Mössbauer spectroscopy. They concluded that carbon atoms were captured from the solid solution by microcracks, which explanation can be very probable.

### Tetragonality reduction during low temperature deformation

#### *Fe-25Ni-0.7C alloy*

It was shown above for the Fe-33.5Ni martensite that deformation at 110 K led to a cubic lattice structure. This was accounted for by the break of coherency at the austenite - martensite interface. Figure 42 shows diffraction patterns of Fe-25Ni-0.7C alloy after subsequent deformations at 110, 120 and 130 K which were made using the deformation sample holder described in Figure 8. Measurements were made at 60 K between each stage of deformation. It is seen that deformation at higher temperature leads to lower tetragonality, which is ascribed to the increased mobility of dislocations. It is obvious that in the beginning, the reduction of tetragonality is caused by the break of coherency at the austenite - martensite interface, but during the higher degree of deformation, the redistribution of carbon atoms must also be taken into account, as proposed in /102,VIII,I/ and confirmed by Mössbauer spectroscopy.

It was ascertained by neutron diffraction measurements that the single peak of martensite appearing after deformation is really related to the cubic symmetry of the lattice and not, for instance, to the texture caused by the deformation or to any surface effect detected by X-rays. The sample for neutron diffraction measurements was prepared by breaking the cold rolled (at 210 K) strips into small pieces in liquid nitrogen. These pieces were transported in liquid nitrogen to the diffractometer

(in St. Petersburg) and inserted in the sample holder in a random order. The neutron diffraction measurement revealed that the martensite peaks were single and symmetrical, which indicates that the lattice is thoroughly cubic.

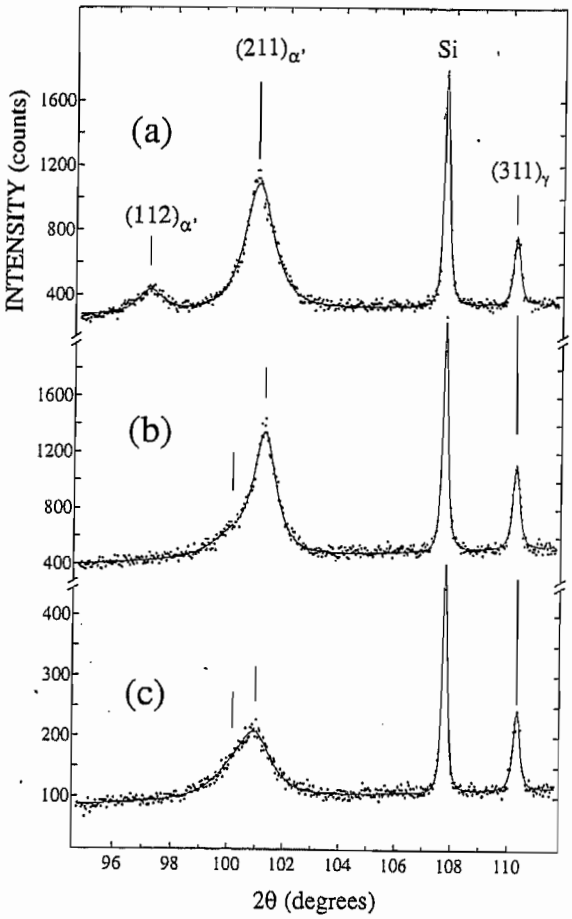


**FIG. 42.** X-ray diffraction patterns of the Fe-25Ni-0.7C martensite: deformed at 60 K and further at 110 K (a), subsequently deformed at 120 K (b) and still further at 130 K (c).

***Fe-9Ni-1.4C alloy***

The X-ray diffraction patterns of the undeformed Fe-9Ni-1.4C martensite measured at room temperature after quenching in liquid nitrogen are shown in Fig. 43c. The tetragonal (112) - (211) doublet and the retained austenite peaks are clearly resolved. The spectra of the martensite deformed at 77 K and at room temperature are presented in Figs. 43a and b, respectively. It is noteworthy that the amount of retained austenite is very small in spectrum 43a, which is due to the formation of the strain induced martensite, when deformed below the $M_d$ temperature. Fig. 43b seems to reveal an increase in the amount of martensite during room temperature deformation. This result is interesting because $M_d$ temperature of this alloy was measured to be above RT. However, the intensity ratio analysis is not very reliable in this case due to a large grain size and texture.

For deformation of the Fe-9Ni-1.4C alloy in liquid nitrogen neither the bending device nor the rolling machine could be used because the samples tended to break. The deformation was performed by pressing the samples between hard plates. At 77 K the sample was broken into small

pieces. These pieces were collected and transported in liquid nitrogen to the sample holder which was simply a horizontally placed rotating shallow cup filled with liquid nitrogen so that the sample was just immersed. No windows were needed in this construction because the vapour of the boiling nitrogen prevented water condensation on the sample surface. The measurement at 77 K revealed a symmetrical single (211) reflection indicating that the martensite lattice had become completely cubic. After the measurement at 77 K the sample was heated to room temperature and measured at RT (Fig. 43). Thereafter the specimen was heated for 2.5 hours at 100 °C. The single martensite (211) reflection remained practically unchanged after aging at these temperatures.

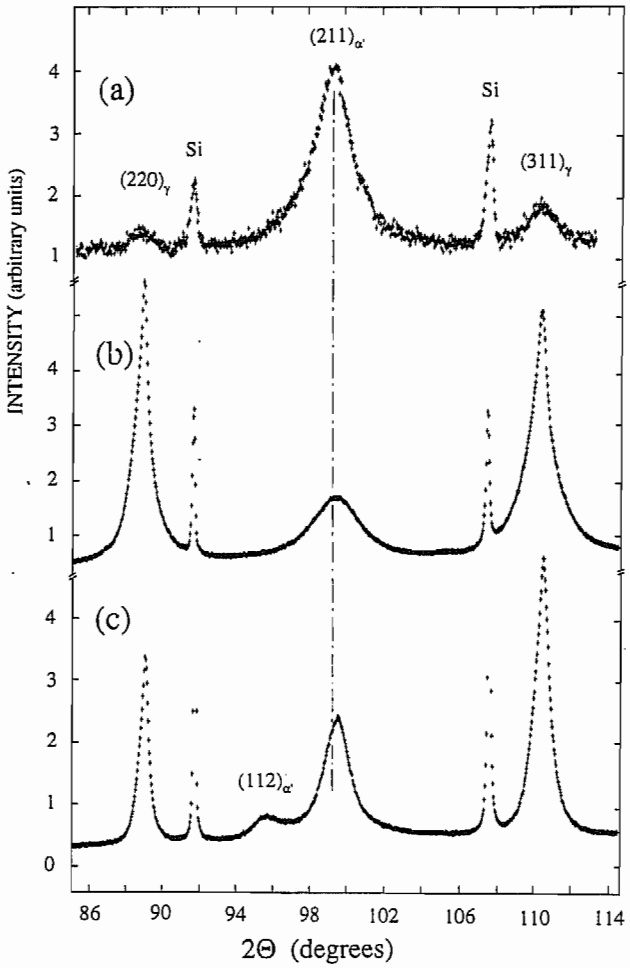


**FIG. 43.** X-ray diffraction patterns of the Fe-9Ni-1.4C alloy:
(a) The freshly formed martensite was deformed at 77 K.
(b) The deformation was performed immediately after heating the sample from liquid nitrogen to room temperature.
(c) Undeformed martensite.
These measurements were made at RT. Silicon powder on the sample surface was used for calibration.

Aged high-carbon martensite is normally very brittle at room temperature. The alloy Fe-9Ni-1.4C martensite is regarded as an example of brittle martensite; microcracking during aging was studied by Pietikäinen (see,*e.g*, /11/) in the alloys which were very close to the present alloy. Figure 44a shows optical micrograph of the Fe-9Ni-1.4C martensite aged at room temperature. Zig-zag martensite lenses with straight midribs are seen. Some microcracks have formed during aging at the intersections of the lenses.

Against this background, the present results of the deformation of this martensite can be regarded as interesting. Deformation of even 75 % could be achieved at room temperature, when deformation was performed immediately after quick heating to room temperature. During such a

heavy deformation the sample cracked but it remained as one piece. Optical micrograph of this sample is shown in Fig. 44b. The martensite lenses are clearly bent and very irregularly shaped. Even the midribs which are straight in undeformed samples are now curved. Besides, practically no microcracks have appeared in the bent lenses. The author emphasizes, however, that the comparison of the number of microcracks must be considered only as an illustration of the difference between the deformed and undeformed martensites. No detailed analysis is made yet. We can conclude that the present martensite was deformed plastically and it was rather ductile. In experiments where deformation was preceded by aging at room temperature, the sample broke in a brittle manner into small pieces during deformation.

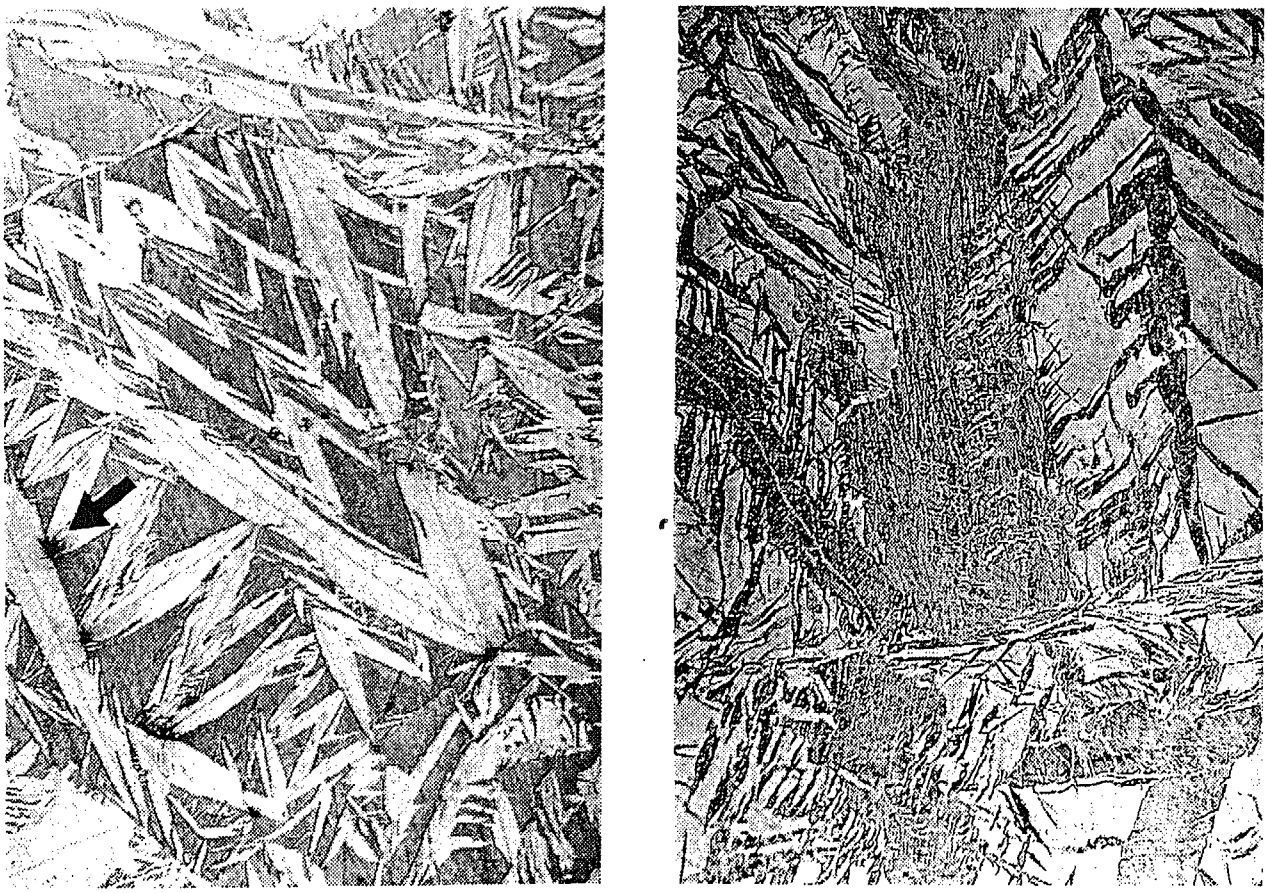

(a) (b)

**FIG. 44.** Optical micrographs of the Fe-9Ni-1.4C martensite (magnification 700x):
(a) Undeformed martensite. Martensite is seen as light areas. Microcracks appear as black spots (indicated by an arrow).
(b) Martensite deformed 75 % at room temperature (the sample is the same as in Fig. 43b). Martensite is seen as dark areas.

*Fe-20Ni-1.2C alloy*

X-ray diffraction results of the deformed Fe-20Ni-1.2C martensite were described in /102,VIII/. It was shown that deformation at 77 K and at 210 K led to a reduction of tetragonality,

but the lattice did not become completely cubic. An extra peak, denoted by C in Figs. 1b-d in /VIII/, appeared during deformation. This peak did not exist in the diffraction pattern of the undeformed martensite (Fig. 1a in /VIII/). The mutual intensity ratios in Figs. 1b-d exclude the possibility that peak C would be a component of an orthorhombic reflection. Probably, it belongs to the cubic martensite phase formed during deformation. An intermediate peak between the reflections $(211)_{\alpha'}$ and $(112)_{\alpha'}$ observed in undeformed lenticular Fe-18Ni-0.9C martensite was discussed by Chen *et al.* /44/. They hypothesized that this peak could be due to a local redistribution of interstitials over *a*-, *b*- and *c*- type octahedral interstices at locations of high internal stresses, such as at martensite plate intersections. This proposal was discussed in more detail in /105/. In the present Fe-20Ni-1.2C martensite (which is thin plate by morphology) this intermediate peak does not exist, possibly due to the better accommodation of the plates and lower strains at the intersections in this alloy, but peak C appeared after deformation. Hence, we can assume that peak C is a sign of cubic martensite which is produced by deformation. Possibly the degree of deformation was not high enough to produce more of this phase in the experiment presented in /VIII/.

## Redistribution of carbon atoms during deformation

### *Mössbauer spectroscopy*

The redistribution of carbon atoms during the low temperature deformation of the Fe-20Ni-1.2C martensite was studied by Mössbauer spectroscopy. Because the details of this measurement are reported elsewhere /VIII/, only the main results are discussed here. The fitting of the binary high-nickel alloys can be performed only by using distributions of hyperfine fields. Nickel alloying causes broad and asymmetrical peaks with different widths. It is evident that when adding carbon to this system, the number of different Ni- and C- configurations around iron atoms expands too high for performing exact calculations. This problem can be avoided by the utilization of the carbonless Fe-20Ni reference patterns as was done in /106,VII/. The advantage of this method is the very small number of fitting parameters, which leads to more reliable results. The simplified version of this fitting procedure used for the present analyses is presented in /VIII/.

The Mössbauer patterns of the deformed Fe-20Ni-1.2C martensites are shown in Fig. 3 in reference /VIII/. Two different models for the distribution of carbon atoms were tested. In the first model carbon atoms were assumed to reside only in the octahedral sites on the *c*- axis and in the second model all axes were considered equal. In both cases the carbon atoms were assumed to be randomly distributed in the octahedral sites. The difference between the two models lies in the intensities of the different component patterns corresponding to the different carbon atom configurations seen by an iron atom. The energy parameters (hyperfine field, quadrupole splitting and isomer shift) were the same in both of the models. It turned out that the broad lines of the spectra prevented the conclusive determination of which distribution is right, but the intensities of the second

and the fifth peaks in the spectra provided indirect information about the distribution of carbon atoms between the different sublattices.

The intensities of peaks $I_2$ and $I_5$ depend on the direction of magnetization in the sample in the following way: if $I_2 = I_5 = 0$, magnetization is perpendicular to the sample surface and if all the intensities (in pure Fe) are related as $I_1 : I_2 : I_3 : I_4 : I_5 : I_6 = 3 : 2 : 1 : 1 : 2 : 3$, the distribution of the magnetization is random. The fitting revealed that $I_2$ and $I_5$ were so small that magnetization must tend to be perpendicular to the sample surface. If the magnetization in the unit cell is assumed to be parallel to the *c*- axis, as shown by Entin *et al.* /107/, the fitting result obtained in /VIII/ means that the *c*- axes of the martensite lattices also tend to be perpendicular to the surface. This means that deformation at 77 K has produced texture. Intensities $I_2$ and $I_5$ of the spectra corresponding to the further deformation at 210 K revealed quite a random distribution of magnetization. It seems improbable that texture would have disappeared during this deformation. Instead, we can assume that texture remains, but magnetization is no longer fixed to the *c*- axis and it can orient more freely in the unit cell, which must also lead to magnetic softening of martensite.

It was shown above that low temperature deformation produces cubic martensite. Besides, the *a*-, *b*- and *c*- axes have become equal also magnetically. There are two possibilities to explain this behavior: in deformed martensite, carbon atoms occupy all octahedral sites equally as proposed in /103,102/ or carbon atoms have left the solid solution and are trapped, *e.g.*, by the microcracks /104/. Capture of carbon atoms by the dislocations does not serve as an explanation here, because dislocations cannot absorb carbon atoms more than about 0.2 wt% according to Speich /108/ (for Fe-C martensites) and 0.08 % according to Oketani *et al.* /109/ (for Fe-Ni-C martensites). In addition, internal friction measurement made after deformation at 130 K by twisting (10 %) during heating of the freshly formed Fe-20Ni-0.7C martensite revealed that very high peak $A_3$ centered at 210 K appeared (Fig. 45). This result reveals that the number of mobile dislocations has increased during deformation: more new dislocations have been generated during deformation than the existing dislocations locked by the pinning by carbon atoms. Similar, but a very small, increase of internal friction was also observed for Fe-33.5Ni(-0.01C) martensite after deformation at 77 K (see Fig. 20). Fig. 45 also shows that coherency peak $A_2$, which is present in the pattern of the undeformed martensite, is absent in the spectrum of the deformed martensite. This result is the same as obtained for the Fe-33.5Ni alloy (Fig. 20) and reveals that deformation has broken the coherency at the interface between martensite and austenite.

In order to be able to conclude how carbon atom distribution chances during deformation, further experimental evidence is required. One interesting possibility would be nuclear magnetic resonance spectroscopy. Measurements made for the samples alloyed with $^{13}C$ isotope would be a useful method to obtain direct evidence for the existence of the carbon enrichment (even graphite) in the possible microcracks of the deformed martensite. Using Mössbauer spectroscopy graphite was

already observed by Gavriljuk and co-workers /104/ in the Fe-C sample which was deformed at room temperature. For direct observations of the variation of the local carbon concentration, the atom probe field ion microscopy would be a suitable method.

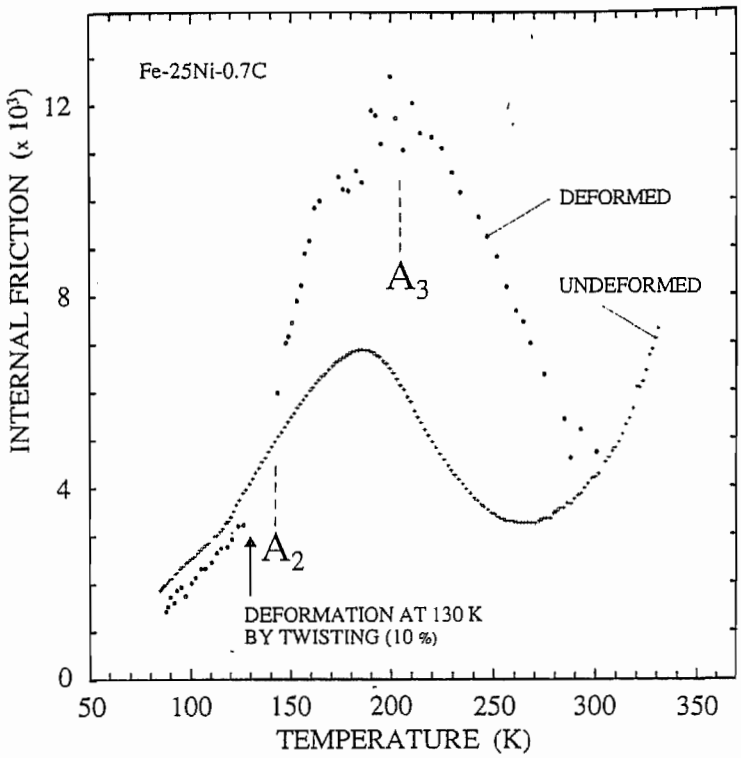


**FIG. 45.** Internal friction of the freshly formed Fe-25Ni-0.7C martensite during heating:
- Undeformed martensite (denoted by crosses)
- Deformed martensite (denoted by points). Deformation was performed during heating at 130 K by twisting.

### Aging of deformed martensite

X-ray diffraction measurements made with the Fe-25Ni-0.7C and Fe-9Ni-1.4C martensites revealed that aging below 100 °C did not cause any essential changes in the lattice: the single peaks of the cubic lattice remained quite well at their positions, having widths and intensities independent of the deformation temperature. The changes in the carbon distribution were significantly smaller than in the undeformed samples. Figure 46 shows the Mössbauer spectra of the Fe-25Ni-0.7C martensite deformed at 77 K and subsequently measured at this temperature (a) and after aging for one hour at room temperature (b). The spectra are quite identical, which reveals that carbon distribution is not essentially changed during aging.

Early stages of aging are characterized by the formation of carbon clusters, which appears as an increase of electrical resistivity (*e.g.*, /81/). It was shown in /VIII/ that this increase is practically absent in the case of the low temperature deformed sample supporting the idea of the prevention of the aging processes. Also dilatometric measurements revealed about six times smaller contraction for the deformed sample than for the undeformed sample below RT.

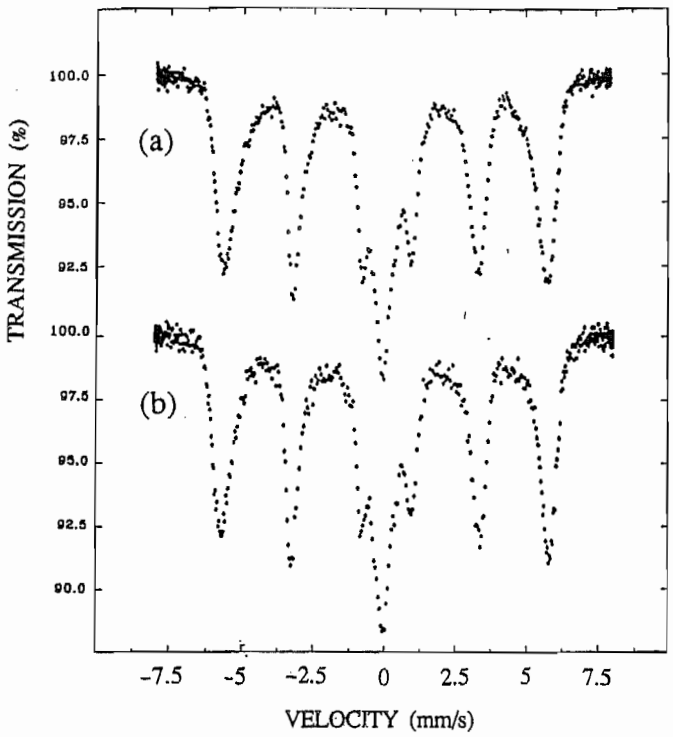


**FIG. 46.** Mössbauer spectra of the Fe-25Ni-0.7C martensite:
(a) deformed at 77 K and measured subsequently at this temperature,
(b) measured at 77 K after aging for 1 h at room temperature.

As mentioned at the very beginning of this work, the freshly formed martensite possesses rather good mechanical properties, but they are lost by aging /1/. From the technologial point of view, it would be important to avoid the aging processes and sustain the low temperature properties at ambient temperatures. One promising way to affect the aging processes is deformation at low temperatures, but it is not a very useful method in practice as long as very low temperatures are required. However, some deformation experiments showed that even high-carbon (low-nickel) martensite can be quite heavily deformed at room temperature in certain circumstances. Also the aging seemed to be prevented or at least significantly retarded after deformation. Further experimental work has to be done in this field. Another important direction for future research is alloying with nitrogen. Martensitic steels where nitrogen is substituted for carbon totally or only partially can improve many properties (*e.g.*, corrosion resistance, mechanical properties and wear resistance) in a very inexpensive way. The present research serves also as some basis for understanding the role of nitrogen in the aging phenomena.

## 4 CONCLUSIONS

1. The abnormally high *c/a* ratio in the freshly formed Fe-Ni-C martensite is caused by strains arising from the coherent bond between the retained austenite and the virgin martensite. Stresses are increased in the retained austenite due to martensitic transformation, but there is no hydrostatic stress component and they are caused by the coherent bond between the freshly formed martensite and the retained austenite in the case of the plate martensite morphology and by

dislocations generated during martensitic transformation in the case of lenticular martensite. A break of coherency occurs during aging at temperatures below 200 K when dislocations become mobile (the first stage of aging), which is accompanied by a decrease of tetragonality. There is no redistribution of carbon atoms affecting the value of tetragonality at such low temperatures.

2. The second stage of the low temperature aging develops at temperatures above 200 K with the pinning of dislocations by carbon atoms and with the clustering of carbon atoms in a solid solution. The pinning of dislocations, evidenced by the internal friction and the positron-lifetime measurements, includes formation of the Snoek atmospheres, *i.e.*, ordering of carbon atoms in a stress field of moving dislocations, as a preceding process. The morphology of martensite controls the density of dislocations and therefore the extent of their interaction with carbon atoms.

3. Clustering of carbon atoms occurs during aging at temperatures above 200 K (the third stage of aging) in accordance with the available transmission electron microscopy studies where some signs of spinodal decomposition near room temperature were revealed. The essential feature of clustering is the increase of the fraction of iron atoms with two carbon atoms as nearest neighbors. A striking difference between the decomposition of virgin martensites in Fe-C and in Fe-N alloys during low temperature aging is the absence of clustering in the Fe-N alloys, if clustering is defined as an increase of the number of interstitial atoms in the immediate surrounding of iron atoms. The structure of carbon-rich regions in the aged Fe-C martensite is not isomorphous with the structure of $\alpha''$ - $Fe_{16}N_2$ in the aged Fe-N alloy. According to Mössbauer data it can be described as $Fe_4C_x$ with $x < 1$. The decrease of the *c/a* ratio in the third stage of aging in Fe-Ni-C martensites is due to the decomposition of martensite, and its starting temperature is lower with the higher nickel content as a result of an increase of diffusivity of carbon by nickel. This effect is also verified by the resistivity and susceptibility results. The increase of tetragonality during aging of Fe-C and Fe-Mn-C martensites below 200 K is not ascribed to the clustering of carbon atoms and needs further studies.

   Shear modulus shows large increase during aging. Its behavior is quite linear and it seems to be rather insensitive to the processes of the three stages of aging.

4. Deformation of the freshly formed martensites at low temperature leads to a decrease in tetragonality and a redistribution of carbon atoms. Carbon atoms may move from octahedral sites on the *c*-axis to the sites on the *a*- and *b*-axes or to microcracks. In both cases, energy stored in the stress fields of distortion dipoles around carbon atoms is reduced. During aging, clusters are formed to minimize the total strain energy. Hence, it is expected that deformation prevents clustering, which is evidenced by X-ray diffraction, Mössbauer, electrical resistivity and dilatometric measurements.

## REFERENCES


1. J. Pietikäinen, J. Iron and Steel Inst., 1968, vol. 206, pp. 74-78
2. P.G. Winchell and M. Cohen, Trans. ASM, 1962, vol. 55, pp. 347-361.
3. G.T. Eldis and M. Cohen, Metall. Trans., 1983, vol. 14 A, pp. 1007-1012.
4. L.I. Lysak, S.A. Artemjuk and Ju.M. Polischuk, Phys. of Metals and Metallogr., 1973, vol. 35, No. 1, pp. 196-199
5. L.K. Mikhajlova, Dokl. Akad. Nauk SSSR (in Russian), 1974, vol. 216, pp.778-780
6. L.I. Lysak and Ya.N. Vovk, Phys. of Metals and Metallogr., 1971, vol. 31, No. 3, pp. 208-211
7. L.I. Lysak and Ya.N. Vovk, Fiz. Metall. Metalloved. (in Russian), 1965, vol. 20, No. 4, pp. 540-545
8. I.Ya. Georgijeva and O.P. Maximova, Phys. of Metals and Metallogr., 1971, vol.32 , No. 2, pp. 135-146
9. I. Tamura, In: Proceedings of First JIM International Symposium on New Aspects of Martensitic Transformations, May 10-12, 1976, Kobe, Japan, Supplement to Trans. JIM, vol. 17, 1976, pp. 59-68
10. M. Umemoto, E. Yoshitaka and I. Tamura, J. of Mater. Sci., 1983, vol. 18, pp. 2893-2904
11. J. Pietikäinen, Trans. ISIJ, 1985, vol. 25, pp. 340-344
12. G.V. Kurdjumov and A.G. Khachaturjan, Acta Metall., 1975, vol. 23, pp. 1077-1088
13. G.V. Kurdjumov, Metall.Trans. 1976, vol. 7A, pp. 999-1011
14. L.I. Lysak, Phys. of Metals and Metallogr., 1978, vol. 45, No. 6, pp. 94-106
15. L.I. Lysak, N.A. Storchak and A.G. Drachinskaja, Phys. of Metals and Metallogr. 1977, vol. 43, nr .3, pp. 138-143
16. S.D. Prokoshkin and E. Ju. Marejeva, Phys. of Metals and Metallogr., 1985, vol. 59, No. 5, pp. 130-142
17. V.I. Bondar, V.Je. Danil`chenko and V. A. Okhrimenko, Phys. of Metals and Metallogr., 1988, vol. 66, No. 1, pp. 157-161
18. J-M. R. Génin and P.A. Flinn, TMS AIME, 1968, vol. 242, pp. 1419-1430
19. W.K. Choo and R. Kaplow, Acta Met., 1973, vol. 21, pp. 725-732
20. N. DeCristofaro, R. Kaplow and W.S. Owen, Metall. Trans., 1978, vol. 9A, pp. 82-825
21. V.N Gridnev, V.G. Gavriljuk, V.V. Nemoshkalenko, Ju. A. Polushkin and O.N. Razumov, Phys. of Metals and Metallogr., 1977, vol. 43, No. 3 pp. 109-116
22. S. Nagakura and M. Toyoshima, Trans. JIM, 1979, vol. 20 , p. 100
23. M.K. Miller, P.A. Beaven, S.S. Brenner and G.D.W. Smith, Metall. Trans., 1983, vol. 14 A, pp. 1021-1024.
24. S. Nagakura, I. Hirotsu, M. Kusunoki, T. Suzuki and J. Nacamura, Metall. Trans., 1983, vol. 14A, pp. 1025-1031.

25. K.A. Taylor, L. Chang , G.B. Olson , G.D.W. Smith , M. Cohen and I.B. Van der Sande, Metall. Trans., 1989, vol. 20A, p. 2717-2737.
26. J.-M.R. Génin, Metall. Trans., 1987, vol. 18A, pp. 1371-1388
27. O.N.C. Uwakweh, J.Ph. Bauer and J.-M.R. Génin, Metall. Trans., 1990, vol. 21A, pp. 589-602
28. O.N.C. Uwakweh, J.-M.R. Génin and J.-F. Silvain, Metall. Trans., 1991, vol. 22A, pp. 797-806
29. C. Prioul, M. Carrard, J. de Physique, 1981, Colloque C5, t. 42, pp. 1007-1072.
30. G. Olson and W.S. Owen, (Ed.), "Martensite, A Tribute to Morris Cohen", ASM, The Materials Science Society, 1992, p. 331
31. K. Härkonen, I. Tittonen, J. Westerholm and K. Ullakko, Phys. Rev. B., 1989, vol. 39, p. 7251
32. E. Ikonen, J. Hietaniemi, K. Härkönen, M. Karppinen, T. Katila, J. Lindén, L. Niinistö, H. Sipola, I. Tittonen and K. Ullakko, High Temperature Superconductors, (Plenum, New York 1988), pp. 209-215
33. V. Kelhä and T. Niinikoski, Acta Polytechnica Scandinavica, No 76, Helsinki 1971, p. 16
34. K. Ullakko, Licentiate Thesis, Helsinki University of Technology, Espoo, Finland, 1986, p.71
35. K. Ullakko and J. Pietikäinen, In: Proc. of The International Conference on Martensitic Transformations (1986), Japan Institute of Metals, pp. 291-295
36. A.S. Nowick and B.S. Berry, "Anelastic Relaxation in Crystalline solids", Academic Press, New York, 1972, p. 677
37. H. Kleemola, S. Pekonen, M. Sulonen, Acta Polytechnica Scandinavica, Phys. including Nucleonics Series No.75, Helsinki 1971, p. 15
38. E.J. Saxl and M. Allen, Phys. Rev. D, Vol. 3, No. 4, 1971, pp. 823-825
39. K. Ullakko, Y. Liu and X. Xie, Proc. of the XXV Annual Conference of the Finnish Physical Society, Report No. 119 (1991), Dept. of Physics, University of Oulu, Finland
40. A. Tiitta, "Astacus, A Reverse Neutron Time-of-Flight Diffraction using a Fourier Chopper", Publication 27, Technical Research Centre of Finland, Electrical and Nuclear Technology, Espoo, (1980), p. 48
41. O. Antson, "Development and Applications of the reverse Neutron Time-of-Flight Method with Fourier-type Beam Chopper", Doctoral Thesis, Helsinki University of Technology, 1991; Technical Research Centre of Finland, Publications 82, Espoo 1991, Finland, 41 p. + 7 Appendices
42. I. Tamura, Suppl. to Trans. JIM, 1976, vol. 17, pp. 59-68
43. T. Maki and C.M. Wayman, Ibid., pp. 75-80
44. P.C. Chen, B.O. Hall and P.G. Winchell, Met. Trans. A, 1980, vol. 11A, pp. 1323-1331

45. M.A. Krivoglaz, "Theory of X-ray and Thermal-Neutron Scattering by real Crystals", Plenum Press, New York, 1969, p. 235
46. M. Hayakawa, Y. Uemura and M. Oka, Metall. Trans, 1981, vol. 12A, pp. 1545-1547.
47. S. Kajiwara, T. Kikuchi and S. Uehara, In: Proceedings of The International Conference on Martensitic Transformations (ICOMAT-86), August 26-30, 1986. The Japan Institute of Metals, 1986, pp.301-306.
48. M. Hayakawa and M. Oka, Acta Met., 1983, vol. 31, pp. 955-959.
49. C.A.V. de A Rodriques, C. Prioul and L. Hyspecka, Metall. Trans., 1984, vol. 15A, pp. 2193-2203.
50. C. Prioul, J. de Physique, 1985, Colloque 10, t. 46 , pp. 665-668.
51. J.M. Humphreys, A. Plumtrie and W.J. Bratina, Acta Met., 1969, vol. 17, pp. 89
52. G.V. Kurdjumov and A.G. Khachaturjan, Metall. Trans.,1972, vol. 3A, pp. 1069-1076
53. Ju.N. Koval and V.V. Kokorin, Phys. of Metals and Metallogr. ,1975, vol. 39, No. 4, pp.129-133
54. A.L. Roitburd and A.G. Khachaturjan, Phys. of Metals and Metallogr., 1970, vol. 30, No. 6, pp. 68-77
55. M. Hayakawa, M. Tanigami and M. Oka, Metall. Trans., 1985, vol. 16A, pp. 1745-1750
56. L.I. Lysak, V.Je. Danil´chenko, Ju.M. Polischuk and A.I. Ustinov, Dokl. Akad. nauk SSSR (in Russian), 1975, vol. 224, No. 1, pp. 76-79
57. V.Je. Danil´chenko, Phys. of Metals and Metallogr., 1987, vol. 64, No. 4, pp. 110-114
58. V.N. Gridnev, V.G. Gavriljuk, V.V. Nemoshkalenko, Ju.A. Polushkin and O.N. Razumov, Phys. of Metals and Metallogr., 1978, vol.46, No. 2, pp. 107-114.
59. K.Ja. Golovchiner, Phys. of Metals and Metallogr., 1974, vol. 37, No. 2, pp. 126-130
60. V.M. Jershov and N.L. Oslon, Fiz. metall. Metalloved. (in Russian), 1968, vol. 25, pp. 874-881
61. V.N. Gridnev and V.I. Trephilov, Dokl. Akad. Nauk SSSR (in Russian), 1957, vol. 116, pp. 60-62
62. P.G. Winchell and G.K. Speich, Acta Met., 1970, vol. 18, pp. 53-62
63. V.G. Veeraraghavan, C.F. Eagen, H.R. Harrison and P.G. Winchell, J. Appl. Phys., 1976, vol. 47, pp. 4768-4771
64. G.V. Kurdjumov and L.C. Khandros, Dokl. Akad. Nauk. SSSR, 1949, Vol. 66, p.211
65. H.C. Ling and W.S. Owen, Acta Met., 1981, Vol. 29, pp. 1721-1736
66. J. Pietikäinen, J. de Physique, Colloque C4, 1982, t. 43, pp. 479-484
67. Y. Liu, Z. Xie, K. Ullakko and J. Pietikäinen, In: Proc. of the XXIV annual Conference of the Finnish Physical Society, 1990, Tampere, Finland; Tampere University of Technology, Dept. of Electrical Engineering Physics, Report 7 - 90, 1990
68. T. Maki and C.M.Wayman, Acta Met., 1977, vol. 25, pp. 695-710

69. L.I. Lysak, A.G. Drachinskaja and N.A. Storchak, Phys. of Metals and Metallogr., 1972, vol. 34, No. 1, pp. 74-79.
70. V.V. Kokorin, Martensitic transformations in inhomogeneous solid solutions, Kiev, "Naukova Dumka" ed., 1987, 166 pp.
71. V.M. Danilenko, D.R. Rizdvyanetsky and A.A. Smirnov, Fiz. Metall. Metalloved. (in Russian), 1963, vol. 15, p. 194
72. D.R. Ryzdvyanetsky, Metallofizika, 1971, vol. 38, p. 19
73. A. Vehanen, P. Hautojärvi, J. Johansson, J. Yli-Kauppila and P. Moser, Phys. Rev. B, 1982, vol. 25, No. 2, pp. 762-780
74. P. Hautojärvi, J. Johansson, A. Vehanen, J. Yli-Kauppila and P. Moser, Phys. Rev. Lett., 1980, vol. 44, No. 20, pp. 1326-1329
75. P. Hautojärvi, A. Vehanen and V.S. Mikhalenkov, Appl. Phys., 1976, vol. 11, pp. 191-192
76. J.P. Hirth and J. Lothe, Theory of dislocations, McGraw - Hill book company, New York, 1968, 780 p.
77. H. Ino, K. Umezu, S. Kajiwara and S. Uehara. In: Proceedings of the International Conference on Martensitic Transformations, August 26-30, 1986, Nara, Japan. The Japan Institute of Metals, 1987, pp. 307-312
78. M. Ino, T. Ito, S. Nasu and U. Gonser, Acta Met., 1982, vol. 30, pp. 9-20
79. A.M. Sherman, G.T. Eldis and M. Cohen, Metall. Trans., 1983, vol. 14A, pp. 995-1005
80. M. Carrard, C. Prioul, I. Plusguellec and P.Azou, In: Proceedings 3rd European Conf. "Internal Friction and Ultrasonic Attenation in Solids", July 18-20, 1979, Manchester, ed. by C.C. Smith, Pergamon Press, 1981, pp. 281-286.
81. K. Ullakko and J. Pietikäinen, Proc. Int. Congr. on Heat Treatment of Materials, Berlin, Germany, 1985, p.361
82. P. Rochegude and J. Foct, Phys. Stat. Sol. (a), 1986, vol. 98, pp. 51-62
83. N. De Cristofaro and R. Kaplow, Metall. Trans., 1977, vol. 8A, pp. 35-43
84. J.-M.R. Génin, Metall. Trans., 1990, vol. 21A, pp. 2083-2086
85. G.B. Olson, K.A. Taylor and M. Cohen, Ibid., p. 2086
86. J.-M.R. Génin and J. Foct, Phys. Stat. Sol. (a), 1973, vol. 17, pp. 395-406
87. V.G. Gavriljuk, V. M. Nadutov and O. Gladun, Phys. of Metals and Metallogr., 1990, vol. 69, No. 3, pp. 128-134
88. L.R. Walker, G.K. Wertheim and V. Jaccarino, Phys. Rev. Lett., 1961, vol. 6, pp. 98-101
89. V.N. Bugaev, V.G. Gavriljuk, O.V. Gladun, S.P. Efimenko, and V.M. Nadutov and V.A. Tatarenko, Proc. of the Int. Conf. on High-nitrogen Steels HNS 90, Aachen, Germany, 1990, pp. 95-99
90. E.I. Mittemeijer, Liu Cheng, P.J. van der Schaaf, G.M. Brackman and B.M. Korevaar, Met. Trans., 1988, vol. 19A, pp. 925-932
91. Liu Cheng and E.I. Mittmeijer, Metall. Trans., 1990, vol. 21A, pp. 13-26

92. A.V. Suyazov, M.P. Usikov and B.M. Mogutnov, Phys. of Metals and Metallogr., 1976, vol. 42, No. 4, pp. 69-77
93. N.V. Edneral and Ju.A. Skakov, Fiz. Metall. Metalloved. (in Russian), 1968, vol. 26, No. 5, pp. 850-856
94. S. Murphy and J. Whitemann, Metall. Trans., 1970, vol. 1, pp. 843-848
95. G. Le Caer, A. Simon, A. Lorenzo and J.-M. R. Génin, J. Phys. Chem., 1982, vol. 86, pp. 4799-4808
96. D.W. Hoffman and Morris Cohen, Acta Met., 1973, vol. 21, pp. 1215-1223
97. L.I. Lysak and B.I. Nikolin, Fiz. Metall. Metalloved., (in Russian), 1966, vol. 22, No. 5, pp. 730-736
98. D.A. Mirzajev, S.V. Rushitz, A.I. Ustinov and Yu.N. Goikhenberg, Metallofizika, 1982, vol. 4, pp. 684-693
99. M. Kajatkari, Doctoral Thesis, Acta Polytechnica Scandinavica, Chemical Technology and Metallurgy Series No. 163, Espoo, Finland, 1985, p. 60
100. M. Kajatkari and J. Pietikäinen, Scripta Metallurgica, vol. 17, (1983), pp. 1351-1351
101. R. H. Richman, In: R.E. Reed-Hill *et al.* (ed.), Deformation Twinning, New York, 1964, Gordon and Breach, pp. 386-389
102. K. Ullakko and J. Pietikäinen, In: Proc. of the Int. Conference of The Martensitic Transformation in Science and Technology, Bochum, Germany, DGM Informationgesellschaft Verlag, 1989, p. 405
103. Yu.L. Al'shevskiy and G.V. Kurdjümov, Phys. Metals and Metallogr., vol. 30, 1970, p. 197
104. O.G. Baharev, V.G. Gavriljuk and V.M. Nadutov, Fiz. Metall. Metalloved. No. 11, 1990, pp. 196-198 (in Russian)
105. Liu Cheng, N.M. van der Pers, A. Böttner, Th.H. de Keijser and E.J. Mittemeijer, Met. Trans. A, vol. 22A, 1991, pp. 1957-1968
106. K. Ullakko, Diploma work, Helsinki University of Technology, 1982, Espoo, Finland (in Finnish)
107. I.R. Entin, V.A. Somenkov and S.M. Shil'shtein, DAN SSSR, vol. 206, 1096 (1972)
108. G.R. Speich, Trans. AIME, vol. 245, 1969, p. 2553
109. S. Oketani, S. Hitomi and S. Nagokuva, J. Jpn. Inst. Met., vol. 26, 1962, p. 494